EPA/#
September 2000

Recommended Methods for Ambient Air Monitoring of NO, NO_2, NO_Y, and Individual NO_Z Species

edited by

W.A. McClenny
Human Exposure and Atmospheric Sciences Division
National Exposure Research Laboratory
U.S. Environmental Protection Agency
Research Triangle Park, NC 27711

National Exposure Research Laboratory
Office of Research and Development
U.S. Environmental Protection Agency
Research Triangle Park, NC 27711

NERL-RTP-HEASD-00-243

TECHNICAL REPORT DATA

1. Report No. EPA/600/R-01/005	2.	3. Recipient's Accession No.
4. Title and Subtitle Recommended Methods for Ambient Air Monitoring of NO, NO_2, NO_Y, and Individual NO_Z Species		5. Report Date September 2000 6. Performing Organization Code
7. Author(s) W.A. McClenny and others		8. Performing Organization Report No.
9.Performing Organization Name and Address Atmospheric Methods and Monitoring Branch, Human Exposure and Atmospheric Sciences Division, National Exposure Research Laboratory, U.S. EPA, Research Triangle Park, NC, 27711		10. Program Element No. E-3917 11. Contract/Grant No. 68-D5-0049
12.Sponsoring Agency Name and Address Atmospheric Methods and Monitoring Branch, Human Exposure and Atmospheric Sciences Division, National Exposure Research Laboratory, U.S. EPA, Research Triangle Park, NC, 27711		13. Type of Report and Period Covered 14.Sponsoring Agency Code

15. Supplementary Notes

16. Abstract The most appropriate monitoring methods for reactive nitrogen oxides are identified subject to the requirements for diagnostic testing of air quality simulation models. Measurements must be made over one hour or less and with an uncertainty of equal to or less than 20% (10% for NO_2) over a typical ambient concentration range extending from a lower limit of 1ppbv. NO, NO_2, HNO_3, PAN, and other reactive nitrogen oxides that exist at the 1ppbv level and above, along with the compound sets designated as NO_Y, NO_X, and their difference, NO_Z are included in this measurement requirement. New and/or improved measurement techniques for NO_2 monitoring including laser-induced fluorescence, photolytic conversion/NO,O_3 chemiluminescence, differential optical absorption spectroscopy, and NO_2/luminol chemiluminescence are examined with reference to literature citations and to field monitoring as part of the 1999 SOS Summer Field Study in Nashville, TN. Existing approaches to monitoring the other most prevalent reactive oxides of nitrogen are reviewed. At the lower end of the ambient monitoring range, research-grade instruments are often needed and operator skill, experience, and close attention are critical to proper instrument operation, calibration, and maintenance. If the most appropriate methods are used and other species and atmospheric parameters relevant to ozone production and accumulation are also accurately measured, air quality simulation models can be diagnostically tested and the basis for regulatory decisions such as the NO_x SIP Call can be evaluated.

17. KEY WORDS AND DOCUMENT ANALYSIS

A. Descriptors - Nitrogen Oxides, Ozone, Nitrogen Dioxide, Nitrogen Oxide, Nitric Acid	B. Identifiers / Open Ended Terms	C. COSATI

18. Distribution Statement	19. Security Class *(This Report)*	21. No. of Pages
	20. Security Class *(This Page)*	22. Price

File: S:\HEASD\Forms\Tech-Form-2220-i

Notice

The U.S. Environmental Protection Agency through its Office of Research and Development assembled the information in this report with input from a number of prominent scientists and funded a research effort to provide field data for this report under Contract 68-D5-0049 to ManTech Environmental Technology, Inc. The report has been subjected to the Agency's peer and administrative review and has been approved for publication as an EPA document. Mention of trade names or commercial products does not constitute endorsement or recommendation for use.

Abstract

The most appropriate monitoring methods for reactive nitrogen oxides are identified subject to the requirements for diagnostic testing of air quality simulation models. Measurements must be made over 1 h or less and with an uncertainty of ≤20% (10% for NO_2) over a typical ambient concentration range extending from a lower limit of 1 ppbv. NO, NO_2, HNO_3, PAN, and other reactive nitrogen oxides that exist at the 1-ppbv level and above, along with the compound sets designated as NO_Y (all reactive nitrogen oxide compounds), NO_X ($NO + NO_2$), and their difference, NO_Z, are included in this measurement requirement. New and/or improved measurement techniques for NO_2 monitoring, including laser-induced fluorescence, photolytic conversion/NO, O_3 chemiluminescence, differential optical absorption spectroscopy, and NO_2/luminol chemiluminescence, are examined with reference to literature citations and to field monitoring as part of the 1999 Southern Oxidants Study (SOS) summer field study in Nashville, TN. Existing approaches to monitoring the other most prevalent reactive oxides of nitrogen are reviewed. At the lower end of the ambient monitoring range, research-grade instruments are often needed and operator skill, experience, and close attention are critical to proper instrument operation, calibration, and maintenance. If the most appropriate methods are used and other species and atmospheric parameters relevant to ozone production and accumulation are also accurately measured, air quality simulation models can be diagnostically tested and the basis for regulatory decisions such as the NO_X State Implementation Plan (SIP) Call can be evaluated.

Foreword

The National Exposure Research Laboratory, Research Triangle Park, North Carolina, performs research and development to characterize, predict, and diagnose human and ecosystem exposure, giving priority to that research which most significantly reduces the uncertainty in risk assessment and most improves the tools to assess and manage risk or to characterize compliance with regulations. The Laboratory seeks opportunities for research collaboration to integrate the work of ORD's scientific partners and provides leadership to address emerging environmental issues and advance the science and technology essential for understanding human and ecosystem exposures. One aspect of the Laboratory's mission is to support the iterative process of comparing model predictions with experimental observations so that ultimately the reconciliation of differences is accomplished. In the case of ozone production in the ambient atmosphere through photochemical processes, this support includes the identification and/or development of monitoring instrumentation of sufficient quality to evaluate the impact of control strategies.

EPA has established a strategic plan for its scientific program of research and development that includes production of reports that respond to the perceived needs in support of public interest through compliance with the Government Performance and Results Act (GPRA). The current report is GPRA Annual Performance Measure (APM) #442; it contains a summary of published methods for monitoring nitrogen oxides and identification of the best available methods. Resources for the production of this report are provided as part of EPA's NARSTO program, which includes the study of ozone precursors and the relationship between emissions of these precursors and the production of ozone in the troposphere. Information provided herein is needed to understand the priorities for instrumentation improvements and to appreciate the current viable alternatives available to the atmospheric scientist. The objective of identifying the best methods is ultimately to obtain the best ambient air data in support of air quality simulation models so as to predict the occurrence of ozone in terms of the presence of ozone precursor compounds, one category of which is the nitrogen oxides.

This report incorporates information on the need for monitoring methods for nitrogen oxides, on their required level of performance, on alternatives available in both the commercial and research arenas, on the operating principles of several monitoring methods, and on the literature that documents information on methods. A major monitoring need is for diagnostic testing of air quality models (AQMs) so that refinements can be made to existing models (see Chapter 4). These refinements would then enhance the relevance of model predictions with respect to recommendations on the control of nitrogen oxide emissions and of ozone concentrations. Discussion of the various alternatives indicates where improvements in monitoring methods are most likely to be made so that scarce resources can be allocated accordingly. For all the reactive oxides of nitrogen considered here, commercial and/or research-grade instruments meet the needs for monitoring with respect to diagnostic testing of AQMs, although improvements are almost universally indicated to avoid the often tedious monitoring protocols that are currently required.

Gary J. Foley, Ph.D.
Director
National Exposure Research Laboratory
Research Triangle Park, NC 27711

Contents

Figures

Tables

Acronyms and Abbreviations

APM	annual performance measure
AQM	air quality model
BRD	balanced ratiometric detector
CF	conversion factor
CIMS	chemical ionization mass spectrometry
CMAQ	Community Multiscale Model for Air Quality
CRDS	cavity ring-down spectroscopy
DIAL	differential absorption lidar
DOAS	differential optical absorption spectroscopy
ECD	electron capture detector
FTIR	Fourier transform infrared
GC	gas chromatography
GC/MS	gas chromatography/mass spectrometry
GPRA	Government Performance and Results Act
HC	hydrocarbon subset of VOCs
IC	ion chromatography
IR	infrared
LIF	laser-induced fluorescence
LOD	limit of detection
MIESR	matrix isolation electron spin resonance
MPAN	peroxymethacrylyl nitrate
MS	mass spectrometry
NAAQS	National Ambient Air Quality Standards
NARSTO	National Atmospheric Research Strategy for Tropospheric Ozone
NH_X	sum of gaseous ammonia and particulate ammonium
NIST	National Institute of Standards and Technology
nm	nanometer
NOAA	National Oceanic and Atmospheric Administration
non-$(NO_Y)_i$	nitrogen-containing compounds not part of NO_Y (e.g., NH_3, HCN)
NO_X	sum of NO plus NO_2
NO_Y	sum of NO_X and other reactive nitrogen compounds
NO_Z	$NO_Y - NO_X$
NRC	National Research Council
O_X	sum of all species that can act as reservoirs for atomic oxygen
PAMS	Photochemical Assessment Monitoring Stations
PAN	peroxyacetyl nitrate
PC	photolysis-chemiluminescence
PDA	photodiode detector array
PDE	partial differential equation
pm	picometer
PM	particulate matter
PMT	photomultiplier tube
ppbv	parts per billion by volume
ppbC	parts per billion carbon
ppbv•m	parts per billion by volume times meters
ppmv	parts per million by volume
PPN	peroxypropionyl nitrate
pptv	parts per trillion by volume
PPS	pseudo-photostationary state
RADM	Regional Acid Deposition Model
ROC	reactive organic compounds
SDM	slotted disk machine
SIP	State Implementation Plan
slpm	standard liters per minute
SNR	signal-to-noise ratio
SOS	Southern Oxidants Study
TDL	tunable diode laser
TDLAS	tunable diode laser absorption spectroscopy
TOPAS	Tropospheric Optical Absorption Spectroscopy
TTFMS	two-tone frequency-modulated spectroscopy
UAM-IV	Urban Airshed Model version IV
UV	ultraviolet
VOC	volatile organic compound

Acknowledgments

This report is a joint effort involving members of the monitoring and modeling communities who have graciously provided information in their areas of expertise or have carefully peer reviewed the manuscript. Special acknowledgment goes to Dr. J.E. Sickles of the National Exposure Research Laboratory, U.S. EPA, for his advice on various aspects of this document; to Dr. G.M. Russwurm of ManTech Environmental Technology, Inc., for his assistance in understanding the subtleties of differential optical absorption spectroscopy; to Dr. E.H. Daughtrey, Jr., of ManTech Environmental Technology, Inc., for his contributions to organizing the ManTech field studies that provided some of the data used in this report; and to Dr. P.K. Dasgupta of the Texas Tech University who has freely shared his knowledge on microchemistry, an area in which he pioneers. Thanks also to Dr. F. Fehsenfeld of the NOAA Aeronomy Laboratory, Dr. D. Stedman of the University of Denver, and Ms. Joann Rice of the OAQPS, U.S. EPA, for peer review prior to publication.

Dedication

This report is dedicated to the memory of Dr. J.A. Hodgeson, an EPA research chemist who pioneered the use of gas-phase chemiluminescence for the monitoring of ambient trace gases, particularly the nitrogen oxides. His contributions in the early years after EPA's formation were significant in setting the direction for subsequent progress in monitoring technology.

Contributors

J.R. Arnold, Atmospheric Modeling Division, National Exposure Research Laboratory, U.S. EPA, Research Triangle Park, NC

R.C. Cohen, University of California at Berkeley, Berkeley, CA

R.L. Dennis, Atmospheric Modeling Division, National Exposure Research Laboratory, U.S. EPA, Research Triangle Park, NC

K.G. Kronmiller, ManTech Environmental Technology, Inc., Research Triangle Park, NC

D.J. Luecken, Human Exposure and Atmospheric Sciences Division, National Exposure Research Laboratory, U.S. EPA, Research Triangle Park, NC

W.A. McClenny, Human Exposure and Atmospheric Sciences Division, National Exposure Research Laboratory, U.S. EPA, Research Triangle Park, NC

J. Stutz, Department of Atmospheric Sciences, UCLA, Los Angeles, CA

J.A. Thornton, University of California at Berkeley, Berkeley, CA

G.S. Tonnesen, CE-CERT, University of California at Riverside, Riverside, CA

M. Wheeler, ManTech Environmental Technology, Inc., Research Triangle Park, NC

E.J. Williams, Aeronomy Laboratory, NOAA Environmental Research Laboratories, Boulder, CA

P.J. Wooldridge, University of California at Berkeley, Berkeley, CA

Chapter 1
Introduction

by

W.A. McClenny, U.S. EPA

The objective of this report is to recommend the best monitoring methods for NO, NO_2, NO_X, NO_Y, and speciated NO_Z to support the current national strategy on regional transport of ozone. Definitions for the compound groupings NO_X, NO_Y, and NO_Z are given in section 1.3. Such instrumentation will be used to evaluate the effectiveness of NO_X emissions reduction as initially envisioned in the September 1998 final Regional Transport of Ozone Rule (NO_X State Implementation Plan [SIP] Call). As part of this document (*Federal Register*, 1998), the Federal government originally proposed that 22 eastern states and the District of Columbia reduce source emissions of NO_X (NO + NO_2) so as to lower the ground-level O_3 concentrations at downwind sites. An average targeted reduction in NO_X emissions of 28% was determined assuming that reasonable, cost-effective control measures were applied. Subsequently, on 25 May 1999, the U.S. Court of Appeals for the D.C. Circuit issued an order partially staying the implementation of the NO_X SIP call. Arguments before the Court were presented on 9 November 1999, and on 3 March 2000 the Court of Appeals generally upheld the NOx SIP Call provisions. On 22 June 2000, the deadline for states to submit SIPs was set as 30 October 2000, and on 30 August 2000 the compliance deadline for the SIP call provisions was extended to 31 May 2004.

In related actions, on 17 December 1999 EPA granted petitions filed by four northeastern states seeking to reduce ozone pollution through reductions in nitrogen oxide emissions from other states. These petitions were filed under Section 126 of the Clean Air Act. Understanding the effectiveness of the actions carried out as a result of the NO_X SIP Call and the Section 126 petitions will ultimately require experimental measurements of ozone and ozone precursors including the nitrogen oxides. Ideally, these measurements along with those of other trace species and atmospheric variables will vindicate the current national strategy of controlling O_3 production by selectively reducing NO_X and/or reactive organic compound (ROC) emissions. Measurements before and after implementation of emission controls will be required to establish a basis for quantifying changes.

1.1 Rationale for the Need to Measure Nitrogen Oxides

A detailed discussion of the rationale for obtaining measurements of individual nitrogen oxide species including NO, NO_2, HONO, HNO_3, organic nitrates, particle nitrate, and NO_Y is presented in Chapter 4. This discussion, titled "On the Need for Better Ambient Observations of Important Chemical Species for Air Quality Model Evaluation," emphasizes diagnostic testing of air quality models (AQMs). In diagnostic testing, field measurements of key trace species and of process rates (reaction rates, photolysis rates, etc.) are compared to the model results at preliminary output levels in the modeling procedure for predicting ambient ozone. Given sufficiently accurate and precise measurements, the results of these comparisons identify the strong and weak points in the model simulations of the ambient atmosphere. Measurements of key trace species concentrations taken with a short temporal resolution compared with typical significant changes in daytime ozone concentration are most desirable. Chapter 4 establishes the required frequency of measurement as significantly less than one hour. The discussion gives specific recommendations for prioritizing variables for a broad range of parameters, including those nitrogen oxides of specific interest, along with some estimates of the measurement certainty required for meaningful comparison tests with the predictions of AQMs. Measurements of NO_2 with an uncertainty of 10% at the 1-ppbv and higher concentration levels and of no greater than 20% for individual NO_Z components are given as two requirements. Measurements of individual NO_Z species such as HNO_3 and PAN-like compounds are used in "air mass history resultant

photochemistry tests" where their ratios to other compounds are formed (see below). Additional requirements on these monitors may be imposed.

1.2 Note about Recommendations of this Report

The recommendations of this report are for monitoring methods that have been shown to meet the rather stringent monitoring requirements for diagnostic testing and atmospheric research. A method's potential may only have been realized with customized instrumentation assembled from component parts in the research laboratory. While this is most often the case, the existence of the National Ambient Air Quality Standards (NAAQS) for NO_2 and other criteria pollutants has created a large market for commercial instruments designed for routine monitoring. In some cases redesign of these instruments has improved performance levels to meet research requirements. Therefore commercial instruments will be mentioned as part of the discussion of methods in cases where they have been used to experimentally demonstrate a potential for research monitoring applications. One example is the monitoring of total NO_Y and NO by NO, O_3 chemiluminescence, which is the reference method for NAAQS criteria monitoring of NO_2. In this case, commercially available instruments have been appropriately modified and used to demonstrate the potential of the chemiluminescence method. The different monitoring methods are mentioned in Chapter 2 as part of the conclusions and are discussed in more detail in Chapter 5 where information on alternative methods is given. Often several methods have been successful in achieving the monitoring requirements of diagnostic testing of AQMs and the scientist must choose among these based on the perception of advantages and disadvantages.

1.3 Definition of Compounds of Interest

As noted by Kliner et al. (1997), NO_Y consists of all oxides of nitrogen in which the oxidation state of the N atom is +2 or greater, i.e., the sum of all reactive nitrogen oxides including NO_X (NO + NO_2) and the remaining set of compounds that collectively are denoted by NO_Z, i.e., $NO_Y - NO_X = NO_Z$. For the purposes of this document, the most prevalent subset of NO_Z compounds will be treated. These compounds are known to account for almost all of the reaction products of NO_X in ambient air. This operational set of NO_Z compounds consists of nitric and nitrous acids (HNO_3 and HONO); the organic nitrates including peroxyacetyl nitrate anhydride (PAN), peroxymethacrylyl nitrate (MPAN), and peroxypropionyl nitrate (PPN); and particulate nitrates. The nitrogen oxides covered in order of presentation are NO_Y, NO, NO_2, HNO_3, HONO, PAN, PPN, MPAN, $RONO_2$, and particle nitrate.

1.4 Previous Survey of Instrumentation

Sickles (1992) provides excellent documentation in the open literature of sampling and analysis techniques for ambient oxides of nitrogen and related species including references up to a certain point in 1990. His work is also available in Volume I, Chapter 6, of EPA publication EPA/600/8-91/049aF (August 1993) titled "Air Quality Criteria for Oxides of Nitrogen." For the present report, two types of references are listed in the reference section (Chapter 7): those resulting from a literature search for the period between 1990 and 2000 and certain pre-1991 references that are required to establish discussion points in the text. The reader is referred to Sickles (1992) for a comprehensive listing of the pre-1991 references.

Parrish and Fehsenfeld (2000) provide a review of methods for gas-phase measurements that includes the nitrogen oxides. Their article is part of a special issue of *Atmospheric Environment* titled the *NARSTO Ozone Assessment—A Critical Review*.

1.5 Point and Path Monitors

Most major contributors to the nitrogen oxides can be monitored by either point or open-path monitors. Point monitors sample ambient air through an inlet to the interior of the monitor where the sample is probed and examined in a controlled environment. Sample conditioning to selectively eliminate interferences and/or to concentrate the sample is possible. Instrument calibration is typically performed by providing a known concentration of the target gas at the inlet. Responses to ambient air samples are then referenced to a calibration curve to infer the ambient air concentration of target species.

Open-path monitors typically monitor by probing the ambient air with a beam of radiation over significant distances (0.1–5 km). Radiation missing from the transmitted spectra is attributed to a combination of absorption and scattering by specific gases and airborne particles distributed along the path length. No sampling is performed and hence no sampling artifacts occur. The sampling environment is uncontrolled so that sample conditioning to remove interferences or to cause sample concentration is impossible. The parameter measured by open-path monitors is the product of gas concentration and distance usually stated in parts per billion by volume times meters (ppbv•m). Dividing this product by a known path length, the average concentration is obtained. As a result of the spatial averaging, the extent of variations in concentration along the path is reduced from that monitored by a point monitor, but the path-averaged value is more representative over the extended distances typical of AQMs. Calibration is performed by comparing field spectra to reference spectra taken in the laboratory (ideally with the same instrument) and/or by placing calibration cells filled with known target gas burdens (ppbv•m) in the optical

beam along a portion of the measurement path. Certain types of open-path measurements can be range resolved by analyzing the backscattered light from pulsed radiation sources. For example, short pulses of laser radiation are backscattered from atmospheric particles and received at the laser location as a function of time. By using multiple wavelengths to establish a difference in absorption along the path, range resolved measurement of target gases can be obtained. These systems are referred to as differential absorption lidar (DIAL) systems and are most frequently used to map dispersing source plumes. Pulsed laser systems can also be used for column burden measurements (ppbv•m). In this case the difference in absorption at multiple wavelengths is obtained using an aircraft-mounted source/receiver and the earth's surface as a diffuse backscatter of radiation.

1.6 Other Important Issues for Tropospheric Monitoring of Nitrogen Oxides

Calibration of the different trace species can be a limiting factor in achieving the level of accuracy required to meet the data quality objectives needed for diagnostic testing of AQMs. Procedures are firmly established for on-site calibration of NO and NO_2 monitoring instruments due to the NAAQS program, but have to be extended to measure the low to sub-ppbv levels sought in atmospheric research measurements. Reliable standards for other nitrogen oxides are not so routinely available and require a concentrated effort to establish. Although recommendations for calibration techniques are beyond the scope of work attempted in this document, the method references listed in Chapter 7 document the procedures for calibration used for specific methods.

Measurements in the vertical dimension are required for a complete description of the air quality mixture affecting ground-level ozone. Measurements from aircraft, from tethered balloons, from radiosondes, and by remote monitoring systems such as sodar, radar, and lidar are made to provide this information. The use of instrumentation for measuring the vertical distribution of nitrogen oxides is not specifically discussed in this document, but a number of the ground-based methods have been adapted to aircraft and/or modified to meet the special requirements of rapid response and orientation insensitivity that are required. Results of comparison studies of instrumentation used in aircraft, including NO instrumentation (Hoell et al., 1987), NO_2 instrumentation (Gregory et al., 1990a), and PAN instrumentation (Gregory et al., 1990b), have been documented by scientists at NASA Langley.

1.7 Organization of the Report

The report is organized to provide a basis and rationale for recommending monitoring methods for tropospheric nitrogen oxides. Following the Introduction, Conclusions, and Recommendations, Chapter 4 presents the rationale for using measurements for diagnostic testing of AQMs. The instruments available for NO_Y and individual reactive nitrogen oxides are discussed in Chapter 5, including the rationale for choosing among alternatives. Chapter 6 reviews some of the data obtained with commercially available NO_2 monitoring systems used in the Nashville Southern Oxidants Study (SOS) '99 summer field study. Supplemental information to highlight recent and/or pertinent experimental and theoretical work is provided in the Appendices. Appendix A explains the importance of the NO, O_3 gas-phase reaction in the inlet to sampling systems for NO, NO_2, and O_3. Appendix B provides documentation on the design features and performance characteristics of the open-path monitoring systems based on differential optical absorption spectroscopy (DOAS). Appendix C discusses the characteristics of photolytic converters as an alternative to thermal converters for conversion of NO_2 to NO prior to chemiluminescence detection of NO. Appendix D provides documentation of recently completed research on the use of laser-induced fluorescence (LIF) for direct NO_2 monitoring. Appendix E is a discussion of the applications of luminol-based monitoring of NO_2 and related procedures for monitoring NO, NO_X, and NO_Y.

Chapter 2
Conclusions

by

W.A. McClenny, U.S. EPA

Chapter 4 explains that many factors determine the production and accumulation of ozone downwind of fuel-fired electric utilities and other major point sources of NO_X emissions. AQMs have been developed to incorporate representations for all these factors and to assign the proper role to each. Based on AQM predictions, the U.S. EPA has determined that reduction in NO_X emissions from major sources in the Northeast U.S. will lead to significant reduction of downwind ambient O_3 concentrations and thereby significantly mitigate the detrimental effects of high ozone concentrations on human health and the ecology. Responsibilities with respect to transport of ozone and ozone precursors across state boundaries in the Northeast and across the international boundary with Canada are also of concern. To evaluate implementation of controls on these sources, AQM predictions will be compared to experimental measurements both before and after control implementation. The effect of the emissions reduction must be separated from other factors to show the real consequences. Since separation of factors must occur, the adequacy of all model constructs must be evaluated using a holistic or "one atmosphere" approach. Among the critical components is the accurate measurement of reactive nitrogen oxides.

The accomplishment of this objective and others of comparable importance is equivalent to being able to show relationships among ozone, its precursors, and other variables that are consistently interpretable and lead to changes that have known attribution. This process is referred to later in this document as *diagnostic testing of the models*. Only through diagnostic testing can the accuracy and validity of the model be determined and a consistent understanding of the interplay of different causal factors contributing to ozone production and accumulation be achieved.

Based on the requirements for adequate diagnostic testing of AQMs as delineated in Chapter 4, methods for monitoring ambient reactive nitrogen oxides at stationary, ground-level monitoring sites must have temporal resolution of significantly less than 1 h and a measurement uncertainty at 1 ppbv and higher of 20% for NO, NO_Y, and the major components of NO_Z (PAN, PPN, MPAN, HNO_3, HONO, and nitrate particulate [as equivalent NO]) and 10% for NO_2 (see Chapter 4). Monitoring methods that can meet these requirements or that appear to have the potential are discussed in Chapter 5. Those methods that are recommended for diagnostic testing and atmospheric research based on documented experimental testing are summarized in sections 2.1 through 2.6.

2.1 Recommendations for Monitoring Total Reactive Oxides of Nitrogen (NO_Y)

Thermal conversion/NO, O_3 chemiluminescence. Use of a thermal converter to convert reactive nitrogen oxides to NO followed by detection of NO by its chemiluminescence reaction with an excess of O_3 is recommended.

Reference (among others): Williams et al. (1998)

Note: Conversion of all reactive nitrogen oxides to NO, followed by chemical conversion to NO_2, and then detection by LIF or luminol fluorescence is an option, but involves two conversions for all species except NO_2.

2.2 Recommendations for Monitoring Nitric Oxide (NO)

NO, O_3 chemiluminescence. Detection of NO by its chemiluminescence reaction with an excess of O_3 is recommended.

Note: All point monitors are subject to sampling losses of NO in the inlet lines due to reaction with co-collected ambient O_3 and the walls of the inlet lines. Thus, rapid transit of the lines is desirable. Two seconds or less of residence time in the inlet,

including both the lines and any sample conditioner (e.g., photolysis cell), ensures that NO is reduced no more than 10% before reaching the detector (see Appendix A).

References (among others): Fontijn et al. (1970), Bollinger (1982), Ridley et al. (1988a)

2.3 Recommendations for Monitoring Nitrogen Dioxide (NO_2)

There are at least four successful methods to monitor NO_2 over its ambient concentration range, as noted below. The use of a photolytic converter with NO, O_3 chemiluminescence is probably the most viable at this time, while the use of LIF in its current incarnation is an excellent research tool. The use of DOAS open-path measurements and luminol chemiluminescence is also viable since interferences are generally known and can be accounted for.

Luminol chemiluminescence. Detection of NO_2 by liquid-based luminol chemiluminescence has been used as a simple, sensitive method subject to interferences (PAN, O_3, and HONO) that can be reduced if not eliminated by adjusting the composition of the luminol solution and using chemical scrubbers (see Appendix E). The method is subject to nonlinearity of response at the lower end of the ambient NO_2 concentration range. At low NO_2 concentrations these issues must be addressed if accurate monitoring is to be achieved. GC/luminol detector combinations are used to obtain PAN, MPAN, PPN, and NO_2 over short cycle times (see section 2.6.).

References (among others): Kelly et al. (1990), Maeda et al. (1980), Wendel et al. (1983)

Differential optical absorption spectroscopy. Detection of NO_2 by DOAS (see Appendix B) is direct and does not require sampling; thus, no sampling losses occur. Uncertainties in this measurement are subject to the choice of spectral fitting routine and the ambient environment (mixture of permanent and trace species, some of which may be unknown interferences). It is clear that agreement between DOAS techniques and the point monitoring techniques listed above is possible across the typical monitoring range of NO_2 in ambient air, provided a path of sufficient length is used. The existence of unknown spectral interferences may require post-run analysis of spectra.

Reference (among others): Platt (1994)

Photolytic conversion/chemiluminescence. Detection of NO_2 by photolytic conversion to NO followed by its chemiluminescence reaction with an excess of O_3 achieves monitoring objectives and is known to compare well with LIF and DOAS measurements in field tests (see Appendix D). HONO is a significant interference since it is photolyzed to an extent depending on the exact nature of the spectral bandwidth of radiation being used (37% is photolyzed in one state-of-the-art system [Ryerson et al., 2000]). See Appendix C for a discussion.

References (among others): Ryerson et al. (2000), Gao et al. (1994)

Laser-induced fluorescence. Detection of NO_2 by LIF is now a demonstrated, field-proven monitoring method using a practical, frequency-doubled Nd^{3+}:YAG laser to pump a dye laser and is a direct method for NO_2 monitoring over the entire range of ambient concentration (see Appendix D). As solid-state laser technology advances, tunable diode lasers are expected to replace the dye laser excitation systems, yielding a more compact, lightweight, and technically simplified instrument.

Reference: Thornton et al. (2000)

2.4 Recommendations for Monitoring Nitric and Nitrous Acids (HNO_3 and HONO)

Note: Nitric acid is highly soluble in water and interaction with surfaces has been a problem for sampling into point monitors.

Diffusion scrubber/ion chromatography. This technique involves the capture of HNO_3 and HONO (as well as SO_2 and other acid gases) in water solution followed by separation by ion chromatography and detection of anions. The use of some type of wet-wall gas-phase scrubber to remove HNO_3 and HONO from the sample stream while passing nitrate particles is required.

Reference (among others): Simon and Dasgupta (1995a)

Chemical ionization mass spectrometry. This technique measures nitric acid with more than adequate sensitivity (15 pptv in 1 s) and is the preferable approach aboard aircraft due to its rapid response.

References (among others): Huey et al. (1998), Mauldin et al. (1998), Fehsenfeld et al. (1998)

Chemiluminescence differencing technique. This technique involves two sample streams, each passing through its own sampling channel. One channel includes a nylon filter that retains nitric acid, and both channels have identical thermal converters. The difference in signal is due to HNO_3. Decomposition of ammonium nitrate particles during sampling is a potential problem.

Reference (among others): Tanner et al. (1998)

2.5 Recommendations for Monitoring Particle Nitrate

Collection on filters placed downstream of acid gas denuders followed either by water extraction and ion chromatographic analysis or by thermal desorption and conversion to NO for chemiluminescence detection is recommended.

References (among others): Simon and Dasgupta (1993), Stolzenburg and Hering (2000)

2.6 Recommendations for Monitoring PAN, PPN, and MPAN

The GC/ECD and GC/luminol chemiluminescence methods have the time resolution and sensitivity to make these measurements. One version of the GC/luminol method has been designed to provide NO_2 measurements as well.

References (among others): Roberts et al. (1989), Gaffney et al. (1998)

2.7 Additional Comments

The discussion in Chapter 5 on methods for monitoring the reactive nitrogen oxides provides the rationale for these choices in terms of the interpretation of information obtained from the scientific peer-reviewed references cited in the text and the experimental work performed by those who have contributed to the current effort. The recommended methods have the potential to meet the monitoring objectives to support diagnostic testing of AQMs. However, this has not been done on a routine basis with automated calibration and monitoring such as done for NAAQS monitoring. To use these monitoring methods successfully, quality assurance measures, including calibration, maintenance, and instrument performance checks (e.g., converter efficiency checks, background determinations), are critical and must be performed with extreme care and diligence, especially at the lower end of the ambient concentration range.

The goals of diagnostic testing can best be accomplished by making a complete set of measurements, including speciated volatile organic compounds (VOCs), OH, and HO_2, and process variables such as the photolytic production rates of OH from HCHO, etc. Typically, these measurements are performed by professional scientists in field-intensive studies. These studies bring together instrumentation based on different principles and/or instruments that use different protocols for the measurement of each individual species. Agreement among these methods means additional confidence can often be assigned to critical measurements. This is particularly important at the lower end of the concentration monitoring range where interferences and environmental variables can be relatively more important.

Chapter 3
Recommendations

by

W.A. McClenny, U.S. EPA

The following recommendations address opportunities for improvements in the quality of measurements for reactive nitrogen oxides and are based on the detailed information provided in Chapters 4, 5, and 6.

- Continue support of comprehensive field intensives for building consensus on the best methods for monitoring reactive nitrogen oxides, and for diagnostic testing of models (specifically the modeling of changes in ozone photochemistry as the NO_X SIP Call reductions are implemented and the modeling of regions with significant persistent ozone exceedances).

- Support research and stimulate commercial interest to improve methods for sampling and analyzing reactive nitrogen oxides, which includes the following actions:

  - Identification and testing of a more stable thermal converter configuration by redesign or by identification of a different type of converter.

  - Further development and commercialization of an auxiliary photolytic converter for conversion of NO_2 to NO so that the specificity of NO_2 measurements can be improved over that available with the thermal converters used in the current U.S. installed instrument base of NO, O_3 chemiluminescence monitors.

  - Further development of a cost-effective LIF monitor by redesign as cost-effective component parts become available.

  - Further development of a DOAS open-path system with full access to spectra and spectral fitting routines that will facilitate postprocessing of data.

  - Further development of a near real-time nitric/nitrous acid monitor based on wet denuders and ion chromatography or on an alternate approach.

  - Further evaluation and application of a near real-time monitor for NO_2/PAN measurements based on gas chromatography (GC) coupled to a NO_2-specific detector.

- Investigate interest by NIST in the production of the following:

  - An ultraviolet (UV)/visible spectral database similar to the NIST reference library of infrared (IR) spectra.

  - A NO_2 reference photometer and monitor similar to those used for O_3. Recent research published in the open literature implies this is now possible.

  - Calibration gas standards (e.g., *n*-propyl nitrate) for checking thermal converter efficiency in NO_Y measurements.

Chapter 4
On the Need for Better Ambient Observations of Important Chemical Species for Air Quality Model Evaluation

by

Robin L. Dennis and J.R. Arnold, Atmospheric Modeling Division, NERL, and
Gail S. Tonnesen, CE-CERT, University of California at Riverside

Chapter 4 describes a suite of measurements required to evaluate the predictive accuracy of AQMs, an explanation of why these measurements are needed, and at what concentration levels and accuracy they are needed. This information is of significant value in the information exchange between modelers and monitoring groups and is given here for the nitrogen oxides summarized in this report and also for the entire array of measurements associated with AQMs. The reader interested only in a listing of measurement requirements will find them in section 4.9, "General Requirements of Observations for Diagnostic Model Evaluation," and Tables 4.2 and 4.3.

4.1 Introduction

Air quality is determined by a complex system of coupled chemical and physical processes. These processes include emissions of pollutants and pollutant precursors, chemical reactions, transport, and deposition. For ozone production, this system is nonlinear (Seinfeld and Pandis, 1998). Multiple spatial and temporal scales, multiple gaseous and particulate pollutants, and environmental issues such as acid or nutrient deposition to ecosystems and visibility degradation are involved. The integrated nature defined by these environmental factors and the feedback cycles in them means that tropospheric air quality can best be treated as "one atmosphere" (Dennis, 1998) in which multiple precursors, intermediates, and products interact and react over several scales of time and space.

But even from the integrated one-atmosphere perspective, O_3 is a pollutant of especially high concern because of its key position in the processes and cycles affecting other pollutants and its widespread effects on ecological and human health (National Research Council [NRC], 1991). For reasons explained in Chapter 5, the oxidized nitrogen species collectively referred to as NO_Y are crucial to the process of O_3 and particulate matter (PM) formation and fate. Because characterizing the dynamics of the formation, transport, and fate of tropospheric O_3 conveniently simplifies the more complex interactions among multiple pollutants, tropospheric O_3 is being used to illustrate the utility of high-quality ambient measurements of NO_Y species and other important aspects of the urban and regional troposphere for evaluating numerical photochemical AQMs.

4.2 Air Quality Process Models in Pollutant Management

AQMs represent the chemical and physical dynamics of the polluted troposphere using a set of coupled nonlinear partial differential equations (PDEs) to describe mathematically the mass conservation equation for each chemical species (Russell and Dennis, 2000):

$$\frac{\partial C_i}{\partial t} = -\nabla\left(\overline{U}C_i\right) + \nabla\left(K_e \nabla C_i\right) + P_i - L_i + E_i - R_i + \left.\frac{\partial C_i}{\partial t}\right|_{clouds} \quad (4\text{-}1)$$

for $i = 1,\ldots,N$

where N is the number of chemical species represented in the AQM, C_i is the concentration of species i, U is the wind vector, K_e is the turbulent diffusion coefficient, E_i is the source due to emissions for species i, R_i is the removal term for species i via various processes (e.g., dry and wet deposition), P_i is the chemical production term for species i, L_i is the loss rate of species i via gas-phase chemical reactions, and $(\partial C_i/\partial t)_{clouds}$ is the production and/or loss of species i by cloud or aqueous-phase

chemical processes. The set of PDEs is coupled because P_i and L_i are functions of the species concentration vector (C). Equation 4-1 cannot be solved analytically, but various numerical methods can be used to obtain approximate solutions. AQMs generally use operator splitting to solve each of the terms in Equation 4-1 separately, greatly shortening solution times (McRae et al., 1982) and improving numerical accuracy, to predict the temporal evolution of the species concentration fields. Due to computational constraints, AQMs typically do not save or output the contributions of each of the processes in Equation 4-1 to the change in species concentrations; however, AQMs can be "instrumented" to store this process rate information and make it available for additional postprocessing and analysis. (Instrumentation of the model is described in section 4.5.)

Among the most recent and scientifically advanced AQMs is U.S. EPA's Models-3/Community Multiscale Model for Air Quality (CMAQ) (Byun and Ching, 1999), which has been designed and built specifically to treat problems from a one-atmosphere perspective. CMAQ and other AQMs were developed for the purposes of better understanding tropospheric dynamics and assisting with pollutant management strategies. Both purposes rely on model predictions of future O_3 concentrations ($[O_3]$) that might result from reductions in emissions of nitrogen oxides ($NO_X = NO + NO_2$) and/or VOCs (or HCs, the hydrocarbon subset of VOCs), the two precursors necessary for O_3 buildup in the troposphere.

For each purpose—scientific understanding and pollutant management—the fundamental task of the model is predicting pollutant concentrations for the nonlinear photochemical system of the troposphere. However, to advance our understanding of the photochemical system and to allow us to specify better, more insightful empirical measures of that system as simulated by the model, these predictions must be accompanied by causal explanations of how the model produced them. Explanation is in fact a unique distinction of the numerical process models since there exists no means for explaining observations using only the observations themselves. That is to say, there is no currently available set of measurements that can be used to fully account for how any one observation at one place came about. However, analysis of results from a properly instrumented model can be used to build explanations of the model's predictions and should be done so as to increase confidence in using AQMs as guidance for air quality policy making. Without a proper understanding of the causal mechanisms for the model's predictions available in this analysis of model processes, there is greater risk for error when using AQMs in developing and selecting emissions control strategies. Since it is estimated that the annual cost of compliance with regulations for managing urban and regional O_3 alone in the U.S. exceeds US$1 billion (U.S. EPA, 1997), the cost of bad guidance can be very high.

4.3 Need for Diagnostic Testing In AQM Evaluation

Because of the large economic and social costs of decisions affecting air pollutant control, we wish to avoid potential errors where possible by using scientifically advanced AQMs like CMAQ to provide a realistic simulation of future conditions and an accurate appraisal of the type and amount of emissions control necessary to meet mandated air quality goals. This need to use the models entails adequate testing in an evaluation that

- indicates the validity of the model's scientific formulations,
- assesses the realism of the model's simulations, and
- characterizes the credibility of the model's realism relative to its intended applications.

There remains, however, a difficult problem for providing a meaningful evaluation of the model to guide decision making: how to tell whether the model is producing seemingly appropriate results from incorrect model formulations or bad input data, i.e., how model performance can appear right for the wrong reasons.

Evaluation efforts to date have been largely inadequate for addressing the problems of AQM evaluation for regulatory use or scientific understanding (Russell and Dennis, 2000). This inadequacy derives from a general lack of high-quality ambient measurements in a sufficiently dense spatial and temporal domain and the concomitant tendency to base the model evaluation on tests using simple statistical measures on outcome variable residuals ($Concentration_{predicted} - Concentration_{observed}$) only for O_3 and, less often, for what is typically reported as NO_X. Because O_3 concentrations are a nonunique function of precursor emissions, and because the system contains several nonlinear feedback effects that effectively buffer the $[O_3]$ (i.e., reduce the variability of its response to changes in any one part of the system [see section 4.4]), the realism of model simulations cannot be usefully evaluated using only comparisons of modeled and observed ambient $[O_3]$ data. Such an analysis cannot test whether good fits of the model to observations might be due to compensating errors in the representation of modeled processes; this greatly reduces our confidence in the usefulness of models for providing guidance in air quality management decisions.

Inadequate evaluations have significant consequences for use of the model in that they allow the possibility of finding a model acceptable for an application when in fact it is not. The lack of diagnostic tests for a model and its component modules in most current AQM evaluations has allowed models to be

judged acceptable for several applications when large and significant errors remained. For example, using the U.S. EPA–recommended performance evaluation statistics for [O_3] (U.S. EPA, 1991) of

- ±5 to ±15 % bias,
- ±30 to ±35% gross error, and
- ±15 to ±20% unpaired peak prediction accuracy,

urban applications of the Urban Airshed Model version IV (UAM-IV) (U.S. EPA, 1991) have performed acceptably well even when errors in the meteorological model produced wind speeds of zero in all grid layers above the surface (Tesche and McNally, 1995). In other cases (described in Tesche et al., 1992), data in VOC inventories used to set up a model for application evaluations were later shown to be underestimated by a factor of 2 or more, yet, at the time, model applications were found to be acceptable using these recommended performance statistics.

Moreover, because model evaluation for air quality applications is carried out to assist in control strategy development and selection, a failed model evaluation for applications such as these leaves the potential for undocumented bias in estimating the effect of control strategies. Given an undocumented bias in a model, policy makers could select an incorrect level of future reductions, or even the wrong type of control—NO_X or VOC. This possibility has been demonstrated in two recent studies using two different models to simulate the New York domain for July 1988. A series of sensitivity-uncertainty tests performed with UAM-IV (Sistla et al., 1996) and with the U.S. EPA Regional Acid Deposition Model (RADM) (Li et al., 1998) have shown that emissions and meteorological uncertainties in the model setup affect final predicted [O_3] to the extent that preferences for control strategies can shift. The high risk of getting the wrong control strategy has costly economic and social disbenefits. The analyses of [O_3] time-series plots and residual statistics that have been the mainstays of model performance evaluation cannot by themselves reveal such potential biases in the use of a model. Thus, undiscovered biases present a substantial negative implication for any evaluation procedure that uses only residual statistics and other outcome measures.

It is important to note that the examples described above are failures of evaluation more than of the model: better evaluation procedures, including enhanced diagnostic testing, might have detected any errors or problems in the models and the compensating errors in their setup. Hence it is crucial that AQM predictions be evaluated diagnostically, i.e., in a way that both assesses the model's predictive performance and reveals why the model behaves as it does using explanations at the level of the model's own processes and mechanisms. With diagnostic testing the operation of these physically based process models is rendered more transparent, which may increase confidence in their use (Saltelli and Scott, 1997; Helton and Burmaster, 1996). Diagnostic testing is in situ testing of a model's processes and can be performed either internally with one model or across several models, or, most significantly, in comparisons using specially collected aerometric data that emphasize atmospheric processes (see for example Parrish et al., 1993; Trainer et al., 1993).

The need for diagnostic testing of AQMs has long been recognized. Fox's report from an early model evaluation workshop (Fox, 1984) noted explicitly that improvement in model performance is tied to understanding the scientific basis for model behavior in well-defined physical situations, a point repeated in Seinfeld (1988). More recently, Tesche et al. (1992) and Reynolds et al. (1994) have described the need for "stressful" diagnostic testing in a better, more comprehensive model evaluation methodology. And, Arnold et al. (1998) have proposed a revised methodology for both diagnostic and application evaluations that emphasizes the importance of diagnostic tests and the key role of a conceptual model of atmospheric processes to guide their development and interpretation. However, limitations both in the form of the models (see section 4.5) and in the availability of high-quality data (see section 4.8) have slowed incorporation of diagnostic tests in actual evaluations. Hence, evaluations to date have focused more on failure analysis of module components than on true process diagnostics of the full model.

To carry out in situ diagnostic testing of a model's processes requires first a clear and concise conceptual model of those processes, one that codifies our understanding of the system interactions in basic statements at a very high and generalized level. The statements of the conceptual model declare what we know from theory or experience to be true or must act instrumentally as if it were true; they provide a generalized description of what we understand the important chemical and physical processes and interactions to be. A simplified schematic for one such high-level conceptual model for the system cycling of O_3 is shown in Figure 4-1. Additional details of the conceptual model this diagram represents are given just below.

4.4 System- and Process-Level Descriptions of the Tropospheric Photochemistry of O_3

While the conceptual model illustrated in Figure 4-1 provides a general appraisal of the system cycling, it lacks details necessary to understand the process interactions that constitute it. For that we require the richer description of processes and mechanisms at the level of the photochemical processes themselves. That description follows here.

Experimental work in environmental smog chambers and with early numerical models more than 20 years ago showed that the chemistry of O_3 formation and accumulation is highly nonlinear (Dodge, 1977). That is to say, although changing either NO_X or VOC emissions can alter the production of O_3 ($P(O_3)$), changes in $P(O_3)$ are not monotonic with changes in the emissions of precursors, especially for changes in NO_X. In some circumstances NO_X reductions lead to increases in $P(O_3)$ and ultimately to higher [O_3]. To use an AQM for successfully

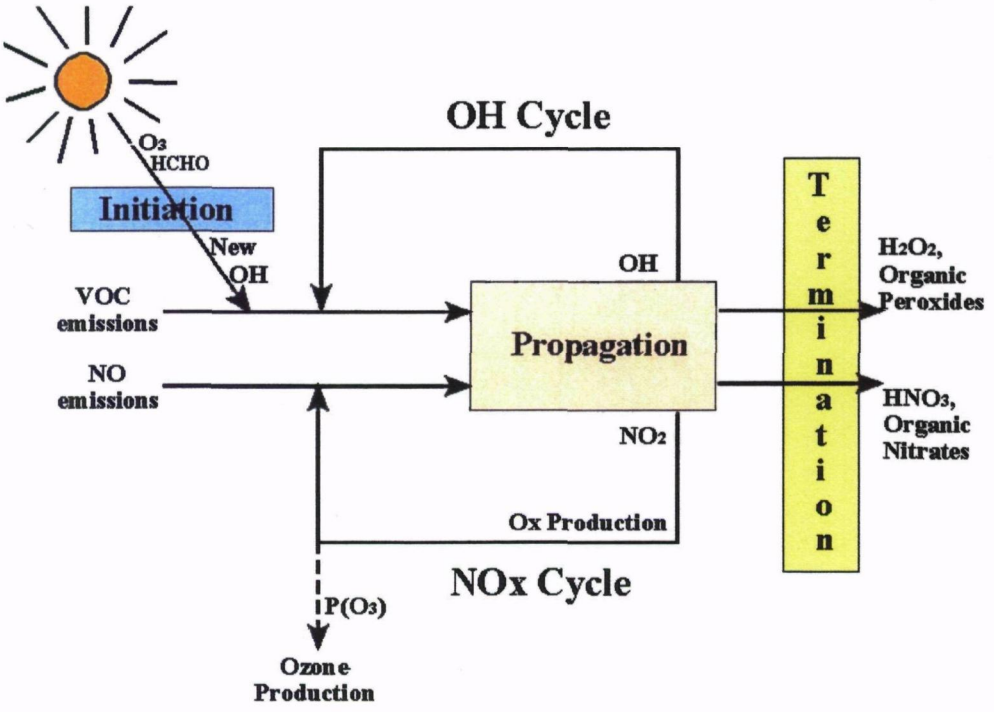

Figure 4-1. High-level conceptual diagram of tropospheric photochemistry showing the major elements of radical initiation, propagation, and termination and the resultant NO and NO_x cycles.

predicting a photochemical system's O_3 response to emissions changes, we must know both the position of that system on its O_3 response surface and the shape of that response surface so that we can successfully predict the system's sensitivity to changed inputs. Figure 4-2 shows the response surface of peak $[O_3]$ to various levels of NO_x and VOC emissions from a simulation for Atlanta, GA, made using a trajectory model. (A description of the model and its setup is found in Tonnesen and Dennis, 2000a.) The isopleth lines of the response surface are derived by fitting contours to the peak predicted $[O_3]$ in multiple model simulations using different NO_x and VOC emissions. Note that many different combinations of NO_x and VOC emissions can produce the same $[O_3]$. This is equivalently showing that solutions to the mass conservation equation (Equation 4-1) governing $P(O_3)$ are nonunique and can be reached through many different combinations of the equation's positive and negative terms. This fact can be seen more easily in the two-dimensional projection shown in Figure 4-3.

The heavy line drawn across the ridges of the surface contour lines is the ridgeline of maximum $[O_3]$ in the simulation and divides the response surface into two domains (A and B). In these two domains, $P(O_3)$ is limited in different ways: Below the ridgeline (domain B), $P(O_3)$ is limited by NO_x availability, and reductions in NO_x decrease $P(O_3)$ while VOC reductions have little influence; above the ridgeline (domain A) radical availability limits $P(O_3)$, and reductions in NO_x can increase $P(O_3)$ while VOC reductions reduce $P(O_3)$. The shape of an O_3 response surface like the one in Figure 4-2 is in fact determined by the nonlinearities in $P(O_3)$, which change over time as the NO_x and VOC levels change throughout the day and from one location to another. The O_3 system response will also be modified by perturbations in the model other than in NO_x and VOC emissions levels, such as by changes in physical parameters of the meteorology driver or in specific details of the chemical mechanism. Uncertainties such as these in a modeling series may in fact alter the spacing and shape of the response surface contour lines, affecting both the change in $[O_3]$ throughout the day and the predicted change in O_3 for changing VOCs and/or NO_x. Consequently, the sensitivity of O_3 to emissions control of these two precursors remains a key variable to the vexing problem of secondary oxidant formation; forecasting that sensitivity is the central problem for regulators seeking successful control strategies for O_3 and is the motivating factor in probing the model at the level of its internal systems and mechanistic processes.

The structure of the O_3 response surface in Figure 4-2 depicts explicitly how $P(O_3)$ in the troposphere varies with VOC and NO_x concentrations. But, in addition to the concentrations of

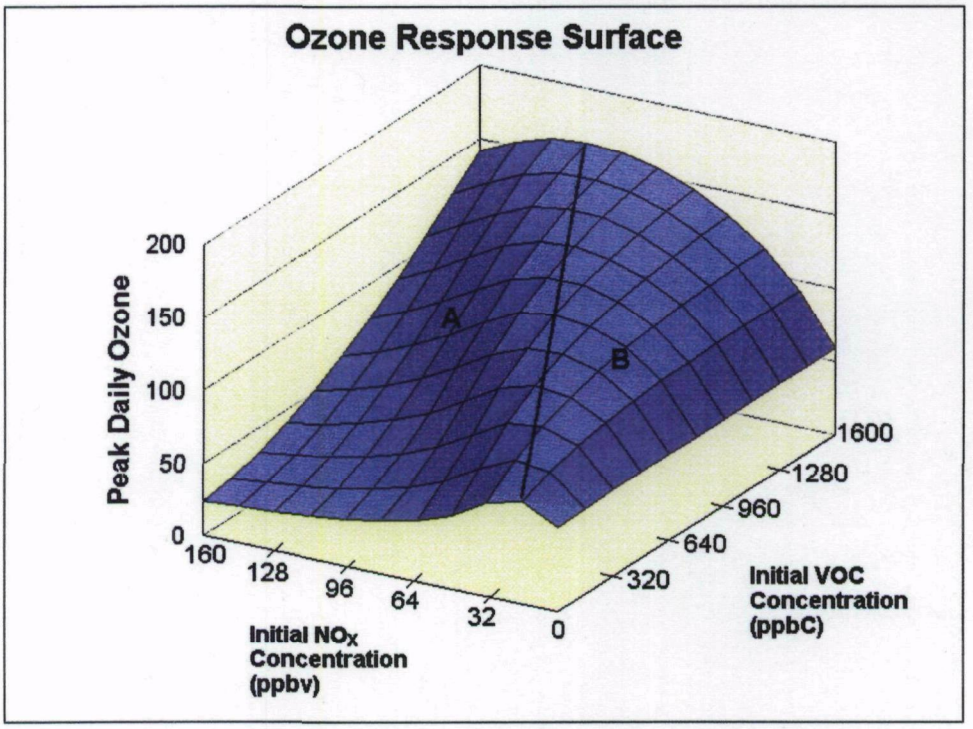

Figure 4-2. Depiction of the nonlinear ozone response surface through plotting daily peak ozone concentrations as predicted by a photochemical box model for a range of initial concentrations of VOCs and NO_X. The heavy line across the top indicates a ridgeline of maximum peak ozone concentrations achieved with the initial concentrations.

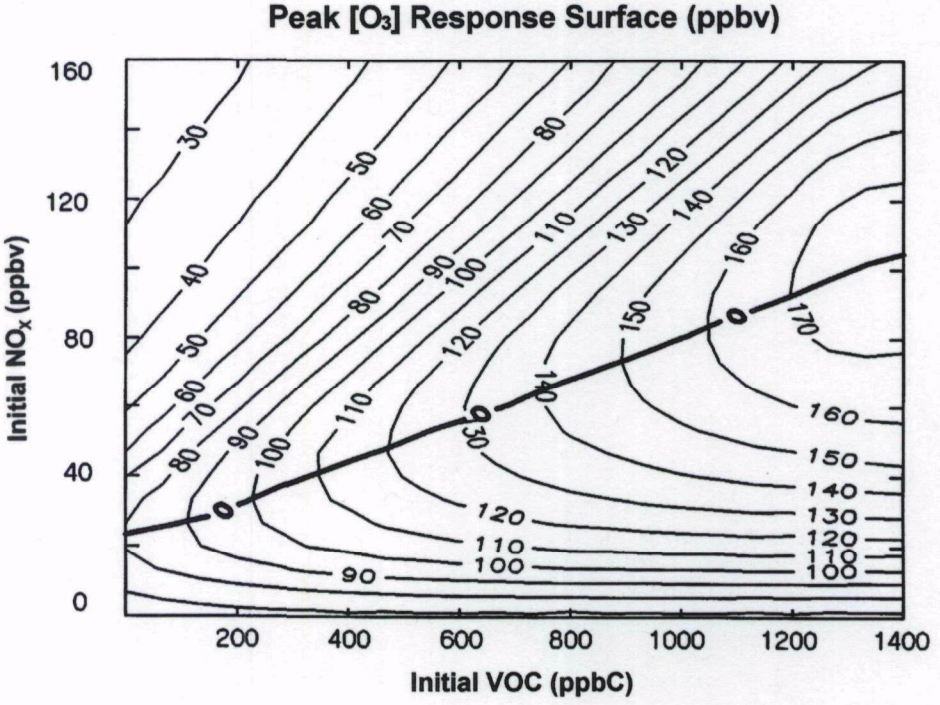

Figure 4-3. Two-dimensional view of Figure 4-2.

these two precursors, $P(O_3)$ is governed by the linked initiation, propagation, and termination of a few important radical species that preferentially attack either VOCs or NO_X as concentrations of all species in the pollutant mix change through time and space. The diagram in Figure 4-4 shows a simplified conceptualization of the relations between the most important radical species and emitted precursors using the most basic HC, CH_4, to illustrate. Here we describe some additional details of that conceptual model in brief system- and process-level overviews of the chemistry of O_3 formation in the troposphere.

$P(O_3)$ is initiated by creation of the hydroxyl radical (OH) through photolysis of O_3 or formaldehyde (HCHO) or HONO as in R1–R5:

$$O_3 + hv \rightarrow O(^1D) + O_2 \quad \text{R1}$$
$$O(^1D) + H_2O \rightarrow 2\ OH \quad \text{R2}$$
$$HCHO + hv \rightarrow CO + 2\ HO_2 \quad \text{R3}$$
$$HO_2 + NO \rightarrow OH + NO_2 \quad \text{R4}$$
$$HONO + hv \rightarrow OH + NO \quad \text{R5}$$

R1–R5 are currently believed to be the major sources of radical initiation; however, there may be other photolysis and decomposition reactions important as radical sources, including photolysis reactions of peroxides and the decomposition reaction of PAN or other unstable intermediate organic species, but there is currently large uncertainty about these.

Once created, the OH radical can react with carbon monoxide (CO) or VOCs to produce peroxy radicals (HO_2 and RO_2) as in R6. At high [NO], peroxy radicals react with NO to split an oxygen-oxygen bond, thereby creating an odd oxygen (O_X) in the form of NO_2, as in R7:

$$OH + VOC + O_2 \rightarrow RO_2 + H_2O \quad \text{R6}$$
$$RO_2 + NO \rightarrow RO + NO_2 \quad \text{R7}$$

The alkoxy radical (RO) produced in R7 can undergo further reactions that re-create the original OH radical:

$$RO + O_2 \rightarrow \text{carbonyl} + HO_2 \quad \text{R8}$$
$$HO_2 + NO \rightarrow OH + NO_2 \quad \text{R4}$$

creating a chain of radical propagation reactions in which a single new OH radical can catalytically mediate the decomposition of several VOC molecules.

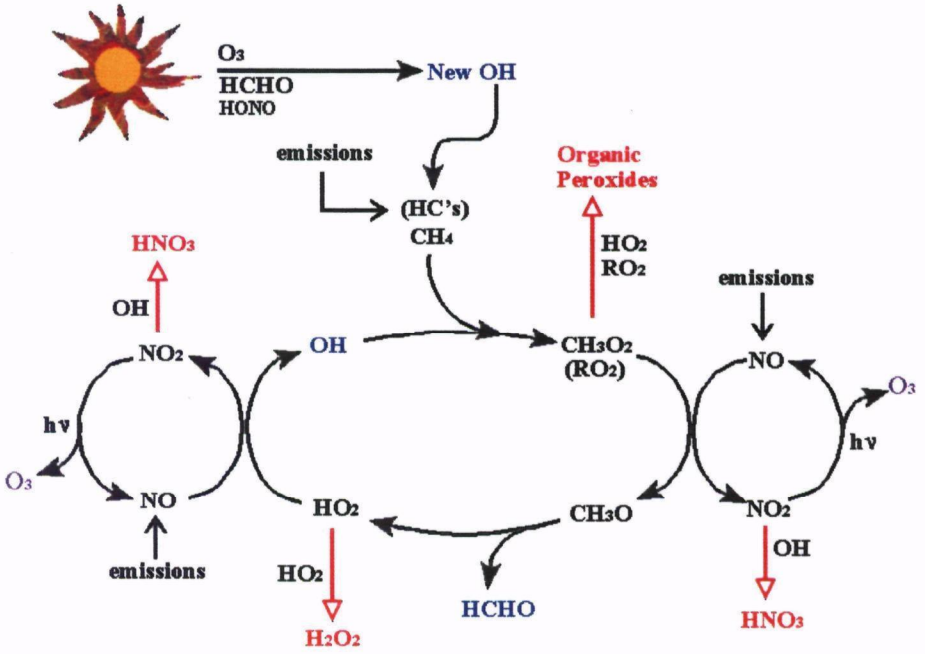

Figure 4-4. Cyclic reaction of methane oxidation (as a surrogate for hydrocarbon oxidation) involving OH and conversion of nitric oxide to nitrogen dioxide, termination to peroxides and nitric acid, and concomitant formation of ozone.

We define O_X as the sum of all species that can act as reservoirs for atomic oxygen, primarily O_3, NO_2, and PAN with minor contributions from some short-lived radical species and HNO_3 and $RONO_2$. In the troposphere, the primary mechanism for production of O_X (and hence O_3) is the oxidation of NO to NO_2 in R4 and R7. A pseudo-photostationary-state (PPS) equilibrium exists between NO_X and O_3 such that at high [NO], in conjunction with radical limitation, the O_X preferentially interconverts to NO_2 through O_3 titration by R9, while at low [NO] the O_X may be converted to O_3 by R10 and R11:

$$O_3 + NO \rightarrow NO_2 + O_2 \quad \text{R9}$$
$$NO_2 + h\nu \rightarrow NO + (O^3P) \quad \text{R10}$$
$$(O^3P) + O_2 \rightarrow O_3 \quad \text{R11}$$

The PPS equilibrium relationship is traditionally written as

$$[O_3] = j_{10}[NO_2]/k_9[NO] \quad (4\text{-}2)$$

where j and k represent photolysis and reaction rate constants, respectively. Equation 4-2 can also be rearranged in terms of [NO] and written as:

$$[NO] = j_{10}[NO_2]/k_9[O_3] \quad (4\text{-}3)$$

Note here that R10 re-creates the original NO, and this re-creation can catalytically mediate multiple conversions of peroxy radicals to O_X.

$P(O_3)$ may proceed by R1–R11 in an autocatalytic cycle until either OH or NO_X is destroyed in termination reactions. Important termination reactions include

$$OH + NO_2 \rightarrow HNO_3 \quad \text{R12}$$
$$RO + NO_2 \rightarrow RONO_2 \quad \text{R13}$$
$$HO_2 + HO_2 \rightarrow H_2O_2 \quad \text{R14}$$
$$HO_2 + RO_2 \rightarrow ROOH \quad \text{R15}$$

but preference for one or another pathway shifts with changing concentrations. At conditions with low VOC/NO_2 ratios, OH radicals preferentially attack NO_2 to produce relatively inert HNO_3 as in R12, and this is the predominant termination reaction for both OH and NO_2 at low VOC/NO_X ratios (Sillman et al., 1990). For systems with high ratios of O_3/NO_2, the PPS equilibrium causes [NO] to decrease, thereby favoring the termination reactions R14 and R15 over the propagation reaction R4.

In this process-level view, the photochemistry of O_3 formation begins with the initiation of new radicals primarily from O_3, HCHO, and HONO. In rural areas, or NO_X-limited areas, the great majority of new OH comes from photolysis of O_3. The subsequent propagation of radicals through the system as RO_2 and HO_2 are formed following OH attack on VOCs, and the re-creation of the OH radical sets up an OH cycle. The OH propagation efficiency (Pr_{OH}) is defined as the average fraction of OH re-created for the cycle of OH reactions. In relation, the OH chain length is defined as the average number of times a new radical cycles through the system until being removed in a termination reaction. The OH chain length can be calculated as

$$\text{OH chain length} = 1 + Pr_{OH} + Pr_{OH}^2 + Pr_{OH}^3 + \ldots = 1/(1 - Pr_{OH}) \quad (4\text{-}4)$$

As Figure 4-1 shows and this process description makes clear, a companion cycle with a similarly defined chain length is set up with the conversion of NO to NO_2 in which NO is re-created or cycled until terminated. Note that the number of molecules potentially processed by this cycling over a period of time can be large when compared to the instantaneous individual species concentrations, i.e., the rates of production and loss control species concentrations.

With this basic understanding, the O_3 ridgeline on the response surface in Figure 4-2 can now be explained in terms of the $VOC\text{-}NO_X\text{-}OH$ cycles. The rate of O_3 production is approximately proportional to the rate of OH attack on VOCs, and this rate is maximized for conditions that maximize the total rate of OH production (P(OH)), which is the product of OH initiation and chain length as in Equations 4-5 and 4-6:

$$P(O_3) \approx k(OH + VOC) \quad (4\text{-}5)$$

$$P(OH) = OH_{initiated} \times 1/(1 - Pr_{OH}) \quad (4\text{-}6)$$

Because of the inverse dependence of P(OH) on $(1 - Pr_{OH})$, $P(O_3)$ will be maximized for conditions that maximize Pr_{OH}, thereby forming the $[O_3]$ ridgeline. This ridgeline separates the response surface into two domains and marks a transition area for the system $[O_3]$ response to changes in NO_X and VOCs. Figure 4-2 shows that as NO_X and VOC levels are changed the photochemical system will change its state and move over this response surface, often crossing the ridgeline into the other domain. This change of state as the system moves over the response surface has important implications for understanding and using an AQM since the photochemical domains above and below the ridgeline are substantially different in important ways.

Systems with a low ratio of VOC/NO_X emissions (domain A in Figure 4-2) are found in the domain above the ridgeline where $P(O_3)$ is limited by the availability of radicals. Under conditions of high $[NO_X]$ in this radical-limited domain, NO_2 reacts with OH and terminates to HNO_3, as in R12, removing both OH and NO_2, which limits $P(O_3)$ by reducing the production of OH. Furthermore, excess NO in this high NO_X region titrates O_3 back to NO_2, as in R9, thereby reducing O_3 photolysis as a source of new OH for additional cycling. For photochemical systems in these radical-limited conditions, the efficiency of $P(O_3)$ per NO_X terminated is low, and $P(O_3)$ is more responsive to reductions in VOCs than in NO_X. In fact, as Figure 4-2 makes clear, reducing NO_X emissions without concomitant VOC reductions for photochemical systems in this domain will cause increases in $[O_3]$.

Conditions below the ridgeline with high VOC/NO_X emissions ratios, however, present a very different case. There, [NO] is relatively low, allowing the peroxy radicals to self-terminate as in R14 and R15. This reduces the number of times OH can be propagated and so lowers the efficiency of $P(O_X)$ per radical. Termination of NO_2 by OH as in R12 is also reduced because the higher VOC/NO_2 ratio causes NO_2 to compete less effectively for the available OH radicals. Hence in these cases, although the efficiency of $P(O_3)$ per NO_X terminated is high, less NO_X is available for reaction, resulting in lower $P(O_3)$ and a lower final $[O_3]$. In contrast to the radical-limited domain above the ridgeline, in this NO_X-limited domain $P(O_3)$ is more responsive to reductions in emissions of NO_X than of VOCs. However, although VOC emission reductions are less effective in reducing $[O_3]$ for photochemical systems in this domain of the response surface, in no case will reductions in either precursor increase $[O_3]$.

4.5 Instrumenting AQMs for Diagnostic Testing

Although the process details described just above inform the structure of the numerical model and are the explicit system pathway components that should be tested diagnostically, they are generally not available in standard AQM output owing to computational processing and storage limits. Therefore, it is necessary to instrument the model code in such a way that these process details are made available for diagnostic testing and analysis. Opening up the system processes by instrumenting the model and then using ambient data to evaluate the accuracy of the model-simulated component processes is useful because it helps identify whether the predictions may have been produced through compensating errors or other unacceptable anomalies in the model. In this way, the model's explanatory power is greatly increased, its predictions are more conclusively confirmed, and confidence in the evaluation is better justified.

The calculated concentrations typically retained at the end of each process step in an AQM simulation run represent only the net effect of the coupled processes; no attempt is made to determine the separate contributions of individual component processes to the final predicted result. But, the model can be instrumented by modifying source code to output the contribution from each process and making that available with the species concentrations already saved by the model, thereby making explicit the model's internal component rates. On a finer mechanistic scale, individual processes such as the nonlinear coupled photochemistry may also be instrumented separately in order to learn more precisely the effects of this chemistry on model predictions. We have applied the techniques of Jeffries and coworkers (Jeffries and Tonnesen, 1994; Tonnesen and Jeffries, 1994) to several AQMs developed at U.S. EPA including RADM and CMAQ. Additional details and results of model testing with the instrumented RADM can be found in Dennis et al. (2000). Information specific to instrumenting CMAQ can be found in Gipson (1999); evaluation of the instrumented CMAQ with these process analysis techniques is currently under way.

4.6 A Taxonomy of Diagnostic Tests for Tropospheric Photochemistry

Developing diagnostic or process-oriented measures for understanding model behavior brings together elements and relations of our conceptual mental model with the explicit representation of them in the instrumented numerical model. The purpose here is to devise and assess system-level and process-oriented probes of both the numerical model and the physical environment it represents using in situ tests with measures that can be made in either or, preferably, both systems. We have developed these measures with process-oriented studies using theoretical assumptions, model-derived explanations, and results from instrumented models that can range from 1-D box models to the full 3-D photochemical modeling system; we note that such studies must always include the complete 3-D model so that results are not distorted by the incomplete representations of the more limited models.

A three-level taxonomy of diagnostic measures can usefully be constructed using the terms and relations presented in the schematic diagram of O_3 formation and accumulation depicted in Figure 4-1 and described more fully in Table 4-1.

The first level of the taxonomy holds the individual components of the photochemical process relations, including initiation of new radicals from O_3 and HCHO and HONO and termination of radical cycling as either peroxy radicals self-combine and/or OH and NO_2 are converted to oxidized nitrogen products that no longer react on time scales relevant for the urban and near-regional settings (NO_Z). NO_Z is often represented as the quantity ($NO_Y - NO_X$). The most important species of NO_Z to define individually are particulate NO_3, HNO_3, PAN(s), and $RONO_2$(s).

The second level of the taxonomy holds the photochemical process groupings, including the propagation of radicals through the system as HO_2 radicals are formed and convert NO to NO_2, and the related concepts of Pr_{OH} and chain length. Recall from section 4.4 that Pr_{OH} is the average fraction of OH recreated for each OH radical entering the photochemical cycle and is always less than 1 because termination reactions will remove some fraction of radicals as well. Recall also from reactions R1–R11 that the cycle of OH radicals through attack on HCs and production of HO_2 is closely bound to the conversion of NO to NO_2 such that excess availability of one species, NO, ensures OH propagation, and excess availability of the other, NO_2, leads to OH termination. Linking these two cycles together, Pr_{OH} is approximated by the product of the two halves of these connected cycles that together propagate the OH. This relation can be represented as

$$Pr_{OH} \approx f_{OH+HC} \times f_{HO2+NO} \qquad (4\text{-}7)$$

Owing to the PPS obtained between OH and VOCs and NO_X, the two propagation terms have an opposite dependence on $[NO_X]$: $[NO_X]$ increases the fraction of HO_2 being re-created as OH increases, but the fraction of OH terminating with NO_2 also increases; thus, the fraction of OH attacking HCs to create HO_2 must decrease. The net result of the interrelation of these cycles is that Pr_{OH} is maximized for some intermediate level of NO_X that maximizes the product of these two terms. In so doing, it maximizes the production rate of O_3 and creates the $[O_3]$ ridgeline.

The third level of taxonomy holds elements for understanding the integrated response of the system such as that represented on the O_3 response surface shown in Figure 4-2 and discussed in section 4.4.

The taxonomy is summarized in Table 4-1. Additional description for understanding and using these measures as tests of the model is given in section 4.7.

Table 4-1. Taxonomy of Photochemical Diagnostic Elements

Individual Component Aspects	Radical initiation
	Radical termination
	Competition between termination pathways
	Air mass aging
Process Aspects	OH production
	Radical propagation
	Radical propagation efficiency, Pr(OH)
	OH chain length
	NO_X chain length
	$P(O_3)$ efficiency per NO_X termination
Response Surface Aspects	System state relative to ridgeline
	Location of ridgeline in response space
	Slope of radical-limited response surface
	Slope of NO_X-limited response surface

4.7 Diagnostic Model Evaluation Tests

We have proposed (Arnold et al., 1998) and are using (Tonnesen and Dennis, 2000a and 2000b) two types of diagnostic tests for evaluating and understanding the behavior of the chemical mechanisms in AQMs:

- Process diagnostics that relate to the first two levels of the diagnostic measures taxonomy
- Response surface diagnostics for interpreting the integrated response of the model at the third level of the taxonomy

To date we have applied these tests mostly in the model since process-oriented measurements in the atmosphere are difficult to make and so are very sparse in space and time. However, we strongly desire ambient measurements to compare the model against; hence, we provide here a discussion of the important measurements we would require to evaluate the model using the diagnostic tests we have developed and preliminarily explored. This discussion follows the order and groupings of the model process taxonomy introduced just above but uses the additional distinction of local photochemistry and cumulative photochemistry over the history of an air mass.

Process diagnostics in the more restricted sense we intend from this point are specific tests of key pathways and interactions in the AQM's chemical mechanism. They assess the model's ability to represent actual atmospheric interactions by examining pathways and processes in the model, often using special measurements designed to indicate the activity of such processes in the atmosphere (see, for example, Parrish et al., 1993; Trainer et al., 1993).

The first taxonomic level defines a small number of key photochemical relations that can usefully be summarized as initiation and termination of radicals. Tests can be identified that, in various combinations, would allow examination of the process steps that make up the initiation and termination of radicals in the system. Examples of such tests and how they illuminate model processes include the following:

- Radical initiation pathways using comparisons for $[O_3]$, [HCHO], [HONO], [peroxides], $j(NO_2)$, $j(O_3)$, and other spectral irradiance measures. Total radical initiation in the system is the sum of individual contributions from each of the initiating species.
- Radical termination pathways using comparisons of $[HNO_3]$, [PAN], $[RONO_2]$, and [ROOH]. Total system radical termination is the concentration sum of the species terminated that involve either NO_X (i.e., $NO_Z = NO_Y - NO_X$, or an approximation of NO_Z using NO_3, HNO_3, PAN(s), and $RONO_2$) or peroxides (i.e., species comprising ROOH and H_2O_2).
- The balance between radical initiation and termination.
- Competition among radical termination pathways by comparing production of HNO_3 and $RONO_2$ to that of H_2O_2 and ROOH.
- Speciation of NO_Z to compare competition among NO_Z termination pathways.
- Speciation and relative fractions of NO_X vs. NO_Y, and PAN and total NO_3 vs. NO_Y to delineate pathways of NO_X processing in the history of an aging air mass.

Key concepts in the second taxonomic level of process groupings are Pr_{OH}, OH chain length, and NO_X chain length. Combinations of ambient observations can be defined that allow testing of these process groups; however, describing these tests requires some additional explanation using details we have learned using the instrumented model.

Recall from Equation 4-7 that $Pr_{OH} \approx f_{OH+HC} \times f_{HO2+NO}$. Using the conceptual model, in situ diagnostic measures can be derived for these two fractions. This is done by listing all chemical reactions involving the relevant species and dropping any minor terms, resulting in two explicit expressions to approximate the two fractions:

$$I(NO, t\text{-}RO_2) = \frac{k_{HO2+NO} * [NO]}{k_{HO2+NO} * [NO] + k_{RO2-HO2} * [RO_2 + HO_2] + k_{HO2-O3} * [O_3]} \quad (4\text{-}8)$$

$$I(HC, NO_2) = \frac{\sum k_{OH-HC_i} * [HC_i]}{\sum k_{OH-HC_i} * [HC_i] + k_{OH-NO2} * [NO_2]} \quad (4\text{-}9)$$

where I(NO, t-RO_2) approximates f_{HO2+NO} and I(HC, NO_2) approximates f_{OH+HC}. In Equations 4-8 and 4-9, then, we have a list of species and rates with which we can approximate Pr_{OH}, and, because of the relation given in Equation 4-5, the OH chain length as well. While not all species and rates in these two expressions can currently be measured, with just a few more high-quality observations of the radicals and NO_2, for example, together with some basic assumptions to cover terms not currently measured, it should be possible in a small number of places to begin using this important diagnostic evaluation tool.

The analogous situation for NO_X is not as straightforward. Although the NO_X chain length can be approximated by examining the day-by-day association between O_3 and the NO_X termination products NO_3, HNO_3, PAN(s), and $RONO_2$ for midday temporal stratifications, this approximation is always attenuated by unaccounted deposition loss processes. Hence, we still desire a better test for this important process group.

We note that some process diagnostic tests from these two taxonomic levels will involve comparisons that reflect both local photochemistry and photochemistry over the history of an air mass. However, local photochemistry and the history of an air mass should be carefully distinguished, and it will be necessary to develop diagnostic measures to evaluate model treatment of each. For example, O_3 production rates and OH chain length might be estimated for instantaneous local photochemistry using measured [RO_2], [NO], [NO_2], and [VOC], while cumulative $P(O_3)$ and average NO_X chain length over an air mass history can be approximated using [O_3] and the ratio [O_3]/[NO_Z]. Additionally, the two expressions in Equations 4-8 and 4-9 are among the process diagnostics and species ratios useful for characterizing the radical budgets for local photochemistry, for example, while radical budgets for air mass history might be characterized with these diagnostic tests:

- [O_3]/(2*[ROOH]+2*[H_2O_2]+[NO_Z])
  the slope of which over several days' measurements approximates average OH chain length for an aged air mass

- 2*[ROOH]+2*[H_2O_2]+[NO_Z]
  which describes the major radical termination pathways in an aged air mass

- 2*[ROOH]+2*[H_2O_2] vs. [NO_Z]
  which compares competing radical termination pathways in an aged air mass

Furthermore, ratios of species can be calculated in the model for comparisons at the surface and aloft to provide additional diagnostic information on a model's process treatment of intermediate and product species in an aged air mass. For example, chemical dynamics measures calculated using partitioned NO_X and NO_Y species for aloft and surface concentrations could provide useful information about air mass aging pathways since the species aloft would be more susceptible to transport and dispersion effects and less susceptible to dry deposition effects, and the chemistry can proceed further to completion there. Also, RO_2-RO_2 reactions should be tested in the surface layer of urban areas, where the reaction has little significance, and again aloft at low [NO_X], where the reaction is significant for [O_3] and [H_2O_2].

Other process diagnostic tests for characterizing air mass aging would use CO data with other ratios of species having varying lifetimes to derive additional model-estimated chemical budgets and processing rates. These comparisons would serve as an aid to interpreting results from specific outcome variable testing of the chemical mechanism, helping to separate the influence of chemistry from other physical model processes.

The diagnostic tests from the third taxonomic level, the response surface diagnostics, test a model's ability to track systemic modulation and generally involve use of indicator species and ratios of species thought to correlate consistently with VOC- and NO_X-sensitive $P(O_3)$ in the model. Measures developed for the propagation efficiencies from Equations 4-8 and 4-9 can be adapted to examine the O_3 response surface. Hence, with I(NO, t-RO_2) and I(HC, NO_2) we now have two explicit gauges of a photochemical system's position on the O_3 response surface and, consequently, its relative distance from the [O_3] ridgeline. These measures of the sensitivity of O_3 to NO_X and VOC changes are characteristics of specific photochemical systems in that each system may have particular combinations of NO_X and VOCs that determine its position on the O_3 response surface. However, we have observed in the model that individual systems exhibit a strong diurnal behavior, too, moving from strongly radical limited in the morning to the transition state near the O_3 ridgeline and on into the NO_X-limited domain of the response surface late in the day. Tracking this air mass history with cumulative diag-

nostics is important for understanding the model's behavior relative to its chief intended use of prediction for control strategy development and assessment. This is because, as described in section 4.4, the position of a system in one or the other domains of the response surface determines whether VOC or NO_X controls are to be preferred.

Several indicators of a system's O_3 sensitivity to changing precursor levels have been proposed and are currently under development and active testing in several models (Tonnesen and Dennis, 2000a and 2000b; Sillman, 1995; Chang et al., 1997; Kleinman, 1994), and many appear promising as diagnostic tests for model evaluations. The motivation in developing these indicators is the need to have a robust value that tells whether the model correctly simulates the real-world sensitivity of O_3 to changing precursor emissions. Some examples include $[O_3]/[HNO_3]$, $[O_3]/[NO_X]$, and $[O_3]/[NO_Z]$, which show strong correlations to O_3 sensitivity, correctly predicting conditions either strongly NO_X or strongly radical limited (Tonnesen and Dennis, 2000b). Because these indicator tests bear directly on the chief policy use of the models, it is important to evaluate their significance in the model against values calculated from ambient observations for a wide area across the modeled domain. We hasten to add, though, that indicator values calculated from ambient observations will not replace numerical process models because observation values cannot reveal the overall effectiveness of a control strategy nor even whether a particular control strategy might lead to attainment of an air quality standard as the model can. But, the indicators are uniquely helpful for diagnosing the capability of the models for this important policy goal.

4.8 Priority and Utility of Observations Needed for Diagnostic Testing

Our work with diagnostic tests in the model suggests that there can be no single definitive test constructed from any elements on any level of the taxonomy. Rather, to be useful for understanding the behavior of the system, diagnostic tests will need to probe as many different aspects of the physical and modeled systems as can be done with available analytical technology. Wherever possible, more than one way of testing a particular element or process of either system will be preferred. All possible measures, and hence all species contained in them, will be needed to develop a distortion-free picture of the true behavior of the model. Although we have presented species priorities derived from our taxonomy of diagnostic elements, in the end we would require that all of the species in the diagnostic tests described in section 4.7 be measured simultaneously at a single surface site or aloft in an aircraft and with a response time significantly less than 1 h, perhaps even approaching the 1- to 5-min range in order to evaluate AQMs diagnostically.

Generating a reduced, ordered list of ambient species from the large list of species ultimately needed for testing models is made difficult by the tight interconnections of processes and feedbacks in the troposphere. This means that it very often appears that modelers are asking for all species to be measured everywhere at all times. The taxonomy presented in section 4.6 is our attempt to dispel this appearance and offer a priority ordering of species ranked according to their utility for process comparisons and response surface diagnostic testing, both local and cumulative. In this section, we list the species we would require for making the diagnostic tests described in section 4.7 and show more specifically how ambient observations of them fit together in diagnostic tests of the model.

Recall from section 4.2 that the key policy use of the model is its prediction of O_3 sensitivity to NO_X or VOC control for attainment or maintenance of an air quality standard. Likewise, recall from sections 4.1 and 4.4 the impossibility of making only a single change in the tightly linked one-atmosphere concept that characterizes the troposphere and that any single concentration such as $[O_3]$ is a nonunique solution to the mass conservation equation (Equation 4-1), i.e., that any $[O_3]$ can have been produced through very many different combinations of NO_X and VOCs. Taken together, these suggest that we must understand both the processes of O_3 production and accumulation that lie behind the final predicted O_3 concentration and the potential for changing production and accumulation with changing NO_X and VOCs if the model's predictions are to be used with confidence.

Hence, it is somewhat disturbing to note that previous model evaluations (summarized in Russell and Dennis, 2000) have documented several problems that appear to be common to many AQMs such as generally underpredicted NO_X values and overly fast NO_X aging to NO_Z that may be pointing to systematic errors in model processing pathways or rates, which in turn may be producing a bias in the model-predicted preference for VOC or NO_X controls. Without better diagnostic tests of the model we are currently uncertain whether the errors would best be ascribed

- to wrong emissions setups from bad or incorrectly interpolated data,
- to inaccurate meteorology, both clouds as reactors and as engines of transport and considerations of incorrect actinic flux, or
- to the chemistry, possibly maladjusted through inappropriate tuning exercises of the chemical mechanism and/or larger model to fit specific observed $[O_3]$.

The diagnostic testing program we present here is one attempt to narrow this uncertainty by examining process issues in the chemistry associated with model-predicted preferences for VOC or NO_X control. And the key to these process issues is understanding the linked OH and NO_X reaction cycles as diagrammed and described above, both for local instantaneous photochemistry and cumulative chemistry as the air mass ages. For this reason, the diagnostic tests described here are focused on

understanding O_3 production and the production of O_X, which determines $P(O_3)$ as a means for explaining O_3 accumulation and the model's final predicted $[O_3]$.

Recall from section 4.4 that O_3 is but one component of O_X and that $P(O_X)$ can be defined as the rate of reaction of HO_2 and RO_2 with NO, minus small losses:

$$P(O_X) = k(HO_2 + RO_2)NO - \text{losses} \quad (4\text{-}10)$$

or

$$P(O_x) \approx P(OH) \times f_{OH-HC} = \frac{OH_{initiated} \times f_{OH-HC}}{(1 - Pr_{OH})} \quad (4\text{-}11)$$

$P(O_X)$ can further be defined as $P(O_3)$ plus the rate at which NO is oxidized to other forms of NO_Y, or equivalently, $P(O_3)$ as the rate of O_X production remaining after NO has been oxidized.

Thus, our first-priority desired observations are the species concentrations and reaction rates required to populate the terms in these expressions and thereby provide a means for diagnostic testing of $P(O_3)$ in the model and the atmosphere. Those priority observations are

- accurate actinic flux measurements for O_3, NO_2, and HCHO;
- accurate concentrations for O_3, H_2O, HCHO, and HONO;
- accurate concentrations for NO, NO_2, PAN(s), HNO_3, $RONO_2$ and total NO_3, and NO_Y (where total NO_3 = nitric acid + particulate nitrate);
- accurate concentrations for CO and speciated VOCs;
- accurate concentrations for H_2O_2 and total peroxides; and
- accurate concentrations for HO_2 and RO_2 (may be together with OH).

With this set of measurements we could approximate local $P(O_X)$ using $[HO_2]$, $[RO_2]$, and [NO] as in Equation 4-10. We could also approximate local OH chain length using the combination of concentration measures and rates defined in Equation 4-7, although these may be more difficult to make.

Cumulative diagnostics of the history of an air mass at a site suitably downwind from the urban core are somewhat more easily approximated with concentration observations than are local ones. For example, we can estimate cumulative radical initiation and termination with 2*[peroxides]+$[NO_Z]$ and with the ratio [peroxides]/$[NO_Z]$. The cumulative OH chain length at a downwind site can be approximated with the slope of the ratio $[O_3]$/(2*[peroxides]+$[NO_Z]$) calculated for several days at the site, while the concentration sum of HNO_3, $RONO_2$, total NO_3, and the PAN(s) would approximate a measure of NO_X termination over the air mass history and the sum of $[O_3]$, $[NO_2]$, and $[NO_Z]$ would serve as a measure of cumulative $P(O_X)$. In addition, using the first-priority observations we could calculate ambient values for some of the indicators of O_3 sensitivity to emissions reductions as described above, including the ratios $[O_3]/[NO_X]$ and $[HCHO]/[NO_2]$.

We recognize that this first set of desired observations is quite large, but reiterate that multiple measures are required because there are significant concerns regarding the usefulness of any particular diagnostic test. For example, there can be large uncertainties in the cumulative diagnostics due to the complexity of the chemistry and other heterogeneous effects. The diagnostic 2*[peroxides]+$[NO_Z]$ does not provide a reliable measure of cumulative radical termination because NO_Z can be produced by heterogeneous reactions that do not involve radical termination (Dentener and Crutzen, 1993) and because both peroxides and NO_Z can be removed from the system by deposition and cloud processes.

Thus, many diagnostic tests are required to perform a comprehensive model evaluation, and we would note that most of the observations listed here are useful in more than one test, making them very efficient for model evaluation.

In addition, though, a second set of measures, lower in priority than the first, would provide still more information useful for testing models and moves down in specificity from the rather more aggregate measures given in the first-priority set. This second set includes

- actinic flux measurements for HONO and H_2O_2,
- OH,
- NO_3 radical,
- speciated $RONO_2$,
- methacrolein and methylvinylketone,
- speciated RCHO, and
- aerosol mass and size distribution,

which will be useful in directed tests of intermediate chemical products and in fleshing out our understanding of their processing.

4.9 General Requirements of Observations for Diagnostic Model Evaluation

One distinguishing characteristic of the diagnostic tests is that they involve combinations of multiple variables, either outcome variable concentrations or process variables like reaction rates. Although potential indicators and gauges in new and different combinations are still being developed, the absolute number of species involved in all possible measures has now plateaued, but additional speciation within classes is still desired.

As a consequence, the number of species and process variables needed to test the models diagnostically is approaching completion, or, at the least, all general categories of measures we might desire have been identified. But there remain, in fact, no measurements of process rates in the atmosphere, a key variable type for many potential tests of the model. We leave aside further discussion of this topic, but note that, given our understanding of the chemistry presented in sections 4.4 and 4.7, it appears to be an area that would repay continued work by modelers and measurement developers. Even without addressing the problem of process measures, though, the list of measurements required for structured and complete diagnostic model testing we gave just above is a daunting one. Thus, here we consider the questions of which diagnostic observations can be made at present and what precision and accuracy we require to use them in tests against the model.

In recent years new, state-of-the-science research instrumentation has been developed and put into production in field campaigns that is capable of making ambient observations of many of the key species and variables needed to construct the diagnostic tests described in section 4.7. This represents a significant advance on the part of the analytical community since these observations are made over very short time scales and often at very, very small concentrations. Here we have reordered the list of species we desire for model evaluation according to the current or near-future viability of making the ambient observations of them:

- Species or variables easily measured accurately: O_3, NO, CO, HCHO, and PAN
- Species or variables measured accurately, but with difficulty: NO_2, NO_3, HNO_3, NO_Y, other PAN(s), H_2O_2, HONO, peroxides, some alkyl nitrates, $j(O_3)$, and $j(NO_2)$
- Species for which analytical techniques are being developed and tested and are moving slowly into more general use, if not production: OH, HO_2, total RO_2, speciated RO_2, and NO_3 radical
- Missing classes:
  - Alkyl nitrates from biogenic hydrocarbons
  - Oxygenated hydrocarbons
  - Process rates

We note that observations of only some of the species in the first rank are routinely made in current ambient networks, and it would be our desire to see observations of HCHO and the PAN(s) more routinely made. We are encouraged, given the large list of species required for diagnostic testing, that a significant number of key species are close to being made more routinely both at the surface and aloft.

The specificity of these ambient measures is also crucial for using them successfully as diagnostic tests of the model. Distinguishing individual NO_Y species provides a good example, as can be seen from the number of individual NO_Y species in the lists given above. There is concern that observations reported as NO_2 from the installed ambient networks using chemiluminescence NO_X boxes are contaminated by unknown amounts of other NO_Y species due to the nonspecificity of the chemiluminescence reaction and the setup of the monitor. This presents a problem for using these NO_2 values in both process and response surface diagnostic tests since several of the ratios are designed to indicate the separate contributions of NO_Y species and is a special problem since NO_2 is a key species in the transformation of O_X through the VOC-NO_X-OH chains. Thus, only with more precise NO_2 observations will we be able to test the model's process representation of the OH reaction cycle through the various forms of NO_Y, to provide better estimates of air mass aging (i.e., the extent to which NO_X has been converted to NO_Z), and to better estimate the efficiency of $P(O_3)$ for each NO_Z. For these tests we also need to directly measure the key constituents of NO_Z. Accurate and precise NO_2 measures are also required for meaningful tests of the proposed indicators of O_3 sensitivity to emissions changes since NO_2 appears in the denominators of several of the ratios including $O_3/(NO + NO_2)$, $HCHO/NO_2$, and the OH rate-constant-weighted ratio of VOCs to NO_2.

For comparisons relating to the efficiency of $P(O_3)$, the currently feasible test is to compare the association between O_3 and NO_X termination products for midday conditions as defined by the slope on a scatterplot of O_3 versus NO_Z. We need to be able to reliably distinguish differences in slopes of O_3 versus NO_Z. If slopes differ by 25% or more we will be concerned. Hence, we want to be able to distinguish reliably differences on the order of ±20%. At regional sites for a given value of daytime O_3, a range of 3 ppbv in hourly NO_Z with an overall mean NO_Z of 6 ppbv is not uncommon. We can obtain an estimate of how well we need to know NO_Z if we assume O_3 is measured very well, within 1 ppbv, and characterize observations for regional sites. We also assume that three-quarters of the observed NO_Z range represents irreduceable nonmeasurement error and that the observations are independent. Then, for a modest number of observations, to have a chance at distinguishing slope differences greater than 20%, we need the combined measurement error in determining NO_Z to be between ±15% and ±20%.

The species whose concentrations need to be quantified in situ to calculate the $I(NO,RO_2)$ and $I(HC,NO_2)$ indicators are, by and large, not easy to measure in the field. In fact, some of the methods are still under development. Thus, it is useful to quantify to the fullest extent possible from our modeling studies what we expect will be required of the measurement methods to enable us to calculate ambient values of these indicators with sufficient accuracy to resolve ridgeline conditions. For $I(NO,RO_2)$, we require measurement techniques for total $RO_2 + HO_2$, NO, and O_3 concentrations. Accurate methods are readily available for NO

and O_3, and experimental methods are being developed for HO_2 and RO_2. Conditions that are near the $P(O_X)$ ridgeline typically have [NO] levels of about 1 ppbv and total $[RO_2]$ of 10 to 40 pptv, so a lower detectable limit of 10 pptv and accuracy of ±10 pptv for the total $[RO_2]$ method would be required to distinguish the ridgeline conditions.

For $I(HC,NO_2)$, we require measurement techniques for a subset of the total HC mixture and for NO_2. In our analysis using model simulations, we are able to calculate $I(HC,NO_2)$ using concentrations of CO, CH_4, alkanes, alkenes, aromatics, and isoprene. A sufficient number of these hydrocarbon species are routinely measured at Photochemical Assessment Monitoring Stations (PAMS) sites (U.S. EPA, 1994) and can be easily measured in field studies; however, CO and CH_4 are not part of the PAMS suite of measurements. Methods for NO_2 need to provide a true measurement of NO_2 without interferences, and while these methods are not yet routinely available, NO_2 has been measured both directly and indirectly (see Chapter 5). In our model simulations, NO_2 levels for ridgeline conditions typically range from 1 ppbv in rural areas influenced by anthropogenic NO_X sources to more than 10 ppbv in urban areas. For a relatively low NO_X urban cell, an uncertainty of 10% in the $[NO_2]$ measurement would cause the estimate of $I(HC,NO_2)$ to range from 70% to 74%. For a high-NO_X urban cell, an uncertainty of 10% in the $[NO_2]$ would cause $I(HC,NO_2)$ to range from 90% to 92%, so ±10% accuracy $[NO_2]$ measurements would be adequate to calculate values of $I(HC,NO_2)$ that could distinguish NO_X- and VOC-sensitive conditions.

4.10 Summary

The process diagnostic tests we propose for the taxonomic levels reflecting both local photochemistry and the history of an air mass are summarized in Table 4-2. The priority observations and species concentration measurements are summarized in Table 4-3.

Table 4-2. Summary of Diagnostic Tests

Local Photochemistry Tests	
O_X production, $P(O_X)$	$P(OH) \times f_{OH+HC}$
O_3 production, $P(O_3)$	$\{ P(OH) \times f_{OH+HC} \} - P(NO_Z)$
OH chain length	$1/(1 - Pr_{OH})$
OH production, P(OH)	$OH_{initiated} \times \{ 1/(1 - Pr_{OH}) \}$
OH propagation, Pr_{OH}	$f_{OH+HC} \times f_{HO2+NO}$
Radical initiation	$OH_{initiated}$
Radical termination	$P(NO_Z)$ + P(peroxides)
O_3 ridgeline indicators (NO_X vs. VOC preference)	f_{OH+HC} f_{HO2+NO} $[O_3] / [NO_X]$
Measure of: f_{OH+HC}	$I(HC, NO_2)$
Measure of: f_{HO2+NO}	$I(NO, t\text{-}RO_2)$

Table 4-2. Continued

Air Mass History Resultant Photochemistry Tests	
Cumulative O_X production	Cumulative daily $[O_3] + [NO_2] + [NO_Z]$
Cumulative O_3 production	Cumulative daily $[O_3]$
Indicative OH chain length	Multiday slope of cumulative $[O_3]/\{2*[\text{total peroxides}] + [NO_Z]\}$
Radical termination—NO_X pathway	$[NO_Z]$ or $\{[NO_Y] - [NO_X]\}$ or $\{[HNO_3] + \text{partic.}[NO_3^-] + PAN(s) + RONO_2(s)\}$
Radical termination—peroxide pathway	$2*\{[ROOH] + [H_2O_2]\} = 2*[\text{total peroxides}]$
Indicative NO_X chain length	Multiday slope of daytime O_3 vs. NO_Z
O_3 ridgeline indicators (NO_X vs. VOC preference)	$[O_3] / [NO_X]$; and $[HCHO] / [NO_2]$; and $[O_3] / [HNO_3]$
Air mass age indicators	$[NO_X] / [NO_Y]$; $[HNO_3] / [NO_Y]$; $[PAN(s)] / [NO_Y]$; [CO] combined with $[NO_X]$ or with [VOC(s)] covering a range of lifetimes

Table 4-3. Priority Measurements

First Priority	
Variables	Actinic flux: $j(NO_2)$, $j(O_3)$, j(HCHO)
Species	O_3, NO, NO_2, NO_Y, H_2O, HCHO, HONO, PAN(s), HNO_3, $RONO_2$ and total NO_3, H_2O_2 and total peroxides, HO_2, RO_2, CO, speciated VOCs
Second Priority	
Variables	$j(HONO)$, $j(H_2O_2)$
Species	OH, NO_3 radical, speciated $RONO_2$, speciated RCHO, methacrolein, methylvinylketone, aerosol mass and size distribution

Chapter 5
Methods for Nitrogen Oxides Monitoring: Discussion and Recommendations

by

W.A. McClenny, U.S. EPA

5.1 Introduction

NO_Y is defined operationally as the number of NO molecules resulting after passing ambient air through a thermal converter assuming reduction of all reactive nitrogen oxides to NO, i.e., the sum of nitrogen atoms in ambient reactive nitrogen oxides. After accounting for surface deposition in the ambient air, NO_Y is the conserved quantity in tracking gaseous NO_X emissions from fossil-fired electric utilities and other NO_X sources. In the absence of NO_Z reaction products, nitrogen dioxide is obtained as $NO_Y - NO = NO_2$. Many instruments in the installed instrument base in the U.S. and elsewhere estimate NO_2 by this subtraction and, in so doing, report monitored NO_2 as an upper limit on the actual NO_2 in ambient air. Since the NAAQS for NO_2 (primary and secondary standards both of 53 ppbv NO_2 as an annual average) are not being exceeded in any locations in the U.S. at this time, this overestimation of monitored NO_2 guarantees that actual NO_2 values would show compliance as well. However, for NO_X SIP Call monitoring, $NO_Y - NO$ is recognized as consisting of both NO_2 and NO_Z where the portion of NO_Y due to NO_Z will depend on the history of the specific air mass being monitored. Indeed, the quotient NO_X/NO_Y is often used to suggest the age of an air mass.

5.2 Methods for Total Reactive Oxides of Nitrogen (NO_Y)

A recent article by Williams et al. (1998) documents the results of NO_Y measurements at a field site in Hendersonville, TN, near Nashville, during the period 13 June to 22 July 1994. Scientists from different scientific laboratories (National Oceanic and Atmospheric Administration [NOAA] Aeronomy Laboratory [two systems], Environmental Science and Engineering, Georgia Institute of Technology, Brookhaven National Lab, and the Tennessee Valley Authority [two systems]) operated instruments based on thermal reduction of nitrogen oxides to NO followed by NO detection using NO, O_3 chemiluminescence. The thermal converters were of two types. One consisted of a tube of 24-karat Au used in conjunction with either carbon monoxide (CO) or hydrogen (H_2) as a reductant gas. The other was Mo in mesh form with no reductant gas required. Concentrations of ambient nitrogen oxides ranged from 2 to 100 ppbv at this site and were composed primarily of NO_X. Based on these measurements, a number of conclusions were possible: (1) five of the seven systems agreed when monitoring ambient air, (2) two systems exhibited problems that were attributed to either inefficient conversion (particularly of the NO_Z components) or problems with calibrations, (3) some problems with conversion of NH_3 (not a nitrogen oxide) and variability in conversion of HNO_3 were observed when intentionally adding these compounds to the ambient airstream as a quality control measure, and (4) the average NO_Y measured by two Au converters was 5% lower than the average with three Mo converters. Other observations were that identification of any converter problems (i.e., by spiking ambient air with NO_Y component gases or with surrogate nitrogen compounds) should be done periodically at each installation in order to have a basis for the post-study corrections to the data. Also, when spiking ambient air with compounds for converter efficiency checks, the variations in the ambient signal due to nitrogen oxides introduces uncertainty in quantitation of the spiked component.

Fahey et al. (1985) and Kliner et al. (1997) have addressed the behavior of thermal converters and offer precautions in their use. Specifically, after investigating the thermal conversion of nitrogen oxides for different combinations of reductant gas (H_2 and CO) and metal surfaces (Au, Pt, and stainless steel), the latter concludes that "non-$(NO_Y)_i$ interferences must be individually

assessed for each instrument under appropriate operating and environmental conditions." Because conversion efficiencies depend on converter surface conditions and other variables, e.g., humidity, temperature, ozone concentration, and aging, a "periodic measurement of the conversion efficiencies of the principal $(NO_Y)_i$ species (e.g., NO_2 and HNO_3) and, when relevant, non-$(NO_Y)_i$ species (particularly HCN, CH_3CN, and NH_3) . . ." is recommended. The authors caution about the accuracy of NO_Y measurements made at rural or remote sites where interferences from NH_3 and other non-$(NO_Y)_i$ components are relatively large compared to NO_X. Harrison et al. (1999) inferred that their thermal converters may have developed a sensitivity to NH_X species (sum of gaseous ammonia and particulate ammonium) that could account for deficits between the sum of individual NO_Y species and the larger NO_Y value.

To be successful in NO_Y conversion, the thermal converter must be mounted at the monitor's interface with the ambient air, typically outside the monitoring shelter. Otherwise HNO_3 and other NO_Y components are lost to an unknown extent in passing through the inlet tubing. A thermal converter can effectively destroy any ozone in the sample stream (Kliner et al., 1997) so that losses due to NO, O_3 reactions in downstream tubing are avoided.

5.2.1 Method Recommendations for NO_Y

Thermal conversion of nitrogen oxides to NO defines NO_Y and the associated analytic method of NO, O_3 chemiluminescence is the simplest, most thoroughly evaluated, and most often used method for measuring the resultant NO. However, because of the experimentally verified variation of converter efficiencies for both NO_Y species and non-$(NO_Y)_i$ species, a strong program of quality control is recommended under the direction of a scientist experienced in this area. Considering the scientific consensus developed in recent field comparison studies (Williams et al., 1998) and subject to the cautionary guidance presented in the open literature (Kliner et al., 1997, and Fahey et al., 1985), this method is recommended for NO_Y monitoring for NO_X SIP Call applications in urban and suburban locations and in qualified rural locations. The use of thermal conversion in rural areas has led to summary statements considering multiple-day measurements, but can result in values of the sum of responses from individual NO_Y species divided by the batch NO_Y response, i.e., $\Sigma(NO_Y)_i/NO_Y$, significantly different from 1.0 (Parrish et al., 1993). Obviously, the lower the NO_Y concentration, the more important the quality control procedures. In summary, the limit of detection (LOD) for NO_Y measurement is not generally associated with the analytical finish but instead with the knowledge of the conversion efficiencies for both NO_Y and non-$(NO_Y)_i$ species over the course of measurements. Therefore, real-time measurements at the low single-digit ppbv levels must be substantiated by a strong quality assurance program. As an indication of the quality of NO_Y measurements possible, the hourly averaged data for the best five out of the seven NO_Y measurements reported by Williams et al. (1998) in their Table 5 differed by values of 2.1 ppbv at an average of 13.4 ppbv, 1.7 ppbv at 16.2 ppbv, 3.0 ppbv at 21.0 ppbv, and 6.7 ppbv at 26.9 ppbv. These uncertainties are at the upper limit (20%) specified by modelers (see Chapter 4). Adequate precision is, however, achievable by any of the methods. Based on information from this report, the problem with NO_Y measurement is in the accuracy, i.e., knowing the conversion efficiencies.

5.3 Methods for Nitric Oxide (NO)

5.3.1 NO, O_3 Gas-Phase Chemiluminescence

Nitric oxide in ambient air has been measured by both point and open-path monitors. One of these methods is the homogeneous gas-phase reaction between NO and excess ozone (Fontijn et al., 1970), one product of which is excited-state NO_2 molecules. Subsequent radiative decay of NO_2 produces photons (chemiluminescence) in the visible beginning at 620 nanometers (nm) and extending into the near infrared. To monitor NO, ambient air is channeled into a reaction chamber to which excess O_3 is added. The reaction is rapid and contained within a small volume, typically a few tens to hundreds of cubic centimeters, and occurs mostly within the reaction cell. The arrangement is designed as a rate sensor for which, within certain constraints, the chemiluminescence signal is proportional to the sampling rate and inversely to the reaction chamber pressure. Since the excess ozone needed for the reaction is generated using filtered ambient air, no compressed gases are needed for monitoring (calibration gases are still needed). Instruments designed on this method are generally small in size and light in weight. The reaction chamber design and operating parameters for efficient generation and collection of photons have been optimized as both a research tool and a commercial instrument (see, for example, Steffenson and Stedman, 1974; Delany et al., 1982; Dickerson et al., 1984; Drummond, 1985), and the instrument is widely used for ambient monitoring. The method is a benchmark of air monitoring technology and, along with the similar chemiluminescence method for ozone, marked EPA's departure from predominantly wet chemical techniques for monitoring trace gases. Any other technique for ambient NO monitoring must be competitive.

During ambient monitoring, care must be taken to avoid NO losses in inlet sampling lines due to the gas-phase reaction with ambient O_3 and to the reaction of NO at the tubing wall. These considerations are treated in some detail in Appendix A, where it is shown that a 2-s or less residence time should limit losses from the gas-phase reaction to 10% or less even at the highest ozone concentrations typically encountered. Wall losses can be determined by the use of standard additions of NO to ambient air entering the sampling manifold. Accumulation of this data at times when different ozone levels exist in the ambient air provides a database from which the combined effect of gas-phase reactions and wall reactions are defined. By calculating losses expected from the gas-phase reaction and comparing them with

the experimental total first-order loss rate of NO, the effect of wall reactions can then be inferred (Fehsenfeld et al., 1990).

In most sensitive NO chemiluminescence monitors, a pre-reaction chamber is used. Its purpose is to allow the NO, O_3 reaction to occur just before reaching the reaction chamber and to use any residual signal from the reaction chamber as background for the subsequent measurement of NO. An estimate of the LOD (SNR = 2) for research instrumentation is 10 pptv for a 1-s integration time and ±10% of the measured concentration well above the detection limit (Fehsenfeld et al., 1987).

5.3.2 Differential Optical Absorption Spectroscopy

DOAS research systems for NO have components like those discussed in Appendix B, Determination of Atmospheric Concentration of Nitrogen Oxides by Differential Optical Absorption Spectroscopy. The procedure and system elements for determination of NO or any other reactive nitrogen oxide are similar to that for NO_2. However, since NO is typically detected with wavelengths in the short UV wavelength region, a combination of low source light intensity in this region and the attenuation of radiation by molecular oxygen in this spectral region limit the path length. Operation of the system involves acquiring an oxygen spectrum for the path length used during NO measurement in order to correctly account for the oxygen attenuation. Literature provided by a commercial manufacturer OPSIS AB (Furulund, Sweden), indicates a detection limit of 1–2 ppbv over a 200-m path length with an averaging time of 1 min. Optical components that transmit/reflect efficiently in the lower wavelength UV region must be used.

5.3.3 Tunable Diode Lasers

Tunable diode laser systems have been used as reference methods in field study programs because these systems offer an unambiguous identification of NO through its unique spectral absorption features. More information on tunable diode laser systems is given below in section 5.3.5.

5.3.4 Other Point Monitoring Techniques

Other techniques have been used such as LIF, two-tone frequency-modulated spectroscopy (TTFMS), and passive sampling tubes for sampling combined with an analytical finish (usually ion chromatography). These techniques are covered for the pre-1990 period by Sickles (1992). The simple and inexpensive passive sampling devices have become widely used for time-integrated sampling of trace gases and are of considerable utility in establishing pollutant distributions across major urban areas for the purpose of locating the best monitoring locations (Varns et al., 1999) even though these techniques cannot be used for diagnostic testing. For the most recent work in these areas see relevant citations in the references (Chapter 7).

5.3.5 Method Recommendations for NO

The simple and sensitive NO, O_3 chemiluminescence technique is well researched and established as the best commercial technology for ambient air monitoring of NO. Ground-based instruments with sufficient sensitivity for ambient-level monitoring at any tropospheric location are commercially available, although research-grade instruments are often assembled from components for special applications such as for tropospheric aircraft flights. DOAS technology is available for NO but a lower detection limit at the sub-ppbv level is difficult to obtain.

5.4 Methods for Nitrogen Dioxide (NO_2)

NO_2 is a criteria pollutant in the U.S. for which the NAAQS for health and welfare is an annual average of 53 ppbv. As a result of the NAAQS requirements for monitoring, the commercial incentive for instrument development has spurred innovative development of instrumentation, resulting in many techniques including both point and path monitors. The point monitors measure NO_2 directly by fluorescence, by absorption in the visible or IR, or by luminol chemiluminescence. NO_2 is monitored indirectly by NO, O_3 chemiluminescence after NO_2 conversion to NO with thermal or photolytic converters. DOAS open-path instruments use a relatively interference-free spectral region in the UV/visible to measure NO_2 directly.

As noted earlier in Section 5.2.1, the gas-phase reaction of NO and O_3 in the manifold leading from the ambient air to the location of a point monitor results in the creation of NO_2 and the loss of NO and O_3. As noted there, a 2-s or less residence time ensures that the loss of NO is less than 10% due to its gas-phase reaction with ozone. Since NO is typically less than NO_2, the gain in NO_2 concentration will also be less than 10%.

5.4.1 NO, O_3 Gas-Phase Chemiluminescence

Thermal converters. The installed instrument base for measuring ambient nitrogen dioxide in the U.S. consists mainly of chemiluminescence NO monitors equipped with NO_2-to-NO thermal converters. The NO_2 concentration is estimated by subtracting the instrument response when bypassing the converter from the response when passing the air sample through the converter. These instruments provide data that systematically overestimate NO_2. There are two reasons: (1) thermal converters convert other reactive nitrogen species as well as NO_2, as noted in Section 5.2; and (2) the NO, O_3 reaction increases the NO_2/NO ratio as the sampled air mass is passed through inlet tubing or through addition volumes (e.g., photolytic converters) before reaching the detection chamber. When only one reaction chamber is time shared between measurements of NO and NO_Y, the difference NO_Y – NO is taken between sequential measurements. Hence temporal variability in response can result in errors when the difference NO_Y – NO is used for NO_2.

Even non-NO_Y compounds such as NH_3 and amines can be converted to NO if converter temperatures are excessive (Williams et al., 1998). The NO_2 is estimated by subtracting the signal due to NO (bypassing the thermal converter) from the signal obtained from an airstream passed through the thermal converter (NO_2 + NO + NO_Z). The largest percentage errors in NO_2 occur typically in the afternoon of warm, sunny days when the photochemical conversions of NO_X to oxidation products such as HNO_3, HONO, PAN, and other organic nitrates are optimum. A large percentage of these compounds are converted to NO in the chemiluminescence monitor's thermal converter. Although special inlets using nylon filters to remove nitric acid and nitrate as well as diffusion scrubbers to selectively remove acid and/or basic nitrogen-containing gases are available to condition the sample stream prior to entering the thermal converter, the vast majority of instruments do not have this feature. In fact, the use of an external thermal converter (converters mounted outside monitoring stations and using extremely short inlet lines) ensures high-efficiency conversion of reaction products of NO and NO_2 and minimizes losses of these species to wall adsorption so that an accurate measure of NO_Y can be obtained.

Photolytic Conversion of Ambient NO_2. Photolytic conversion of NO_2 using wavelengths below 400 nm is being perfected with respect to choice of light sources and other design features that allow efficient conversion while limiting undesirable consequences such as NO, O_3 reactions and excessive heating in the photolysis cell. Eric Williams of NOAA addresses these considerations in Appendix C and reviews the different designs that are currently in use. The implementation of photolytic conversion in research instrumentation has already been realized in several laboratories, and a commercial version has been marketed by Eco Physics (Dürnten, Switzerland) as part of a NO_X monitor for several years. Current research and routine monitoring needs for a specific and sensitive monitor of ambient NO_2 is spurring additional development. The prospect of a photolytic converter that can be added to existing chemiluminescence NO monitors appears to be the most practical current approach to obtaining a near-term ambient air database for NO_2 concentrations.

5.4.2 Luminol Chemiluminescence

As noted by Maeda et al. (1980) and Wendel et al. (1983), NO_2 reacts with luminol in water solution and the resulting compound emits visible radiation around 465 nm, resulting in a real-time, direct measurement. In one version of the method, the reaction takes place in a lightproof chamber, on the surface of a wick saturated with the water-based luminol solution and mounted in front of a photomultiplier tube. The solution continuously moves from one reservoir down the vertically mounted wick and into a second reservoir. This reaction is the basis for commercial Luminox instruments available from Scintrex, (Toronto, Canada). The instrument provides a direct measurement of NO_2 but is subject to interferences from other compounds such as O_3 and PAN. Additives to the luminol solution are effective in selectively suppressing response to interferences and enhancing response to NO_2. Schmidt et al. (1995) describe a selective ozone scrubber for application in ambient NO_2 measurements using the Luminox instrument. The reaction between NO_2 and luminol is nonlinear and must be corrected for measurements of NO_2 below a lower concentration level, typically near 2 ppbv. Kelly et al. (1990) evaluated the performance of the Luminox, Model LMA-3, and noted that to obtain accurate measurements of NO_2 at low concentrations, the readings must be corrected for zero offset, nonlinearity, and ozone and PAN interferences, in that order. Fehsenfeld et al. (1990) describe a comparison among NO_2 monitors, one of which was the LMA-3, at a remote site near Niwot Ridge, CO. Corrections for O_3 and PAN interferences in the LMA-3 were noted to be "sufficiently consistent that they could be corrected for by using the measured values of O_3 and PAN down to about 0.3 ppbv NO_2." Gaffney et al. (1998) and Gaffney et al. (1999) have demonstrated the use of a luminol-type detector for NO_2 and peroxyacyl nitrates.

5.4.3 Laser-Induced Fluorescence

LIF was used successfully in the 1970s by combining fixed-frequency lasers and high-discrimination ratio liquid filters (Gelbwachs et al., 1972). Photons resulting from the de-excitation of NO_2 molecules were viewed at right angles to the laser light path through the liquid filters, and sensitive photon counting techniques were used. Flashlamps replaced the fixed-frequency lasers (argon ion laser or helium-cadmium laser) as a light source in later research by this group (Fincher et al., 1977). However, neither approach proved to be as commercially viable as the thermal conversion/NO, O_3 chemiluminescence. LIF has now been revived using practical, high-power, tunable laser sources that permit the matching of light output and the maxima in the NO_2 absorption features. Thornton, Wooldridge, and Cohen discuss the latest advances for this technique in Appendix D of this report in a text arranged through the efforts of Dr. Cohen. Examples are given of recent successful comparison testing against the NO, O_3 chemiluminescence monitoring technique with a photolytic converter as part of the SOS '99 study in Nashville, TN. Projections in this discussion include the ultimate achievement of a version for routine use with a detection limit of 10 pptv.

5.4.4 Differential Optical Absorption Spectroscopy for NO_2

The successful use of DOAS for monitoring NO_2 in the troposphere has been demonstrated using both commercial instruments and instruments assembled from individual components (Edner et al., 1993; Plane and Nien, 1992; Febo et al., 1996). Stevens et al. (1993) compared the measurement of a

commercial DOAS (OPSIS, Furulund, Sweden) to EPA-approved fixed-point methods. In the U.S., OPSIS has achieved equivalency status to the reference technique for monitoring NO_2. The achievement of equivalency means that the instrument meets certain standards of performance and that data obtained with the instrument can be reported by state agencies in satisfaction of the reporting requirements for the NAAQS. McElroy et al. (1993) describe a method for on-site calibration of the OPSIS for NO_2 and other gases.

The commercial instruments using DOAS were developed using certain proprietary operational techniques. For this reason, the specific algorithms for the estimation of uncertainty for NO_2 and other reactive nitrogen species is not generally known in detail and the transmission spectra are not necessarily available to the operator for customized postprocessing. However, the estimated uncertainty is understood to be based on the residuals obtained by fitting field spectra to a set of stored reference spectra, including the target gas spectra and known interferences. High estimated uncertainty can indicate unexpected spectral interferences, a change in wavelength calibration (although this can be periodically corrected), or other problems. Nonlinearity in response to NO_2 concentrations is also a potential problem at the spectral resolution used in typical DOAS instruments. This is an inherent problem with instruments that use spectral transmission data to calculate trace gas concentrations (Russwurm and Phillips, 1999). Unfortunately, the extent of this problem cannot be determined without specifics concerning the algorithm used for signal processing. In commercial units, real-time data processing is emphasized and a concentration measurement with estimated uncertainty is the output of the instrument. The detection limit for NO_2 as stated in the commercial literature (OPSIS, Furulund, Sweden) is estimated at 1 ppbv using a 500-m total optical path length. Uncertainty in the measurement must be less than ±10% to meet the requirements for diagnostic modeling. Appendix B of this report authored by Dr. Jochen Stutz addresses the scientific approach to monitoring of nitrogen oxides by DOAS.

5.4.5 Tunable Diode Laser Absorption Spectroscopy—Middle Infrared

The diode laser has been used as the radiation source in the detection of NO_2 and other nitrogen oxides by using the technique of second derivative absorption spectroscopy. Typically, the ambient sample is drawn into a glass cell with special optics to direct the tunable diode laser (TDL) radiation in a folded path of length up to 100 m (Schiff et al., 1983) or used over an open ambient path (Chaney et al., 1979). The pressure inside the cell is reduced (to the order of 25 torr) to minimize pressure-broadening effects of the absorption line. The TDL is a semiconductor device whose band-gap energy is temperature dependent and whose output frequency is determined by joule heating losses. The laser is held at low temperatures by closed-cycle coolers and tuned by resistive heating of the diode. The output frequency is tunable over several tens of wave numbers by varying the current passing through the diode; it can be made to scan rapidly and repetitively (1 KHz) over a given wave number range by providing the appropriate current control. Very high specificity is obtained because the output frequency has an extremely narrow bandwidth on the order of 10^{-3} wave numbers and therefore does not degrade the shape of the gas absorption line being monitored. This allows a single absorption feature of the target gas to be selected, generally removing the effects of other interfering species.

A sensitive, fast response detector is used to generate the analytical signal. The laser wavelength is maintained at an absorption maxima by the use of a reference signal generated by passing a small fraction of the beam through a reference cell containing the gas of interest. As the beam is tuned across the absorption feature, it is slightly modulated in wavelength by modulating the diode current. This generates a so-called first-derivative signal that switches signs as the laser is tuned past the line center. This zero crossing generates a signal that is used as a reference to keep the laser tuned to line center. The strength of the second-derivative signal after the beam passes through the multipass cell is calibrated and used to measure the target gas concentration in the sample. Ried et al. (1980) indicate that this type of system can achieve sensitivities on the order of 100 pptv.

Since the TDL provides near unambiguous detection of target gases, it has frequently been used as a reference method in field test comparisons. Examples of its use for NO_2 include a comparison with the LMA-3 direct NO_2 monitor at a field monitoring site (Russwurm, 1988) and other pre-1991 research (Sickles et al., 1990) including an intercomparison of NO_2 measurement techniques such as the TDL by Fehsenfeld et al. (1990).

5.4.6 Systems Using Visible/Near Infrared Radiation Laser Sources or LEDs

Allen et al. (1995) and Sonnenfroh and Allen (1996) reported the application of single-longitudinal mode, room-temperature, semiconductor lasers operating in the visible and near IR to in situ monitoring of NO_2. They report a system design that uses the relatively new balanced ratiometric detector (BRD), a novel electronic laser noise-canceling technique. They project a sensitivity for ambient operation of approximately 1 ppbv for a 10-m path assuming a detectable absorbance of 10^{-6}. Mihalcea et al. (1996) report the use of two photometers, one using a commercially available InGaAsP diode laser with output near 670.2 nm and the second using radiation from a prototype frequency-doubled GaAlAs diode laser source with output near 394.5 nm. These systems were used to measure the temperature and pressure dependence of NO_2 absorption at those wavelengths. The experimental results suggest a detection limit of 10 ppbv for a hypothetical system using the lower wavelength and assuming a detectable absorbance of 10^{-5}. Fetzer et al. (1998) also used a frequency-doubled GaAlAs diode laser for demonstrating a capability for NO_2 monitoring.

Fetzer et al. (1998) demonstrated the use of an NO_2 photometer using a GaN light-emitting diode (LED) as source of 450-nm radiation and achieving a detection limit of 1 ppbv with an instrument response time of 1 min. No comparable commercial unit is known to be available at the present time. However, Jung and Kowalski (1986) modified a commercial ozone photometer to a NO_2 photometer by changing the lamp source, optical filter, mirrors, detector, and the absorption cell path length. The unit was used to measure NO_2 at the South Coast Air Quality Management District's air monitoring station at Pomona, CA, and compared with a commercial chemiluminescence monitor.

5.4.7 Method Recommendations for NO_2

Photolytic conversion of NO_2 to NO followed by NO, O_3 chemiluminescence for concentrations across the full range of ambient NO_2 concentrations has been demonstrated using commercially available units. However, unless the time spent in the inlet sampling line, including the photolytic converter, is 2 s or less, an O_3 monitor must also be included to provide information to correct NO_2 readings for conversion of NO to NO_2. Most chemiluminescence systems in the installed instrument base in the U.S. have thermal converters and provide an upper limit on NO_2 as explained above. Since the NAAQS for NO_2 is currently not being exceeded at any location in the U.S., criteria monitoring is not impacted. However, NO_2 monitoring for model evaluation requires a more selective converter.

A successful, commercially available method for NO_2 monitoring in urban and suburban areas is the UV DOAS system. NO_2 is measured directly and without sampling. No sampling artifacts are possible and there are no known interferences. Although the exact method of treating uncertainty depends on the manufacturer, the use of residuals in a least squares fitting procedure across a portion of the absorption spectrum provides a measure of uncertainty. Additional understanding of the uncertainty of the DOAS measurement is needed.

The best available technology for the full range of NO_2 concentration is the LIF technique, a technique that has high commercial potential, but is not yet being manufactured by a commercial vendor. LIF is specific for NO_2 and measures NO_2 directly. Sample transport from the ambient air to the detector is subject to the NO, O_3 reaction in the sample lines so that the same constraints on residence time as for any point monitor are relevant. Photometric measurements of NO_2 in the visible look promising if the new balanced radiometric detector and room temperature tunable diode laser sources are used. The question of whether the photometric approach is viable for practical monitoring of ambient NO_2 must be answered with additional research.

5.5 Methods for Monitoring Nitric and Nitrous Acids (HNO_3 and HONO)

HNO_3 and HONO are frequently used for diagnostic testing of AQMs as noted in Chapter 4. HNO_3 is produced during the day as a reaction product of OH and NO_2 and peaks during the daytime. Because of the high deposition rates of HNO_3, this deposition constitutes the primary termination step for NO_X emitted into the atmosphere. HONO has a short lifetime in the atmosphere during the day because it is readily photolyzed (OH is formed as one product) and shows a minimum during the daytime with a maximum at night. There may be some daytime sources of HONO maintaining a very small concentration at steady state. It has been argued that hydrolytic production of HONO from NO_2 is catalyzed by soot surfaces (Zellweger et al., 1999; Ammann et al., 1998).

In the past, time-integrated systems for sampling and accumulation of nitric and nitrous acids have been widely used. These systems use either filter packs or a combination of coated diffusion tubes and filter packs for sampling. However, the samples must be transported to a laboratory for analysis. Many of these systems typically collect samples over a time period exceeding the time resolution required for performing the diagnostic tests mentioned in the Introduction. These techniques will not be considered for diagnostic testing of AQMs but nonetheless can be important in establishing comparability among different methods for measurements averaged over a longer time period. For information on the denuder/filter pack techniques, the reader is referred to the results of five pre-1991 comparisons of nitric acid techniques, including the *Atmospheric Environment* edition (Vol. 22, No. 8) devoted to the results of the "Nitric Acid Shootout" that took place in 1985 in Pomona, CA. Other references are Anlauf et al. (1985), Spicer et al. (1982), Walega et al. (1991), and Sickles et al. (1990).

5.5.1 Thermodenuders

Thermal denuders with selective coatings such as tungstic acid (Braman et al., 1982; McClenny et al., 1982) have been used for near real-time monitoring with outputs at one-half hour or less. Using a tungstic-acid-coated tube as a denuder, nitric acid chemically combines with the acid and accumulates at the surface of the tube. Subsequent heating of the tube releases NO_X, which is passed to a sensitive NO, O_3 chemiluminescence detector. Roberts et al. (1987) report the lack of significant interferences by NO_2, HCN, PAN, and n-propyl nitrate under most conditions, although the extent of interference becomes greater as the atmospheric humidity is reduced. In field tests conducted at a rural site, comparisons with a nylon filter collection technique gave significant differences at the sub-ppbv concentration

levels, although the interfering gases were not identified. Klockow et al. (1989) describe an automatic thermodenuder system for measurement of HNO_3 and ammonium nitrate in air for a one-half hour sampling period. The system has two denuders in series. Both are coated with $MgSO_4$ and the first is operated at room temperature, while the second is operated at 150 °C. Gaseous nitric acid is collected in the first denuder and ammonium nitrate is decomposed and captured as nitric acid in the second. Subsequent heating to 700 °C liberates HNO_3 and HONO as NO_X, which is detected with a standard NO_X chemiluminescence monitor.

5.5.2 Dual-Channel Chemiluminescence Monitors

Commercial chemiluminescence monitors for NO have been modified to design real-time nitric acid detectors using two inlets, one with only a particle filter and the second with a particle filter and a nylon filter. Sample air entering the monitor from both channels passes through a thermal converter before reaching the chemiluminescence reaction chamber. The difference signal is attributed to HNO_3, including that formed from the decomposition of ammonium nitrate. In some instances, HNO_3 may be removed by substances already present on the particle filter. Tanner et al. (1998) measured the sum of nitrate and nitric acid by using a system comprising two inlet channels, each containing a gold-CO catalyzed converter to reduce all odd nitrogen species (NO_Y) to NO. One channel also contained a nylon filter to capture the sum of nitrate PM and nitric acid. The NO resulting in each channel is detected by NO, O_3 chemiluminescence. This type of system has been used in an intercomparison of HNO_3 methods (Spicer et al., 1982) and aboard aircraft for studies of plume chemistry during the 1995 SOS summer field study in Nashville.

5.5.3 Wet Denuders

Nitric and nitrous acids are often sampled by capture in water followed by ion chromatographic analysis. Capture of nitric acid by a diffusion scrubber based on a wet anion exchange membrane and determination by UV detection was reported more than a decade ago (Dasgupta and Philips, 1987). However, the method was insensitive and not sufficiently selective. A subsequent study (Vecera and Dasgupta, 1990) demonstrated ambient measurements of nitrous acid with 7- to 15-min time resolution and a detection limit of 20 pptv. A porous membrane diffusion scrubber was used for collection and ion chromatography with UV detection for analysis. However, the diffusion scrubbers of this type did not collect quantitatively and calibration efforts were required. Vecera and Dasgupta (1991) introduced the use of a wet denuder, rudimentary low-pressure ion chromatography, and postcolumn colorimetric reaction detection for the determination of HONO and HNO_3 with an 11-min time resolution and 80- and 230-pptv detection limits, respectively. More efficient parallel plate wetted denuders were introduced (Simon and Dasgupta, 1993), which make this approach more sensitive and competitive with a more expensive ion chromatographic finish. However, the diazo coupling chemistry uses a copperized cadmium reactor for reducing nitrite to nitrate and that, although a standard technique used in water analysis laboratories, may not be considered as environmentally friendly. Taira and Kanda (1993) describe a wet effluent diffusion denuder that incorporates a 0.16-cm-i.d. straight glass tube as the denuder. Buhr et al. (1995) disclosed an automated system for nitric acid, particulate nitrate, and particulate sulfate. The method uses a semicontinuous wet effluent denuder and a wet effluent frit for sampling, followed by ion chromatography with conductivity detection. Sample frequency is 15 min and a detection limit of 10 pptv is achieved for each compound. Nitric acid measurements over an ambient range of <0.1 to 4 ppbv were compared with a filter pack method and excellent agreement was obtained. Near real-time monitors with short cycle times on the order of 15–30 min have been reported by Simon and Dasgupta (1995a) for HNO_3 and HONO using a wet-wall parallel-plate denuder and a customized ion chromatograph. The most recent version of this type of monitor is a commercial prototype that was used in the summer 1999 Atlanta SOS study by Dr. P.K. Dasgupta of the Texas Tech University. This latest version differs from the unit described in the open literature in the method for collection of airborne PM. In the newer version, an in-line particle filter is placed downstream of the wet-wall denuder; periodic automatic extraction of this filter occurs followed by ion chromatographic analysis. Figure 5-1 shows the variation of HNO_3 and HONO with a 10-min resolution as measured using this system during a 3-day stretch in the Atlanta SOS study during the summer of 1999. As expected, the diurnal maxima of HNO_3 occurs in the daytime whereas HONO disappears during the day and becomes important at night.

Keuken et al. (1988) developed a wet-wall denuder formed between concentric cylindrical tubes mounted about a horizontal axis. The walls are wetted by maintaining a supply of water in the lower section of the cylindrical annulus and continuously rotating the cylinders. As ambient air is passed through the water-free portion of the annulus, soluble ions accumulate in the water reservoir and are periodically analyzed by ion chromatography. Oms et al. (1996) discuss the use of a later version of this approach in which analysis of HNO_3, HONO, HCl, and SO_2 are automated by computer control at a frequency of 2/h. Detection limits of 2 and 12 ng/m^3 are stated for HONO and HNO_3, respectively. A commercial version of this unit has been constructed by Anderson Inc., Atlanta, GA. Kanda and Taira (1992) reported the measurement of HNO_3 and HONO as NO after capturing the two gases in a NaOH solution and chemically converting the two to NO.

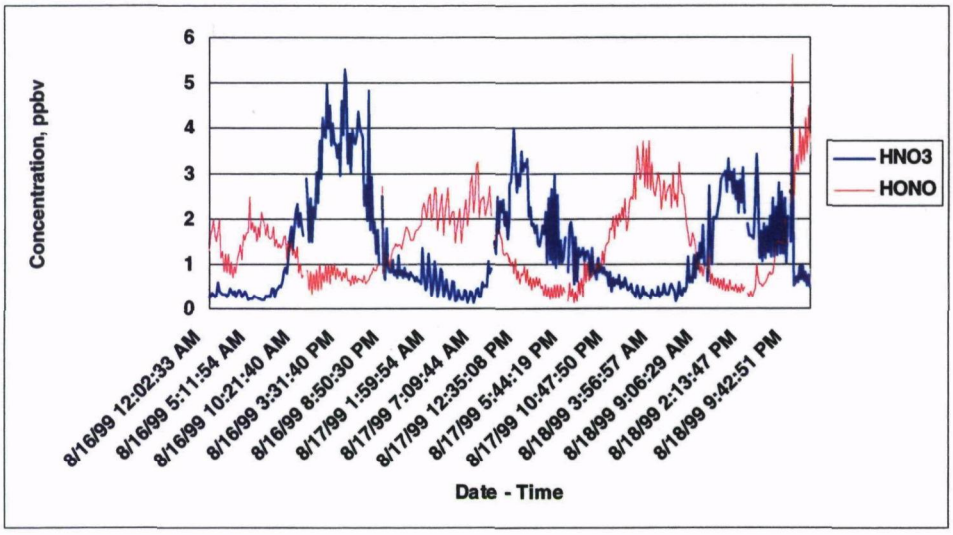

Figure 5-1. HNO_3 and HONO with 10-min resolution as measured using a wet-wall denuder system for a three-day stretch in the Atlanta SOS study during the summer of 1999 (Dasgupta, Texas Tech University, Lubbock, TX).

5.5.4 The Mist Chamber Technique

Cofer et al. (1985) describe a mist chamber technique. Essentially, water soluble components of ambient air are captured by mixing water droplets with the ambient air. The droplets are created inside a collecting vessel by using the venturi action of sample air passing over a water-filled capillary, thereby generating water particles with high surface area to volume ratio. The diffusion of water soluble gases to the particles results in the capture of the gases. The droplets are subsequently collected by impaction against a filter and analyzed by ion chromatography. This system is typically operated with cycle times greater than one-half hour. Talbot et al. (1990) expanded on the use of the mist chamber method and examined differences between results using the mist chamber technique and those using the nylon filter technique as observed in the field experiments.

5.5.5 Chemical Ionization Mass Spectrometry

The most recent addition to real-time measurement of nitric acid is the chemical ionization mass spectrometry (CIMS) technique as reported by Mauldin et al. (1998) and by Huey et al. (1998). These instruments differ in design and in the reagent ion used. Fehsenfeld et al. (1998) has documented the comparison of these two systems and a filter pack technique. Apparent decomposition of ammonium nitrate particles to nitric acid and ammonia on the front filter of the filter pack released nitric acid to be captured as nitric acid and hence biased the filter pack results high. Scatterplots of simultaneous measurements by the two systems indicate a roughly symmetric scatter with about 1:1 agreement and most comparisons fall within ±30% of being identical across the ambient measurement range of 2–1000 pptv (see Figure 4 in Fehsenfeld et al., 1998). CIMS detection limits of less than 15 pptv for a 1-s integration period are cited. The fast response of the system is particularly well suited to requirements of airborne monitoring.

5.5.6 Tunable Diode Laser Absorption Spectroscopy and DOAS Techniques

Optical techniques have often been used for measuring nitric and nitrous acid. Real-time systems employing tunable diode laser absorption spectroscopy (TDLAS) (Schiff et al., 1983) and another using an open-path, multipass Fourier transform infrared (FTIR) system (Tuazon et al., 1981) have been successfully operated for monitoring nitric acid and are particularly useful as reference methods in areas where nitric acid concentrations achieve ppbv concentrations. The TDLAS has a detection limit given as 4 ppbv for nitric acid, while the best FTIR systems provide measurements to 10 ppbv. Commercial DOAS systems are used for monitoring nitrous acid with a quoted detection limit of 0.5 ppbv under standard conditions for a monitoring path of 500 m and a measurement time of 1 min (OPSIS, Furulund, Sweden). Febo et al. (1996) have measured HONO with a commercial DOAS system at values exceeding 10 ppbv in Milan.

5.5.7 DNPH Derivatization and HPLC Analysis

Zhou et al. (1999) have demonstrated a derivatization technique for HONO based on DNPH derivatization and HPLC

analysis with UV detection at 309 nm. HONO is scrubbed from ambient air by passing the sample through a coil sampler along with an aqueous scrubbing solution. Various potential interferences have been examined and results indicated a 1:10,000 interference equivalent for NO2 and 1:1000 for PAN. Limited comparisons with a bubbler/IC method indicate at most a 20% difference for 4-h averages across a concentration range of 80–1200 pptv. The system has been automated with a 5 min cycle time.

5.5.8 Method Recommendations for HNO_3 and HONO

The denuder/ion chromatographic method for monitoring both nitrous acid and nitric acid has been commercialized by Anderson Inc. (Atlanta, GA) by using a rotating annular denuder for collection, and a system design by P.K. Dasgupta of Texas Tech University which uses a wet parallel plate denuder has been tested in several recent field studies (see Figure 5.1). One additional attraction of the denuder/ion chromatographic approach is the information about other compounds that is obtained as part of the ion chromatographic analysis.

DOAS methods using manual inspection of individual spectra may be the most accurate for HONO due to the low detection limits of ≈100 pptv, the absence of significant interferences, and the fact that no sampling is required. However, the use of manual inspection limits automation of the method.

Chemical ionization mass spectroscopy is apparently the best available method for nitric acid based on the recent work at NOAA and the National Center for Atmospheric Research (NCAR). It is not clear that this technique will meet the detection limit requirement for diagnostic testing of models, although the recent side-by-side comparisons showed agreement between two systems of ±30% at sub-ppbv concentrations. Sampling losses through the MS inlet system are apparently minimized due to the rapid airflow rate into the system. Additional comparisons with other viable techniques seem warranted.

5.6 Methods for Monitoring Particle Nitrate

Particle nitrate has been measured downstream of water-soluble gas components in the type of instrument described by Simon and Dasgupta (1995a and 1995b). In the original paper, Dasgupta and coworkers designed the system to grow particles to a large size by adding steam to the sample stream and then to collect the particles for IC analysis by impaction in a cooled maze. Recent design changes include the collection of particles on a filter followed by automated extraction and analysis. Khylstov et al. (1995) describe a similar method using a steam-jet aerosol collector with ion chromatographic detection of inorganic ions. Spicer et al. (1985) describe a thermal decomposition/chemiluminescence method for determining nitrate in which the sample or an aqueous extract of the sample is heated to 425 °C and detection of the resultant gaseous nitrogen oxides is by NO, O_3 chemiluminescence. Yamamoto and Kosaka (1994) also discuss thermal desorption of nitrates to a chemiluminescence detector using a different arrangement for thermal desorption. Stolzenburg and Hering (2000) disclose a method for automated measurement of fine-particle nitrate in the atmosphere with a cycle time of 10 min. Interfering gases such as nitric acid are removed from the airstream by an upstream denuder. Particles are increased in size by humidification and then collected by impaction. This is followed by flash vaporization and chemiluminescence detection of evolved nitrogen species. This approach has been used in the field in several studies and is currently being commercialized by Rupprecht and Patashnik. Inc. (Albany, NY).

5.6.1 Method Recommendations For Particle Nitrate

The available technologies are relatively new and need to be compared in side-by-side field testing. However, the systems based on thermal desorption/chemiluminescence and on filter collection followed by extraction and IC analysis are being used frequently and, in the case of the former a commercial status has been achieved.

5.7 Methods for Monitoring PAN, PPN, MPAN, and Other Organic Nitrates

Kleindienst (1994) summarizes the different measurement techniques for PAN up to a certain point in 1993 in the context of a comprehensive review of the properties of PAN and different aspects of its part in atmospheric chemistry. Table 2 in this article includes a summary of methods for detecting PAN in tropospheric measurements. These include three gas chromatographic methods—electron capture, luminol chemiluminescence, and NO, O_3 chemiluminescence—and two continuous methods—infrared spectroscopy and PAN, amine chemiluminescence. The use of capillary chromatography with either electron capture detectors (ECDs) or luminol chemiluminescence continues to be prevalent in current monitoring efforts for PAN and other organic nitrates. Some researchers still use the older packed chromatographic column technology. A number of additional references, including more recent references, are given below.

PAN thermally decomposes in the atmosphere to form NO_2 and the acetylperoxy radical, and at 298 K (or 77 °F) calculation of the thermal decomposition rate results in an atmospheric lifetime of nearly 1 h, although an increase in ambient temperature to 305 K (or 90 °F) reduces this to roughly 15 min (see Figure 1 of Kleindienst, 1994). Sample integrity of PAN and PAN-like compounds during the measurement process in moving through a point monitor, contacting surfaces, and, in some cases, moving through capillary or packed columns, is a major concern. Thermal decomposition of PAN-like compounds on a precolumn converter is sometimes used to check for the presence of interferences when gas chromatographic separations

with short retention times (e.g., during aircraft measurements) are being used. There is no primary standard for PAN-like compounds, and they are usually synthesized in the laboratory and stored for subsequent dilution at the monitoring site. Conversion of PAN to NO in the well-characterized thermal converters used for NO_Y measurements (see above) often provide a surrogate standard.

Methods for sampling and analysis of alkyl nitrates are reviewed by Parrish and Fehsenfeld (2000) in their article on methods for gas-phase measurements of ozone and aerosol precursors. Direct sample injection or preconcentration followed by GC/ECD analysis is typical.

5.7.1 Gas Chromatography with Specific Detection

The most common current methods for analysis of PAN and PAN-like compounds involve separation of organic nitrates by GC and detection using either an ECD or a luminol chemiluminescence detector for NO_2 (after thermal conversion of nitrates to produce NO_2). As pointed out by Roberts et al. (1989), capillary columns offer better sensitivity of detection compared to packed columns and can separate PAN, PPN, and a number of C1–C5 alkyl nitrates from many light halogenated compounds that have similar retention times. Blanchard et al. (1990) compared two packed-column GC/ECD systems for monitoring ambient air (0.15 to 2 ppbv) and obtained slope and intercept values of 1.14 ± 0.01 and -0.03 ± 0.05, respectively, with a correlation coefficient of 0.995. A comparison between one of these systems and a system with a packed column and a GC/luminol detector for the same monitoring sequence gave slope and intercept values of 1.08 ± 0.03 and 0.08 ± 0.24, respectively, with a correlation coefficient of 0.864. Blanchard et al.(1993) demonstrated the potential of a packed-column GC method for PAN using a postcolumn chemical amplifier and a NO_2 luminol detector. For PAN concentrations < 1 ppbv, a NO_2 amplification factor of 180 ± 20 was observed when 6 ppmv of NO and 8% of CO were added to a postcolumn reactor; this approach was proposed for extending the lower range of detection for PAN. De Santis et al (1996) used an annular denuder coated with a sodium carbonate solution to capture PAN. The PAN is retained as nitrate and the nitrate is extracted for measurement by ion chromatography. Danalatos and Glavas (1997) used a capillary column at subambient temperatures along with an ECD to demonstrate improved response compared to ambient temperature runs and to separate PAN from interfering gases (mainly halogenated compounds). Nikitas et al. (1997) used thermal conversion of PAN to NO_2 to generate a signal of PAN + NO_2 on a luminol detector and subtracted the signal obtained from NO_2 alone by bypassing the thermal converter; PAN was obtained by subtraction. Gaffney et al. (1998) have suggested a method combining chromatographic separation of NO_2, PAN, MPAN, and PBN (peroxybutyryl nitrate) on a 3-m-long, 0.53-mm-diameter capillary column and a modified commercial luminol-based nitrogen dioxide detector for field measurements. The column is coated with 3 μm of DB-1 stationary phase and operated at room temperature. Helium is used as the carrier gas for 1- to 5-mL samples to obtain a chromatogram in 1 min and to achieve a sensitivity in the tens of pptv with synthetic samples. Field measurements of PAN, PPN, and MPAN are now being made with capillary column/ECD systems at total uncertainties of ± 5 pptv + 15%) to infer the contributions of biogenic and anthropogenic sources to ozone formation (Roberts et al., 1998). Detection limits as low as 5 pptv have been achieved. Williams et al. (2000) extended the GC/ECD approach to airborne measurements of PAN, MPAN, and PPN.

While ECDs have been used for many years as chromatographic detectors for PANs and other organic nitrates, the use of radioactive material, typically ^{63}Ni, is coming under increasing scrutiny and restriction. Zedda et al. (1998) have recently applied a new pulsed discharge electron capture detector to the measurement of PAN, PPN, and other atmospheric nitrates. The new detector employs no radioactive components and therefore requires no special consideration for transport and use at field sites.

5.7.2 Gas Chromatography/Negative Ion Chemical Ionization Mass Spectrometry

Tanimoto et al. (1999) report the measurement of PAN, PPN, and MPAN at pptv levels by gas chromatography/negative ion chemical ionization mass spectrometry. For PAN the detection limit is given as 15 pptv with good linearity at the pptv levels. All three compounds are measured within 10 min.

5.7.3 Method Recommendations for PAN, PPN, MPAN, and other Organic Nitrates

PAN and other organic nitrates are monitored using capillary columns for separation and sensitive detectors such as the luminol-based chemiluminescence system or the ECD for detection. These units can be assembled from commercially available products. The sample integrity of PAN during a measurement is subject to its thermal decomposition in the measurement instrument and to potential interferences even in the presence of gas chromatographic separation. Careful experimental and calibration techniques are required to accurately measure PAN and PAN-like compounds, so any routine or network application should only be attempted with a high level of dedication and preparation.

5.8 Methods for Monitoring the Nitrate Radical

The free radical NO_3 is highly reactive and its contribution to NO_Y is generally negligible. However, it is important in nighttime atmospheric chemistry because it oxidizes many primary organic pollutants to form nitric acid, peroxy radicals,

and other products. Platt et al. (1980) recorded the diurnal variations of NO_3 using the DOAS technique. A recent paper (Geyer, 1999) lists the various techniques and shows a favorable comparison between the two most frequently used, i.e., DOAS and matrix isolation electron spin resonance (MIESR). King et al. (2000) describe the first use of cavity ring-down spectroscopy (CRDS) to detect NO_3 in the laboratory with a system achieving a noise equivalent mixing ratio of 2 pptv for a 30-s averaging period.

5.8.1 Method Recommendations For the Nitrate Radical

Research-grade DOAS systems have been used recently in summer intensive studies by the Southern Oxidants Study group and appears to be the best available method.

Chapter 6
Use of Commercially Available Systems for NO_2 Monitoring in the Nashville SOS '99 Study

by

K. Kronmiller and M. Wheeler
ManTech Environmental Technology, Inc.

Interest in gathering information on NO_2 monitoring technology led EPA to participate in the SOS '99 summer field study in Nashville, TN, at the Cornelia Fort site northeast of midtown Nashville. Three other groups were using research-grade instrumentation for the reactive nitrogen oxides at this site. The EPA effort was organized by W.A. McClenny of the Atmospheric Methods and Monitoring Branch, Human Exposure and Atmospheric Sciences Division, National Exposure Research Laboratory, Office of Research and Development, U.S. EPA, and the site coordinator, E.J. Williams of the NOAA Agronomy Laboratory. EPA contractor ManTech Environmental Technology, Inc., prepared and operated commercial instrumentation, in some cases with modifications, for NO_Y, NO_X, NO_2, and NO monitoring. This activity resulted in valuable field monitoring experience and in a database for certain commercial and modified commercial instruments for monitoring nitrogen oxides. Additional monitoring was carried out after the field study at the EPA facility in Research Triangle Park, NC, in order to repeat the types of monitoring executed in Nashville.

Three monitoring systems were operated inside one of the office trailers located at the base of the sampling tower at the Cornelia Fort site. One system consisted of a Model LMA-3 luminol-based NO_2 monitor (Scintrex, Toronto, Canada) with a sampling train designed with alternate routes to condition the sample air before entering the instrument's reaction chamber (Spicer, et al., 1995). This monitoring arrangement is explained more fully in Appendix E. The gases NO_2, NO_X, and NO_Y could be monitored in sequence by using the different sampling routes. Each monitoring mode was maintained for 5 min and repeated every 15 min. The conditioned sample air was also monitored using a TEI Model 42 chemiluminescence monitor with internal thermal converter (Thermo Environmental Instruments, Franklin, MA). The TEI Model 42 provided NO, NO_2, and NO_Y during the first 5 min (no conditioning) of each 15-min cycle. A third monitoring system, a TEI Model 42C was operated inside the office trailer with a Mo thermal converter mounted on the sampling tower. This unit was used to obtain some of the NO_Y measurements shown below.

A fourth system, a commercially available UV/DOAS open-path monitoring system (OPSIS, Furulund, Sweden), of a similar type to the research system described in Appendix B was operated adjacent to the sampling tower at Cornelia Fort. A source/receiver was placed at one end of the monitoring path and a corner-cube retroreflector at the opposite end so as to establish a 200-m total optical open path at an average aboveground height of 3 m. This system provided essentially real-time measurements of ambient NO_2 by measuring the differential absorption of UV/visible radiation along the measurement path.

Figure 6-1 shows the results of a monitoring comparison at the Cornelia Fort during the period 28 June through 5 July 1999 using three of the instruments described above. Figure 6-2 shows the results of a monitoring comparison at the EPA facility in Research Triangle Park, NC, after the Nashville summer study during the period 4–11 October 1999. The same three instruments were used, although the height of the optical path length for the path monitor averaged the same as the inlet height of the point monitors, i.e., 3 m. In both figures, NO_2 is monitored with sufficient accuracy to establish compliance with the NAAQS for NO_2, i.e., an annual average concentration of less than 53 ppbv. However, it is obvious that the monitoring requirements cited in Chapter 4 for modeling, i.e., ±10% at 1 ppbv and above, is not uniformly achieved. Signal offsets occurred at the lower end of the monitoring range and instrument problems caused the loss of a number of monitoring sequences. Since the LMA-3 was

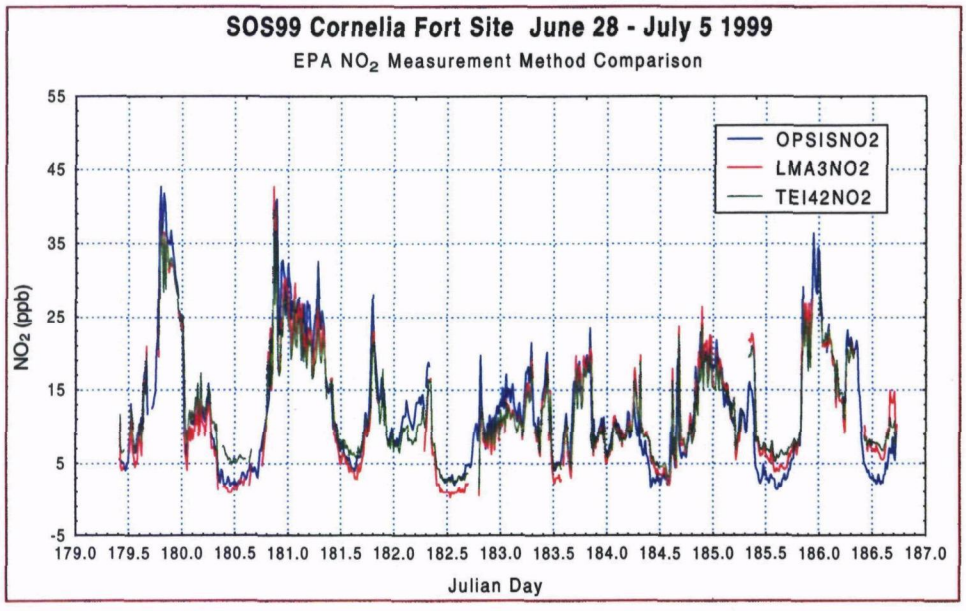

Figure 6-1. Results of a monitoring comparison at the Cornelia Fort during the period 28 June–5 July 1999. Three instruments were used: the UV/DOAS system (OPSIS, Furulund, Sweden) with a 200-m total optical open pathlength at an average aboveground height of 8 ft and two point monitors, the LMA-3 (Scintrex, Toronto, Canada) and the TEI 42 (Thermo Engineering Instruments, Waltham, MA), at a height of 30 m.

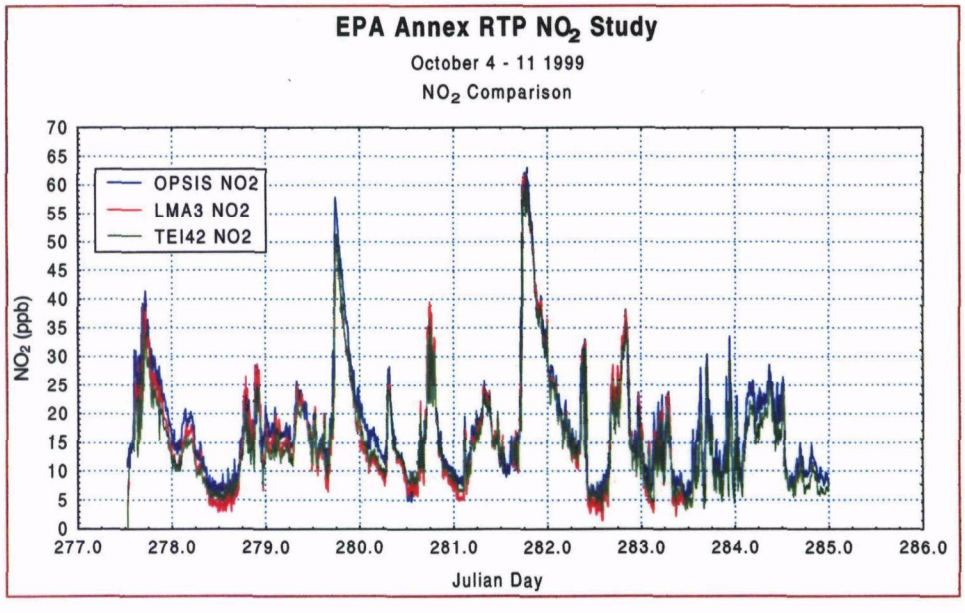

Figure 6-2. Results of a monitoring comparison at the EPA facility in Research Triangle Park, NC, during the period 4–11 October 1999 using the same instruments as in Figure 6-1.

calibrated at high concentrations and corrections for the response nonlinearity (lower slope of response vs. concentration at low concentrations), the lower readings for the LMA-3 are understandable. If not for this effect, the OPSIS and LMA-3 readings should be comparable and somewhat lower than the TEI Model 42 since the Model 42 is responding to $NO_Y - NO$ and therefore establishing an upper bound to NO_2.

Figure 6-3 shows a data comparison for a 24-h period (20–21 June 1999) during the Nashville SOS '99 study between the UV/DOAS system and two research-grade instruments, one based on LIF and the other on NO, O_3 chemiluminescence with photolytic conversion of NO_2 (see Appendices). All these systems are essentially real time and, aside from the difference in height (3 m for the open path and 30 m for the inlet to the point monitors), the readings should agree. As noted on the figure, the average value for those times at which all three monitors were operating is extremely close. Differences between the point and path monitors are also evident, although these differences may be due to the distribution of NO_2 with height. The correlation of responses in time show both positive and negative differences, which would not be the case for a true bias.

Figures 6-4 and 6-5 show comparisons of two chemiluminescence instruments and the LMA-3 for NO_Y. Again the LMA-3 appears to read somewhat low at low concentrations of NO_2 for reasons noted above. However, as shown in these figures, the average value of data from the three units is within 12 ppbv for each of the monitoring sequences. Differences at the low-ppbv levels observed during the daytime and at certain other times are greater than the modeling requirements of ±20% for concentrations ≥ 1 ppbv.

These experimental measurements indicated that commercial instruments as operated in the studies agreed with research-grade instruments to the extent that the conclusions for NAAQS monitoring and trends monitoring of daily averages or maximum values would be valid using either. However, biases due to uncorrected nonlinear response and the possibility of uncompensated interferences from PAN and O_3 in the LMA-3 and from NO_Z compounds in the TEI Model 42 prevent the agreement of the three monitors during periods when NO_2 concentrations are low and photochemical activity produces interfering NO_z compounds. Note from the Figures 6-1 and 6-2 that agreement among the three monitors was significantly better in October 1999 when photochemical activity was lower. The use of single-channel point monitors did not allow the high temporal resolution most desirable for diagnostic monitoring. Also, the time sharing of one channel to determine a difference measurement for NO_2 can lead to erroneous values during conditions of high NO_Y and NO concentration variability. Open-path measurements of NO_2 (3-m average above ground-level height) were made at a different height than the point monitors (30-m inlet) and were often at the stated detection level of the commercial instrument (1 ppbv over a 500-m path length or about 2.5 ppbv over the 200-m path length used) during daylight monitoring.

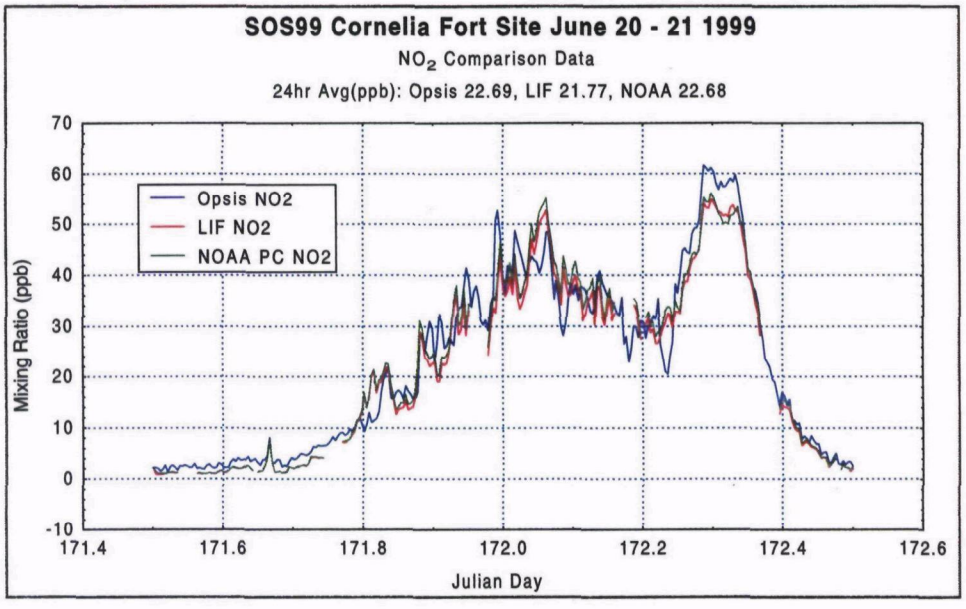

Figure 6-3. Results of comparison data for NO_2 over a 24-h period, 20–21 June 1999, at the Cornelia Fort site—UV/DOAS open-path monitor, LIF (Cohen, UC-Berkeley), and chemiluminescence monitor with photolytic converter (Williams, Aeronomy Laboratory, NOAA, Boulder, CO).

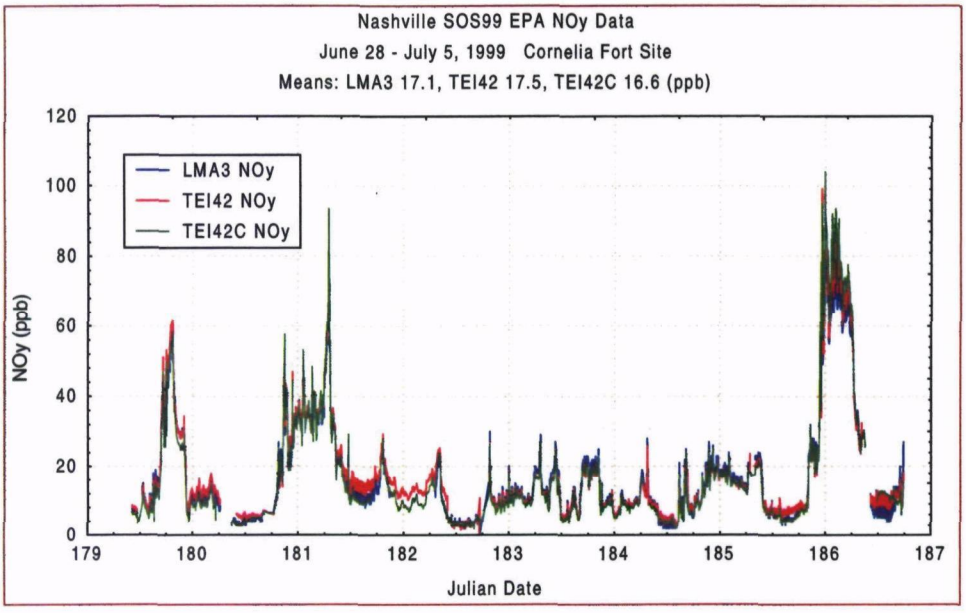

Figure 6-4. Results of comparison data for NO_Y during the period 28 June–5 July 1999 at the Cornelia Fort site—LMA-3, TEI 42, and TEI 42C.

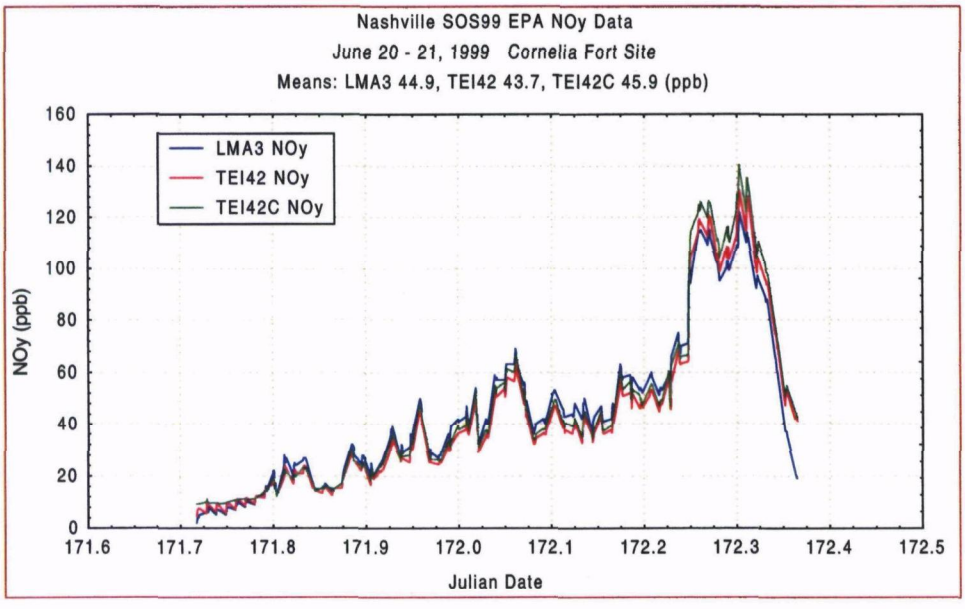

Figure 6-5. Results of comparison data for NO_Y during 20–21 June 1999 at the Cornelia Fort site—LMA-3, TEI 42, and TEI 42C.

Chapter 7
References

Allen, M.G., Carleton, K.L., Davis, S.J., Kessler, W.J., Otis, C.E., Palombo, D.A., and Sonnenfroh, D.M. 1995. Ultrasensitive dual-beam absorption and gain spectroscopy: Applications for near-infrared and visible diode laser sensors. *Appl. Opt.* 34(18):3240–3249.

Ammann, M., Kalberer, M., Jost, D.T., Tobler, L., Rossler, E., Piguet, D., Gaggeler, H.W., and Baltersperger, U. 1988. Heterogeneous production of nitrous acid on soot in polluted air masses. *Nature* 395:157.

Anlauf, K.G., Fellin, P., Wieve, H.A., Schiff, H.I., Mackay, G.I., Braman, R.S., and Gilbert, R. 1985. A comparison of three methods for measurement of atmospheric nitric acid and aerosol nitrate and ammonium. *Atmos. Environ.* 19:325–333.

Arnold, J.R., Dennis, Robin L., and Tonnesen, Gail S. 1998. Advanced techniques for evaluating Eulerian air quality models: Background and methodology. In *Preprints from the 10th Joint Conference on the Applications of Air Pollution Meteorology with the AWMA*, pp. 1–5, Phoenix, AZ. Boston: American Meteorological Society.

Atkinson, R., Baulch, D.L., Cox, R.A., Hampson, R.F., Kerr, J.A., Rossi, M.J., and Troe, J. 1997. Evaluated kinetic photochemical and heterogeneous data for atmospheric chemistry: supplement V, IUPAC subcommittee on gas kinetic data evaluation for atmospheric chemistry. *J. Phys. Chem. Ref. Data* 26:521–1011.

Blanchard, P., Shepson, P.B., Schiff, H.I., Bottenheim, J.W., Gallant, A.J., Drummond, J.W., and Wong, P. 1990. A comparison of calibration and measurement techniques for gas chromatographic determination of atmospheric peroxyacetyl nitrate (PAN). *Atmos. Environ.* 24A:2839–2846.

Blanchard, P., Shepson, P.B., Schiff, H.I., Drummond, J.W. 1993. Development of a gas chromatograph for trace level measurement of peroxyacetyl nitrate using chemical amplification. *Anal. Chem.* 65(18):2472–2477.

Bollinger, M.J. 1982. Chemiluminescent measurements of the oxides of nitrogen in the clean troposphere and atmospheric chemistry implications. Ph.D. thesis, Chemistry Department, University of Colorado, Boulder.

Braman, R.S., Shelley, T.J., and McClenny, W.A. 1982. Tungstic acid for preconcentration and determination of gaseous and particulate ammonia and nitric acid in ambient air. *Anal. Chem.* 54:358–364.

Buhr, S.M., Huhr, M.P., Fehsenfeld, F.C., Holloway, J.S., Karst, U., Norton, R.C., Parrish, D.D., and Sievers, R.E. 1995. Development of a semi-continuous method for the measurement of nitric acid vapor and particulate nitrate and sulfate. *Atmos. Environ.* 29(19): 2609-2624.

Burkhardt, M.R., Maniga, N.I., Stedman, D.H., and Paur, R.J. 1988. Gas chromatographic method for measuring nitrogen dioxide and peroxyacetyl nitrate in air without compressed gas cylinders. *Anal. Chem.* 60:816–819.

Butcher, S.S., and Ruff, R.E. 1971. Effect of inlet residence time on analysis of atmospheric nitrogen oxides and ozone. *Anal. Chem.* 43:1890–1892.

Byun, D.W., and Ching, J.K.S. 1999. *Science Algorithms of the EPA Models-3 Community Multiscale Air Quality (CMAQ) Modeling System.* U.S. EPA report no. EPA/600/R-99/30. Washington, DC: U.S. EPA, Office of Research and Development.

Chaney, L.W., Rickel, D.G., Russwurm, G.M., and McClenny, W.A. 1979. Long-path laser monitor for carbon monoxide: System improvements. *Appl. Opt.* 18:3004–3009.

Chang, T.Y., Chock, D.P., Nance, B.I., and Winkler, S.L. 1997. A photochemical extent parameter to aid ozone air quality management. *Atmos. Environ.* 31:2687–2794.

Cofer, W.R., III, Collins, V.G., Talbot, R.W. 1985. Improved aqueous scrubber for collection of soluble atmospheric trace gases. *Environ. Sci. Technol.* 19:557–560.

Copeland, H. TVA, Mussel Shoals, AL, personal communication, September 1999.

Danalatos, D., and Glavas, S. 1997. Improvement in the use of capillary columns for ambient air peroxyacetyl nitrate monitoring. *J. Chromatogr. A* 786:361–365.

Dasgupta, P.K. and Philips, D.A. 1987. A diffusion scrubber for the collection of gaseous nitric acid. *Sep. Sci. Technol.* 22:1255–1267.

De Santis, F., Allegrini, I., Di Filippo, P., Pasella, D. 1996. Simultaneous determination of nitrogen dioxide and peroxyacetyl nitrate in ambient atmosphere by carbon-coated annular diffusion denuder. *Atmos. Environ.* 30(14):2637–2645.

Delany, A.C., Dickerson, R.R., Melchoir, F.L., Jr., and Wartburg, A.F. 1982. Modification of a commercial NO_X detector for high sensitivity. *Rev. Sci. Instrum.* 53:1899–1902.

Dennis, R.L. 1998. The Environmental Protection Agency's third generation air quality modeling system: An overall perspective. In *Preprints from the 10th Joint Conference on the Applications of Air Pollution Meteorology with the AWMA*, pp. 225–258, Phoenix, AZ: American Meteorological Society.

Dennis, R.L., Arnold, J.R., and Tonnesen, G.S. 2000. Probing the shores of ignorance. In *Forecasting Environmental Change*, ed., M.B. Beck. New York: Elsevier Press (in press).

Dentener, F.J., and Crutzen, P.J. 1993. Reaction of N_2O_5 on tropospheric aerosols: Impact on global distributions of NO_X, O_3, and OH. *J. Geophys. Res.* 98:7149–7163.

Dickerson, R.R., Delany, A.C., and Wartburg, A.F. 1984. Further modification of a commercial NO_X detector for high sensitivity. *Rev. Sci. Instrum.* 55:1995–1998.

Dodge, M.C. 1977. Combined use of modeling techniques and smog chamber data to derive ozone precursor relationships. In *Proceedings of the International Conference on Photochemical Oxidant Pollution and Its Control*, ed., B. Dimitriades, U.S. EPA report no. EPA-600/3-77-001b. Research Triangle Park, NC: U.S. EPA, Office of Research and Development.

Drummond, J.W., Volz, A., and Ehhalt, D.H. 1985. An optimized chemiluminescence detector for tropospheric NO measurements. *J. Atmos. Chem.* 2:287–306.

Edner, Hans, Ragnarson, Pär, Spännare, Stefan, and Svanbery, Sune. 1993. Differential optical absorption spectroscopy (DOAS) system for urban atmospheric pollution monitoring. *Appl. Opt.* 32(3):327–333.

Fahey, D.W., Eubank, C.S., Hubler, G., and Fehsenfeld, F.C. 1985. Evaluation of a catalytic reduction technique for the measurement of total reactive odd-nitrogen NO_Y in the atmosphere. *J. Atmos. Chem.* 3:435–468.

Febo, A., Perrino, C., and Allegrini, Il. 1996. Measurement of nitrous acid in Milan, Italy, by DOAS and diffusion denuders. *Atmos. Environ.* 30(21):3599–3609.

Federal Register. October 27, 1998. 63(207):57355–57404.

Fehsenfeld, F.C., Dickerson, R.R., Hubler, G., Luke, W.T., Nunnermacker, L.J., Williams, E.J., Roberts, J.M., Calvert, J.G., Curran, C.M., Delany, A.C., Eubank, C.S., Fahey, D.W., Fried, A., Gandrud, B.W., Langford, A.O., Murphy, P.C., Norton, R.B., Pickering, K.E., and Ridley, B.A. 1987. A ground-based intercomparison of NO, NO_X, and NO_Y measurement techniques. *J. Geophys. Res.* 92:14710–14722.

Fehsenfeld, F.C., Drummond, J.W., Roychowdhury, U.K., Galvin, P.J., Williams, E.J., Buhr, M.P., Parrish, D.D., Hubler, G., Langford, A.O., Calvert, J.G., Ridley, B.A., Grahek, F., Heikes, B.G., Kok, G.L., Shetter, J.D., Walega, J.G., Elsworth, C.M., Norton, R.B., Fahey, D.W., Murphy, P.C., Hovermale, C., Mohnen, V.A., Demerjian, K.L., Mackay, G.I., and Schiff, H.I. 1990. Intercomparison of NO_2 measurement techniques. *J. Geophys. Res.* 95(D4):3579–3597.

Fehsenfeld, F.C., Huey, L.G., Sueper, D.T., Norton, R.B.,Williams, E.J., Eisele, F.L., Mauldin, R.L., III, and Tanner, D.J. 1998. Ground-based intercomparison of nitric acid measurement techniques. *J. Geophys. Res.* 103(D3):3343–3353.

Fetzer, Gregory J., Miao, Linshi, Chilla, Juan L.A., Pikal, Jon M., and Menoni, Carmen S. 1998. NO_2 photometer based on solid-state light sources. *Appl. Opt.* 37(24):5590–5595.

Fincher, C.L., Tucker, A.W., Birnbaum, M., Paur, R.J., and McClenny, W.A. 1977. Fluorescence ambient NO_2 monitor with flashlamp pumping. *Appl. Opt.* 16(May):1359–1365.

Fontijn, A., Sabadell, A.J., and Ronco, R.J. 1970. Homogeneous chemiluminescent measurement of nitric oxide with ozone:

Implications for continuous selective monitoring of gaseous air pollutants. *Anal. Chem.* 42:575–579.

Fox, D.G. 1984. Uncertainty in air quality modeling: A summary of the AMS workshop (September 1982, Woods Hole, MA) on quantifying and communicating model uncertainty. *Bull. Am. Met. Soc.* 65:27–36.

Gaffney, J.S., Bornick, R.M., Chen, Y.-H., and Marley, N.A. 1998. Capillary gas chromatographic analysis of nitrogen dioxide and PANs with luminol chemiluminescent detection. *Atmos. Environ.* 32(8):1445–1454.

Gaffney, J.S., Marley, N.A., Steele, H.D., Drayton, P.J., and Hubbe, J.M. 1999. Aircraft measurements of nitrogen dioxide and peroxyacyl nitrates using luminol chemiluminescence with fast capillary gas chromatography. Environ. Sci. Technol. 33(19):3285–3289.

Gao, R.S., Keim, E.R., Woodbridge, E.L., Ciciora, S.J., Proffitt, M.H., Thompson, T.L., Mclaughlin, R.J., Fahey, D.W. 1994. New photolysis system for NO_2 measurements in the lower stratosphere. *J. Geophys. Res.* 99(D10):20673–20681.

Gelbwachs, J.A., Birnbaum, M., Tucker, A.W., and Fincher, C.L. 1972. Fluorescence determination of atmospheric NO_2. *Optoelectron.* 4:155–157.

Geyer, A., Alicke, B., Mihelcic, D., Stutz, J., and Platt, U. 1999. Comparison of tropospheric NO_3 radical measurements by differential optical absorption spectroscopy and matrix isolation electron spin resonance. *J. Geophys. Res.* 104(D21):26097–26105.

Gipson, G. 1999. Chapter 16: Process analysis. In *Science Algorithms of the EPA Models-3 Community Multiscale Air Quality (CMAQ) Modeling System*, eds., D.W. Byun and J.K.S. Ching, U.S. EPA report no. EPA/600/R-99/30. Washington, DC: U.S. EPA, Office of Research and Development.

Gregory, G.L., Hoell, J.M., Jr., Carroll, M.A., Ridley, B.A., Davis, D.D., Bradshaw, J., Rodgers, M.O., Sandholm, S.T., Schiff, H.I., Hastie, D.R., Karecki, D.R., Mackay, G.I., Harris, G.W., Torres, A.L., and Fried, A. 1990a. An intercomparison of airborne nitrogen dioxide instruments. *J. Geophys. Res.* 95(D7):10103–10127.

Gregory, G.L., Hoell, J.M., Ridley, B.A., Singh, H.B., Gandrud, B., Salas, L.J., and Shetter, J. 1990b. An intercomparison of airborne PAN measurements. *J. Geophys. Res.* 95:10077–10087.

Harrison, R.M., Grenfell, J.L., Yamulki, S., Clemitshaw, K.C., Pendett, S.A., Cape, J.N., and McFadyen, G.G. 1999. Budget of NO_Y species measured at a coastal site. *Atmos. Environ.* 33:4255–4272.

Helton, J., and Burmaster, D.E. 1996. On the treatment of aleatory and epistemic uncertainty in performance assessment for complex systems. *Reliability Engineering and Systems Safety*, Special Issue 54:91–94.

Hering, S.V., Lawson, D.R., Allegrini, I., Febo, A., Perrino, C., Possanzini, M., Sickles, J.E., II, Anlauf, K.G., Wiebe, A., Appel, B.R., John, W., Ondo, J., Wall, S., Braman, R.S., Sutton, R., Cass, G.R., Solomon, P.A., Eatough, D.J., Eatough, N.L., Ellis, E.C., Grosjean, D., Hicks, B.B., Womack, J.D., Horrocks, J., Knapp, K.T., Ellestad, T.G., Paur, R.J., Mitchell, W.J., Pleasant, M., Peake, E., Maclean, A., Pierson, W.R., Brachaczek, W., Schff, H.I., Mackay, G.I., Spicer, C.W., Stedman, D.H., Winer, A.M., Biermann, H.W., and Tuazon, E.C. 1988. The nitric acid shootout: Field comparison of measurement methods. *Atmos. Environ.* 22:1519–1539.

Hoell, J.M., Jr., Gregory, G.L., McDougal, D.S., Torres, A.L., Davis, D.D., Bradshaw, J., Rodgers, M.O., Ridley, B.A., and Carroll, M.A. 1987. Airborne intercomparison of nitric oxide measurement techniques. *J. Geophys. Res.* 92:1995–2008.

Huey, L.G., Dunlea, E.J., Lovejoy, E.R., Hanson, D.R., Norton, R.B., Fehsenfeld, F.C., and Howard, C.J. 1998. Fast time response measurements of HNO_3 in air with a chemical ionization mass spectrometer. *J. Geophys. Res.* 103(D3):3355–3360.

Jeffries, H.E., and Tonnesen, G.S. 1994. A comparison of two photochemical reaction mechanisms using mass balance and process analysis. *Atmos. Environ.* 28:2991–3003.

Jung, J., and Kowalski, J. 1986. Direct ambient nitrogen dioxide measurement by visible light absorption. In *Proceedings of the EPA/APCA Symposium on Measurement of Toxic Air Pollutants*, Raleigh, NC, APCA publication VIP-7 (EPA Report No. 600/9-86-013).

Kanda, U., and Taira, M. 1992. Simultaneous determination of atmospheric nitric acid and nitrous acid by reduction with hydrazine and ascorbic acid with chemiluminescence detection. *Analyst* 117:883–887..

Kelly, T.J., Spicer, C.W., and Ward, G.F. 1990. An assessment of the luminol chemiluminescence technique for measurement of NO_2 in ambient air. *Atmos. Environ.* 24A(9):2397–2403.

Keuken, M.P., Schoonebeek, C.A.M., Van Wensveen-Louter, A., and Slanina, J. 1988. Simultaneous sampling of NH_3, HNO_3, HCl, SO_2, and H_2O_2 in ambient air by wet annular denuder system. *Atmos. Environ.* 22:2541–2548.

Khlystov, A., Wyers, G.P., and Slanina, J. 1995. The steam-jet aerosol collector. *Atmos. Environ.* 29(17):2229–2234.

King, M.D., Dick, E.M., and Simpson, W.R. 2000. A new method for the atmospheric detection of the nitrate radical (NO_3). *Atmos. Environ.* 34:685–688.

Kleindienst, T.E. 1994. Recent developments in the chemistry and biology of peroxyacetyl nitrate. *Res. Chem. Intermed.* 20:335–384.

Kleinman, L.I. 1994. Low- and high-NOx tropospheric photochemistry. *J. Geophys. Res.* 99:16831–16838.

Kliner, D.A., Daube, B.C., Burley, J.D., and Wofsy, S.C. 1997. Laboratory investigation of the catalytic reduction technique for measurement of atmospheric NO_Y, *J. Geopyhs. Res.* 102(D9): 10759–10776.

Klockow, D., Niessner, R., Malejczyk, M., Kiendl, H., Berg, B. vom, Keuken, M.P., Wayers-Ypelaan, and Slanina, J. 1989. Determination of nitric acid and ammonium nitrate by means of a computer-controlled thermodenuder system. *Atmos. Environ.* 23(5):1131–1138.

Li, Y., Dennis, R.L., Tonnesen, G.S., and Pleim, J.E. 1998. Regional ozone concentrations and production efficiency as affected by meteorological parameters in the Regional Acid Deposition Modeling system. In *Preprints from the 10th Joint Conference on the Applications of Air Pollution Meteorology with the AWMA.* Phoenix, AZ: American Meteorological Society.

Maeda, U.K., Aoki, K., and Munemori, M. 1980. Chemiluminescence method for the determination of nitrogen dioxide. *Anal. Chem.* 52:307–311.

Mauldin, R.L., Tanner, D.J., and Eisele, F.L. 1998. A new chemical ionization mass spectrometer technique for the fast measurement of gas-phase nitric acid in the atmosphere. *J. Geophys. Res.* 103(D3):3361–3367.

McClenny, W.A., Gailey, P.C., Braman, R.S., and Shelley, T.J. 1982. Tungstic acid technique for monitoring nitric acid and ammonia in ambient air. *Anal. Chem.* 54:365–369.

McElroy, F.F., Hodgeson, J., Lumpkin, T.A., Rehme, K.A., Stevens, R.K., Conner, C.P., and Hallstadius, H. 1993. Simultaneous calibration of open-path and conventional point monitors for measuring ambient air concentrations of sulfur dioxide, ozone, and nitrogen dioxide. In *Proceedings of the International Specialty Conference on Optical Sensing for Environmental Monitoring*, Atlanta, GA, October 11–14, 1993 AWMA publication SP-89. Pittsburgh, PA: Air &Waste Management Association.

McRae, G.J., Goodin, W.R., and Seinfeld, J.H. 1982. Development of a second-generation mathematical model for urban air pollution—I. Model formulation. *Atmos. Environ.* 16:679–696.

Mihalcea, R.M., Baer, D.S., and Hanson, R.K. 1996. Tunable diode-laser absorption measurements of NO_2 near 670 and 395 nm. *Appl. Opt.* 35(21):4059–4064.

National Research Council. 1991. *Rethinking the Ozone Problem in Urban and Regional Air Pollution.* Washington, DC: National Academy Press.

Nikitas, C., Clemitshaw, K.C., Oram, D.E., and Penkett, S.A. 1997. Measurements of PAN in the polluted boundary layer and free troposphere using a luminol-NO_2 detector combined with a thermal converter. *J. Atmos. Chem.* 28:339–359.

Oms, M.T., Jongejan, P.A.C., Veltkamp, A.C., Wyers, G.P., and Slanina, J. 1996. Continuous monitoring of atmospheric HCl, HNO_2, HNO_3, and SO_2 by wet-annular denuder air sampling with on-line chromatographic analysis. *Int. J. Environ. Anal. Chem.* 62:207–218.

Parrish, D.D., Buhr, M.P., Trainer, M., Norton, R.B., Shimshock, J.P., Fehsenfeld, F.C., Anlauf, A.G., Bottenheim, J.W., Tang, Y.Z., Wiebe, H.A., Roberts, J.M., Tanner, R.L., Newman, L., Bowersox, V.C., Olszyna, K.J., Bailey, E.M., Rodgers, M.O., Wang, T., Berresheim, H., Roychowdhury, U.K., and Demerjian, K. 1993. The total reactive oxidized nitrogen levels and the partitioning between the individual species at six rural sites in Eastern North America. *J. Geophys. Res.* 98:2927–2939.

Parrish, D.D., and Fehsenfeld, F.C. 2000. Methods for gas-phase measurements of ozone, ozone, precursors, and aerosol precursors. *Atmos. Environ.* 34(12–14):1853–2332.

Plane, John M.C., and Nien, Chia-Fu. 1992. Differential optical absorption spectrometer for measuring atmospheric trace gases. *Rev. Sci. Instrum.* 63(3):1867–1876.

Platt, U. 1994. Differential optical absorption spectroscopy (DOAS). In Monitoring by Spectroscopic Techniques, ed. M.W. Sigrist. New York: John Wiley.

Platt, U., Perner, D., Harris, G.W., Winer, A.M., and Pitts, J.M. 1980. Detection of NO_3 in the polluted troposphere by differential optical absorption. *Geophys. Res. Lett.* 7:89–92.

Reynolds, S.D., Roth, P.M., and Tesche, T.W. 1994. *A Process for the Stressful Evaluation of Photochemical Model Performance.* Glendale, CA: Western States Petroleum Association.

Ridley, B.A., Carroll, M.A., Gregory, G.L., and Sasche, G.W. 1988a. NO and NO_2 in the troposphere: Technique and measurements in regions of a folded tropopause. *J. Geophys. Res.* 93:15813–15830.

Ridley, B.A., Carroll, M.A., Torres, A.L., Condon, E.P., Sachse, G.W., Hill, G.F., and Gregory, G.L. 1988b. An intercomparison of results from ferrous sulphate and photolytic converter techniques for measurements of NO_X made during the NASA CTE/CITE 1 aircraft program. *J. Geophys. Res.* 93(D12): 15803–15811.

Ried, J., El-Sherbiny, M., Garside, B.K., and Ballik, E.A., 1980. Sensitivity limits of a tunable diode laser spectrometer with application to the detection of NO_2 at the 100 ppt level. *Appl. Opt.* 19:3349–3354.

Roberts, J.M., Norton, R.B., Goldan, P.D., and Fehsenfeld, F.C. 1987. Evaluation of the tungsten oxide denuder tube technique as a method for the measurement of low concentrations of nitric acid in the troposphere. *J. Atmos. Chem.* 5:217–238.

Roberts, J.M., Fajer, R.W., and Springston, S.R. 1989. Capillary gas chromatographic separation of alkyl nitrates and peroxycarboxylic nitric anhydrides. *Anal. Chem.* 61:771–772.

Roberts, J.M., and Bertman, S.B. 1992. The thermal decomposition of peroxyacetic nitric anhydride (PAN) and peroxymethacrylic nitric anhydride (MPAN). *Int. J. Chem. Kinet.* 24:297–307.

Roberts, J.M., Williams, J., Baumann, K., Buhr, M.P., Goldan, P.D., Holloway, J., Hubler, G., Kuster, W.C., McKeen, S.A., Ryerson, T.B., Trainer, M., Williams, E.J., Fehsenfeld, F.C., Bertman, S.B., Nouaime, G., Seaver, C., Grodzinsky, G., Rodgers, M., and Young, V.L. 1998. Measurements of PAN, PPN, and MPAN made during the 1994 and 1995 Nashville Intensives of the Southern Oxidant Study: Implications for regional ozone production from biogenic hydrocarbons. *J. Geophys. Res.* (Atmos.) 103(D17):22473–22490.

Russell, A.G., and Dennis, R.L. 2000. NARSTO critical review of photochemical models and modeling. *Atmos. Environ.* (in press).

Russwurm, G.M. 1988. Development of tunable diode laser: A reference method for nitrogen species. Research Triangle Park, NC: Northrop Services, Inc.–Environmental Sciences.

Russwurm, G.M., and Phillips, B. 1999. Effects of a nonlinear response of the Fourier-transform infrared open-path instrument on the measurements of some atmospheric gases. *Appl. Opt.* 38(30):6398–6407.

Ryerson, T.B., Williams, E.J., and Fehsenfeld, F.C. 2000. An efficient photolysis system for fast-response NO_2 measurements. *J. Geophys. Res.* (Atmos.) (in press).

Saltelli, A., and Scott, M. 1997. The role of sensitivity analysis in the corroboration of models and its links to model structural and parametric uncertainty. *Reliability Engineering and Systems Safety* 52:1–4.

Schiff, H.I., Hastie, D.R., Mackay, G.I., Iguchi, T., and Ridley, B.A. 1983. Tunable diode laser systems for measuring trace gases in tropospheric air. *Environ. Sci. Technol.* 17:353A–364A.

Schmidt, R.W.H., Kames, J., Kanter, H.J., Schurath, U., and Slemr, F. 1995. A selective ozone scrubber for application in ambient nitrogen dioxide measurements using the commercial Luminox (LMA-3, Scintrex/Unisearch Inc.). *Atmos. Environ.* 29(8):947–950.

Seinfeld, J.H. 1988. Ozone air quality models: A critical review. *J. Air Pollut. Control Assoc.* 38:616–645.

Seinfeld, J.H., and Pandis, S. 1998. *Atmospheric Chemistry and Physics: From Air Pollution to Climate Change.* New York: Wiley.

Sickles, J.E., II. 1992. Chapter 2: Sampling and analysis for ambient oxides of nitrogen and related species. In *Gaseous Pollutants: Characterization and Cycling,* ed., Jerome O. Nriagu. New York: John Wiley & Sons, Inc.

Sickles, J.E., II, Hodson, L.L., McClenny, W.A., Paur, R.J., Ellestad, T.G., Mulik, J.D., Anlauf, K.G., Wiebe, H.A., Mackay, G.I., Schiff, H.I., and Bubacz, D.K. 1990. Field comparison of methods for the measurement of gaseous and particulate contributors to acidic dry deposition. *Atmos. Environ.* 24A(1): 155–165.

Sillman, S., Logan, J.A., and Wofsy, S.C. 1990. The sensitivity of ozone to nitrogen oxides and hydrocarbons in regional ozone episodes. *J. Geophys. Res.* 95(D2):1837–1851.

Sillman, S. 1995. The use of NO_Y, H_2O_2, and HNO_3 as indicators for O_3-NO_X-HC sensitivity in urban locations. *J. Geophys. Res.* 100(D7):14175–14188.

Simon, P.K., and Dasgupta, P. 1993. Wet effluent denuder coupled liquid/ion chromatography systems: Annular and parallel plate denuders. *Anal. Chem.* 65:1134–1139.

Simon, P.K., and Dasgupta, P. 1995a. Continuous automated measurement of gaseous nitric and nitrous acids and particulate nitrite and nitrate. *Environ. Sci. Technol.* 29:1534–1541.

Simon, P.K., and Dasgupta, P. 1995b. Continuous automated measurement of the soluble fraction of atmospheric particulate matter. *Anal. Chem.* 67:71–78.

Sistla, G., Zhou, N., Hao, W., Ku, J., Rao, S.T., Bornstein, R., Freedman, F., and Thusis, P. 1996. Effects of uncertainties in meteorological inputs on Urban Airshed Model predictions and ozone control strategies. *Atmos. Environ.* 30:2011–2055.

Sonnenfroh, D.M., and Allen, Mark G. 1996. Ultrasensitive, visible tunable diode laser detection of NO_2. *Appl. Opt.* 35(21):4053–4058.

Spicer, C.W. Howes, J.E., Jr., Bishop, T.A., Arnold, L.H., and Stevens, R.K. 1982. Nitric acid measurement methods: An intercomparison. *Atmos. Environ.* 16:1487–1500.

Spicer, C.W., Joseph, D.W., and Schumacher, P.M. 1985. Determination of nitrate in atmospheric particulate matter by thermal decomposition and chemiluminescence. *Anal. Chem.* 57:2338–2341.

Spicer, C.W., Kelly, T.J., and Ward, G.F. 1995. *An Evaluation of Two Approaches for Improved Nitrogen Oxides Monitoring in Urban Atmospheres,* U.S. EPA report no. EPA-600/R-95/031. Columbus, OH: Battelle, EPA Contract 68-DO-0007.

Steffenson, D.M., and Stedman, D.H. 1974. Optimization of the operating parameters of chemiluminescent nitric oxide detectors. *Anal. Chem.* 46:1704–1709.

Stevens, R.K., Drago, R.J., and Mamane, Y. 1993. A long path differential optical absorption spectrometer and EPA-approved fixed-point methods intercomparison. *Atmos. Environ.* 27B: 231–236.

Stolzenburg, M.R., and Hering, S.V. 2000. Method for the automated measurement of fine particle nitrate in the atmosphere. *Environ. Sci. Technol.* (in press).

Taira, M., and Kanda, Y. 1993. Wet effluent diffusion denuder for sampling of atmospheric gaseous nitric acid. *Anal. Chem.* 65:3171–3173.

Talbot, R.W., Vijgen, A.S., and Harriss, R.C. 1990. Measuring tropospheric HNO_3: Problems and prospects for nylon filter and mist chamber techniques. *J. Geophys. Res.* 95(D6):7553–7561.

Tanimoto, H., Hirokawa, J., Kajii, U., and Akimoto, H. 1999. A new measurement technique of peroxyacetyl nitrate at part per trillion by volume levels: Gas chromatography/negative ion chemical ionization mass spectrometry. J. Geophys. Res. 104 (D17):21343–21354.

Tanner, R.L., Valente, R.J., and Meagher, J.F. 1998. Measuring inorganic nitrate species with short time resolution from an aircraft platform by dual-channel ozone chemiluminescence. *J. Geophys. Res.* 103(D17):22387–22395.

Tesche, T.W., Roth, P.W., Reynolds, S.D., and Lurmann, F.W. 1992. *Scientific Assessment of the Urban Airshed Model (UAM-IV).* Crested Butte, CO: Alpine Geophysics.

Tesche, T.W., and McNally, D.E. 1995. *Assessment of UAM-IV Model Performance for Three St. Louis Ozone Episodes.* Covington, KY: Alpine Geophysics, LLC.

Thornton, J.A., Wooldridge, P.J., and Cohen, R.C. 2000. Atmospheric NO_2: In situ laser-induced fluorescence detection at parts per trillion mixing ratios. *Anal. Chem.* 72:528–539.

Tonnesen, G.S. and Dennis, R.L. 2000a. Analysis of radical propagation efficiency to assess ozone sensitivity to hydrocarbons and NO_X. Part 1: Local indicators of instantaneous odd oxygen production sensitivity. *J. Geophys. Res.* (in press).

Tonnesen, G.S., and Dennis, R.L. 2000b. Analysis of radical propagation efficiency to assess ozone sensitivity to hydrocarbons and NO_X. Part 2: Long-lived species as indicators of ozone concentration sensitivity. *J. Geophys. Res.* (in press).

Tonnesen, G.S., and Jeffries, H.E. 1994. Inhibition of odd oxygen production in the Carbon Bond 4 and generic reaction set mechanisms. *Atmos. Environ.* 28:1339–1349.

Trainer, M., Parrish, D.D., Buhr, M.P., Norton, R.B., Fehsenfeld, F.C., Anlauf, K.G., Bottenheim, J.W., Tang, Y.Z., Wiebe, H.A., Roberts, J.M., Tanner, R.L., Newman, L., Bowersox, V.C., Meagher, J.F., Olszyna, K.J., Rodgers, M.O., Wang, T., Berresheim, H., Demerjian, K.L., and Roychowdhury, U.K. 1993. Correlation of ozone with NO_Y in photochemically aged air. *J. Geophys. Res.* 98:2917–2925.

Tuazon, E.C., Winer, A.M., and Pitts, J.N., Jr. 1981. Trace pollutant concentrations in a multiday smog episode in the California south coast air basin by long path length Fourier transform infrared spectroscopy. *Environ. Sci. Technol.* 15:1232–1237.

U.S. Environmental Protection Agency (U.S. EPA). 1991. *Guideline for Regulatory Application of the Urban Airshed Model*, U.S. EPA report no. EPA-450/4-91-013. Research Triangle Park, NC: Office of Air Quality Planning and Standards, Technical Support Division.

U.S. Environmental Protection Agency (U.S. EPA). 1993. *Air Quality Criteria for Oxides of Nitrogen*, U.S. EPA report no. EPA/600/8-91/049aF. Washington, D.C.: Office of Research and Development.

U.S. Environmental Protection Agency (U.S. EPA). March 1994. *Photochemical assessment monitoring stations implementation manual*, U.S. EPA report no. EPA-454/B-93-051. Research Triangle Park, NC: Office of Air Quality Planning and Standards.

U.S. Environmental Protection Agency (U.S. EPA). 1997. *Regulatory Impact Analyses for the Particulate Matter and Ozone National Ambient Air Quality Standards and Proposed Regional Haze Rule*. Research Triangle Park, NC: Office of Air Quality Planning and Standards (OAQPS).

Varns, J.L., Mulik, J.D., Sather, M.E., Lister, M.K., Glenn, G., Smith, L., Williams, D.D., Berz, E.A., and Hines, A.P. 1999. The Passive Ozone Network in Dallas (POND Concept)—A Modeling Opportunity with Community Involvement, poster presentation at the 31st Annual Air Pollution Workshop, April 26–29, Corvallis, OR.

Vecera, Z., and Dasgupta, P.K. 1991. Measurement of ambient nitrous acid and a reliable calibration source for gaseous nitrous acid. *Environ. Sci. Technol.* 25:255–260.

Vecera, Z., and Dasgupta, P.K. 1991. Measurement of atmospheric nitric and nitrous acids with a wet effluent diffusion denuder and low-pressure ion chromatograph-postcolumn reaction detection. *Anal. Chem.* 63:2210–2216.

Walega, J.G., Dye, J.E., Grahek, F.E., and Ridley, B.A. 1991. Compact measurement system for the simultaneous determination of NO, NO_2, NO_Y, and O_3 using a small aircraft. In *Proceedings of SPIE—The International Society of Optical Engineering*, 1433:232–241. Bellingham, WA: International Society for Optical Engineering.

Wendel, G.J., Stedman, D.H., and Cantrell, C.A. 1983. Luminol-based nitrogen dioxide detector. *Anal. Chem.* 55:937–940.

Williams, E. NOAA Agronomy Laboratory, personal communication, January 2000.

Williams, E.J., Baumann, K., Roberts, J.M., Bertman, S.B., Norton, R.B., Fehsenfeld, F.C., Springstone, S.R., Nunnermacker, L.J., Newman, L., Olszyna, K., Meagher, J., Bartsell, B., Edgerton, E., Person, J.R., and Rogers, M.O. 1998. Intercomparison of ground-based NO_Y measurement techniques. *J. Geophys. Res.* 103:22261–22280.

Williams, J., Roberts, J.M., Bertman, S.B., Stroud, C.A., Fehsenfeld, F.C., Baumann, K., Buhr, M.P., Knapp, K., Murphy, P.C., Nowick, M., and Williams, E.J. 2000. A method for the airborne measurement of PAN, PPN, and MPAN, in preparation for submission to *J. Geophys. Res.*

Winer, A.M., Peters, J.W., Smith, J.P., and Pitts, J.N., Jr. 1974. Response of commercial chemiluminescence NO-NO_X analyzers to other nitrogen-containing compounds. *Environ. Sci. Technol.* 8:1118–1121.

Yamamoto, M., and Kosaka, H. 1994. Determination of nitrate in deposited aerosol particles by thermal decomposition and chemiluminescence. *Anal. Chem.* 66:362–367.

Zedda, D., Keigley, G.W., Joseph, D.W., and Spicer, C.W. 1998. Development of a new high sensitivity monitor for peroxyacetyl nitrate and results from the west-central Mediterranean region. In *Air Pollution VI—Sixth International Conference on Air Pollution*, 79-88. eds., C.A. Brebbia, C.F. Ratto, and H. Power, Southampton: WIT Press.

Zellweger, C., Ammann, M., Hofer, P., and Baltensperger, U. 1999. NO_Y speciation with a combined wet effluent diffusion denuder aerosol collector coupled to ion chromatography. *Atmos. Environ.* 33:1131–1140.

Zhou, X., Qiao, H., Deng, G., and Civerolo, K. 1999. A method for the measurement of atmospheric HONO based on DNPH derivatization and HPLC analysis. *Environ. Sci. Technol.* 33:3672–3679.

Appendix A
Correction to Point Monitor Readings of O_3, NO, and NO_2 Due to the Reaction of NO and O_3 during Transport of Ambient Air to the Point of Measurement

by

William A. McClenny and Deborah J. Luecken
Human Exposure and Atmospheric Sciences Division, National Exposure Research Laboratory, U.S. EPA

The measurement of NO, NO_2, and O_3 by point monitors requires the transport of sample air from the ambient air through a length of tubing and eventually into the measurement region of the monitor. During this transport the gas-phase reaction of NO and O_3 occurs, leading to their mutual decrease and a corresponding equal increase in the NO_2 concentration. This is a widely recognized sampling artifact (Ridley et al., 1988a; Sickles, 1992) that should be minimized and/or accounted for to allow accurate monitoring of NO and NO_2 in ambient air. Butcher and Ruff (1971) showed there could be significant changes (changes greater than the precision of measurement) in these gas concentrations under certain situations, e.g., in rural air where ozone is high compared to NO and NO_2, an ambient temperature of 25 °C or higher is assumed, and a transport time on the order of 10 s occurs.

In revisiting this issue in order to correct monitoring data taken in Nashville during the 1999 Southern Oxidants Study (SOS '99) summer study, the reaction rate for NO and O_3 was taken from the latest compilation by Atkinson et al. (1997). This rate constant was used to determine losses of NO in the sampling manifold assuming a sample gas temperature of 30 °C (86 °F) corresponding to a hot day in the southeast USA. Significant percentage decreases in NO concentration were noted to occur in a sample containing high O_3 concentrations. Depending on ambient NO_2 concentrations, significant percentage increases in NO_2 could also occur in the sampling manifold. Since there is no official requirement referred to in the *Federal Register* other than that the residence time should be less than 20 s (40CFR58, Appendix E, Section 9), additional information has been developed to provide guidance in NO_2 monitoring using point monitors and is included in this report to clarify an important aspect of NO and NO_2 monitoring.

A.1 Development of Technical Guidance for NO_2 Monitoring

The ambient NO concentration is exponentially attenuated during transport through the inlet tubing by its reaction with ozone, such that, assuming a constant ozone concentration well above the NO and NO_2 concentrations, the final NO concentration is given by

$$[NO]_f = [NO]_i \exp(-k\,[O_3]_i\,t) \qquad \text{(A-1)}$$

where $[NO]_f$ = final (entrance to detection chamber) NO concentration in ppbv
$[NO]_i$ = initial (ambient) NO concentration in ppbv
k = 0.044267*exp(-1370/T) in 1/ppbv-s
T = temperature in °Kelvin; pressure assumed at 1 atm
$[O_3]_i$ = initial O_3 concentration in ppbv which is assumed constant
t = residence time in seconds

As examples of NO concentration losses, values of the ratio $[NO]_f/[NO]_i$ for 50 and 100 ppbv O_3 concentrations are shown in Figure A-1.

For an ozone concentration of 100 ppbv in air samples at temperatures of 30 °C, the residence time for ambient NO in a sampling line must be less than 2.20 s to limit the NO losses to10% (and 1.06 s to limit the NO losses to 5%). In reality, the ozone concentration decreases by the same amount as the NO concentration, and NO losses will be slightly less than predicted under the assumption of constant O_3 concentrations.

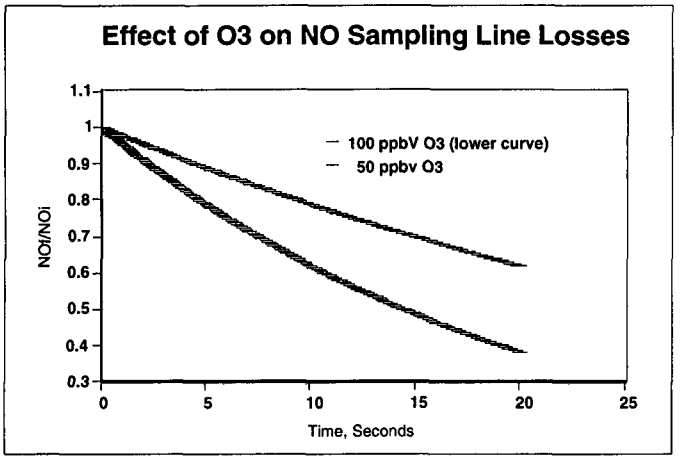

Figure A-1. *Effect of O_3 on NO sampling line losses.*

Short residence time values are not always achieved in practice. In such cases, a correction to the data should be made by rearranging Equation A-1, i.e., by multiplying the recorded NO concentrations, $[NO]_f$, by the factor $\exp(k\,[O_3]_i\,t)$:

$$[NO]_i = [NO]_f\,[\exp(k\,[O_3]_i\,t)] \qquad \text{(A-2)}$$

Also, the decrease in NO concentration $[NO]_f[\exp(k\,[O_3]_i\,t) - 1]$ must be subtracted from the recorded NO_2 concentrations to correct it, i.e.,

$$[NO_2]_i = [NO_2]_f - [NO]_f\,[\exp(k\,[O_3]_i\,t) - 1] \qquad \text{(A-3)}$$

For the most general treatment to account for any set of initial O_3, NO_2, and NO concentrations, numerical integration software was used to determine O_3 and NO losses (and NO_2 gains) during transport. Information on this software is available from Human Exposure and Atmospheric Sciences Division, National Exposure Research Laboratory, U.S. EPA (Deborah Luecken, [919-541-0244]). However, the corrections obtained based on Equation A-1 are nearly identical to those obtained by numerical integration in most ambient monitoring situations in which corrections are important.

Experimental monitoring data has shown that the ratio of final to initial NO concentrations is less than calculated and that to account for this, the effective reaction rate, k, in the above equation must be higher. The reaction of O_3 and NO at the surface of the transport tubing is believed to be the cause of this additional loss, although the exact mechanism has not been determined. Fehsenfeld et al. (1990) describe experimental procedures that can be used to determine the effective first-order reaction rate constant accounting for both NO, O_3 reactions and wall losses. This method involves the standard addition of a known amount of NO at the entrance of the sampling manifold at times when different O_3 concentrations are present in ambient air. The experimental value of this reaction rate is expected to be greater than the gas-phase reaction rate alone.

A.2 Conclusion on Gas-Phase Reaction between O_3 and NO

Sampling manifolds used for establishing compliance with the NAAQS and for research studies of ambient air should be examined to ensure that the transit time of air samples through the sampling manifold and into the monitoring instrument is short. The longer the residence time the greater the chance for reaction of NO and O_3 to form NO_2 and change the concentrations of these gases from their values in the ambient air. If the transit time is not short, the measured NO and NO_2 concentrations should be corrected as shown in Equations A-2 and A-3.

Wall reactions between O_3 and NO to form NO_2 have been neglected here since creation of NO_2 at tubing walls is subject to the type and condition of the wall. In one case, loss has been observed to be 25% higher than that due to the gas-phase reaction (Fehsenfeld et al., 1990). However, actual wall losses must be measured at the specific monitoring location and should be tested periodically (every 3 months) or as may be indicated by local conditions, and the manifold should be cleaned to prevent buildup of particles. Other elements of the inlet manifold system, notably gas-line filters, may contribute substantially to conversion of NO to NO_2 and should be tested accordingly.

If a 10% loss of NO is acceptable at 100 ppbv of O_3 and 30 °C, then a manifold residence time of 2.2 s (round to 2.0 s) is appropriate. Assuming that $NO_i \leq NO2_f$ (NO is generally less than NO_2 away from NO sources) where $NO_{2f} \leq 20$ ppbv, that $[O_3] \leq 100$ ppbv, and that $T \leq 30$ °C, the overestimation in $[NO_2]$ due to the NO, O_3 dark reaction during a 2-s residence time in the sampling manifold is also calculated to be less than 10%. Lower ozone concentrations and/or lower temperatures are expected during almost all sampling periods in any given year at most locations. Hence corrections to the annual average for NO_2 concentrations are expected to be small. However, corrections to monitoring data will be useful in providing better data for input to air quality simulation and observationally based models during periods when ozone concentrations are high. Corrections to the NO_2 at any location and time will obviously depend on manifold design (residence time), the prevalence of ozone and NO, and the temperature during the ozone season, as indicated in Equation A-3 above.

If the chemiluminescence monitoring system includes a vacuum pump then pressure reduction at the sampling inlet effectively eliminates the homogeneous chemistry inlet losses.

Appendix B
Determination of Atmospheric Concentration of Nitrogen Oxides by Differential Optical Absorption Spectroscopy

by

Jochen Stutz
Department of Atmospheric Sciences, UCLA

B.1 Introduction

Spectroscopic methods are among the oldest analytical techniques used to identify and quantify atmospheric trace constituents. In general, their advantages are high selectivity and low detection limits. And, in the case of open-path measurements, no calibration is necessary. One of the most successful spectroscopic techniques in the atmosphere is differential optical absorption spectroscopy (DOAS) (see Platt and Perner, 1983; Plane and Nien, 1992; Platt, 1994; and Plane and Smith, 1995, for reviews). In the 1970s, DOAS was used to measure stratospheric (Noxon, 1975) and tropospheric (Platt, 1978) nitrogen dioxide, NO_2, and other trace gases (Perner and Platt, 1979; Platt et al., 1979). Today it is used to monitor trace gases such as NO_2, NO, HONO, NO_3, SO_2, O_3, HCHO, and others (Platt, 1994). The following text gives a short introduction to the technique and discusses its advantages, disadvantages, and problems for monitoring nitrogen oxides.

B.2 Theory of DOAS

DOAS is a method that determines the concentration of atmospheric trace gases by measuring their narrow-band absorption. Unlike *typical* absorption spectroscopic techniques, the light path of DOAS is placed in the open atmosphere with path lengths of a few hundred meters to several kilometers. Because the light path is placed in the open atmosphere, there are several problems that DOAS has to overcome. The following section describes how DOAS solves the problem introduced by the location of the light path.

B.2.1 Principle

A schematic setup of a DOAS instrument is shown in Figure B-1. Light, with an intensity $I_0(\lambda)$ emitted by a suitable spectral broadband source, passes through the open atmosphere, is collected at the end of the light path, and is spectroscopically analyzed.

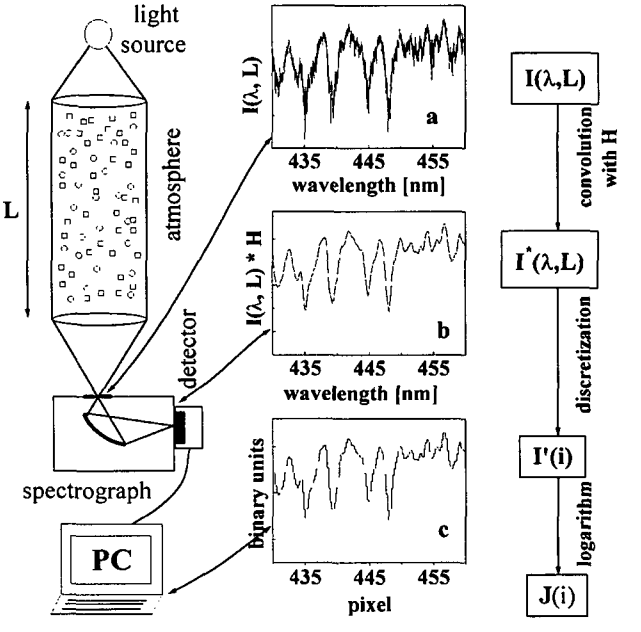

Figure B-1. Schematic overview of DOAS measurements.

The absorption of trace gases can be described by Lambert-Beer's law:

$$I(\lambda) = I_0(\lambda) \times e^{-\sigma(\lambda) \times C \times L} \quad \text{(B-1)}$$

where $I_0(\lambda)$ and $I(\lambda)$ are the light intensities at the beginning and end of the light path with a length L. The absorption of the trace gas is described by its absorption cross section $\sigma(\lambda)$ and its concentration C. As the light travels through the atmosphere, it also undergoes extinction due to absorption processes by different trace gases and to scattering by air molecules and aerosol particles. The transmitivity of the instrument (mirrors, grating, retroreflectors, etc.) will also decrease the light intensity; we will assume here that this decrease is already included in $I_0(\lambda)$. Therefore, the determination of $I_0(\lambda)$ would require removal of the respective gas from the air along the light path. The principle of DOAS is based on the fact that extinction processes and many trace gas absorptions show very broad or even smooth spectral characteristics.

The basic concept behind DOAS is the separation of the absorption spectrum and cross section $\sigma = \sigma_B + \sigma'$ into two parts: σ_B, which represents broad spectral features, and the differential absorption cross section σ', which represents narrow spectral structures (see Figure B-2).

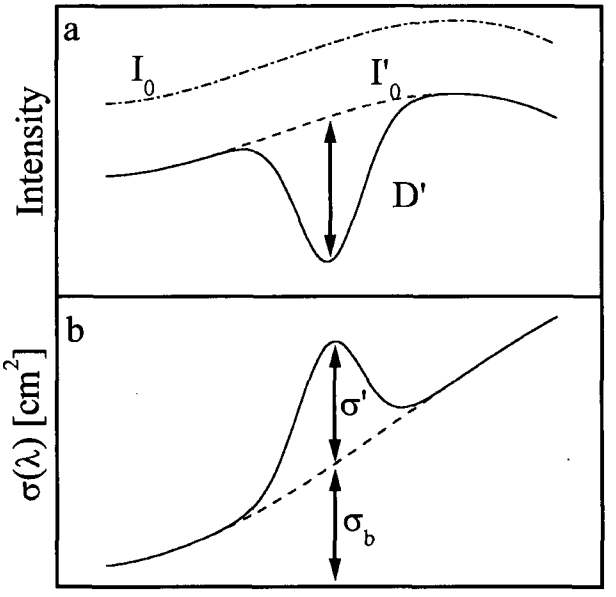

Figure B-2. The principle of DOAS.

Equation B-1 then transforms to

$$I(\lambda) = I'_0(\lambda) \times e^{-\sigma'(\lambda) \times C \times L} \quad \text{(B-2)}$$

where

$$I'_0(\lambda) = I_0(\lambda) \times e^{-\sigma_B(\lambda) \times C \times L} \quad \text{(B-3)}$$

contains all the broadband parts of the spectrum. Therefore, considering only σ' eliminates interferences with extinction and other broadband absorptions. It will also eliminate any dependence of the light intensity on the instrument transmitivity, which typically also shows a broad spectral characteristic. This separation can be performed by a suitable filtering procedure (see below).

By defining a differential optical density, the depth of a narrow absorption band at a wavelength λ', the concentration C can be calculated:

$$D'(\lambda') = \ln\left(\frac{I_0(\lambda')}{I(\lambda')}\right) \qquad C = \frac{D'(\lambda')}{\sigma' \times L} \quad \text{(B-4)}$$

In contrast to a simple absorption measurement at one wavelength, DOAS requires the measurement of a long enough wavelength interval to perform the described filtering and to separate overlapping absorptions of different trace gases showing differential absorption in the same wavelength interval. This separation is possible because the σ are physical constants that identify an individual trace gas like a "fingerprint." A calibration is, in principle, not necessary (we will see below that for real instruments a calculation to adapt the cross section to the spectral resolution of the individual instrument is indeed necessary). Therefore, DOAS is, if applied correctly, an absolute analytical method for atmospheric nitrogen dioxide and other trace gases.

It should be noted that, for simplicity, the integration of the product $\sigma(\lambda) \times C \times L$ over the light path and the sum over a number of trace gases was omitted here. DOAS measures the average concentration in the air mass crossed by the light path.

B.2.2 Practical Considerations

A more detailed examination of the physical and mathematical background that is involved in the measurement of the light after it has traveled through the atmosphere is necessary to understand some of the problems associated with DOAS. Since this is beyond the scope of this paper, only a qualitative description will be given here. For a more thorough mathematical description of DOAS refer to Stutz and Platt (1996).

Figures B-1A, B-1B, and B-1C illustrate how the spectral shape of an absorption spectrum—for example, here the NO_2 absorption (Harder et al., 1997)—changes during the measurement. After the path through the atmosphere, the shape is dominated by the natural spectral width of the trace gas absorption. In some trace gases, like NO_2, this leads to structures with spectral widths in the 100-picometer (pm) range overlaid by narrower structures in the 1- to 10-pm range (see Figure B-1a). Other trace gases such as HONO and NO_3 do not show this very narrow absorption, and the absorption bands have widths in the range of 0.1 to 3 nanometers (nm) (Platt, 1994). Due to the

limited spectral resolution of the spectrographs (in the range 0.1–1 nm full width, half maximum) used in DOAS instruments, the shape of this spectrum changes during the measurement (See Figure B-1b). The mathematical description of this process is the convolution of the spectrum shown in Figure B-1a, with the instrument function H of the spectrometer. Since the shape of the spectrum changes during the measurement, the depth of the absorption bands also changes. Therefore, the differential optical absorption D′ will change depending on the instrument. It is thus essential for DOAS to determine the differential absorption cross section that corresponds to the respective absorption spectrum and instrument. As will be described in more detail below, this can be done either by determining H and simulating the absorption spectrum or by measuring it with the same instrument. The last step of the measurement process is detection of the spectrum at the exit of the spectrograph by a detector, digitizing it in intensity and wavelength (see Figure B-1C).

B.3 Experimental Realization

DOAS measurements can be subdivided into several steps. The first step is the actual measurement of the atmospheric trace gas absorption, which is accompanied by several auxiliary measurements. In the next step, the absorption cross sections have to be adapted to the instrumental function of the instrument, or alternatively, a cell with the known trace gases has to be measured with the same instrument. If the DOAS instrument is stable, this step has to be repeated only from time to time, particularly after any changes of the instrument. The last step is the filtering and separation of the absorptions in a so-called fitting procedure. This last step is also used to estimate the error of the actual measurement. The following section will discuss the different parts of DOAS measurements, pointing out the crucial aspects of the individual steps.

B.3.1 Experimental Setup

In general, DOAS instruments consist of a light source, transfer optics to send the light through the atmosphere, and a spectrograph detector system that records the spectral structure of the light.

Three different light-path setups are currently used in DOAS instruments. The classical arrangement developed by Platt et al. (1979) has a xenon arc lamp combined with a collimating mirror on one end of the light path and a receiving telescope on the other. Although this setup is still used in some commercial DOAS instruments, it has been replaced by an arrangement that folds the light path once by aiming a combined sending and receiving telescope at one or more quartz cube corner retroreflectors (Axelsson et al., 1990). The main advantages of this approach are its simpler setup and the ability to aim the telescope at different retroreflector setups and thus vary length, orientation, and height of the light path. In the third setup the light path is folded into a small length (on the order of 1–20 m) by multiple reflection on mirrors (White, 1942; White, 1976; Ritz et al.,1992). This setup is experimentally more demanding, but has the advantage of better comparability with in situ techniques (see below).

Several types of spectrographs have been used in the past. The type is not as important as certain properties of their construction. The most important of these properties are the stability of instrument function and the spectral position. Since changes can often be attributed to temperature drift, the temperature of the spectrometer is usually kept constant to within ±0.5 K by means of regulated heating and insulation (Stutz, 1996). Another problem, especially in the UV, is stray light from wavelengths other than the desired wavelength in the spectrograph (Pierson and Goldstein, 1989; Stutz, 1996). Careful spectrograph design and the use of bandpass filters can reduce stray light. In any case, an accurate characterization of the spectrograph stray light should be performed.

The spectral resolution chosen has to be high enough to resolve the differential structures of the different gases, but low enough to allow a large enough wavelength interval to be observed (Platt, 1994). To avoid aliasing effects, a certain amount of oversampling is necessary. For pixel array detectors a typical minimum width of the instrument function of 4 pixels is necessary.

Two types of detectors are used in DOAS instruments. The slotted disk machines (SDMs) developed by Platt (1979) move a slit rapidly over the focal plain of the spectrograph, scanning the spectrum by converting wavelength-intensity information into time-intensity information with a photomultiplier. More modern instruments use photodiode array detectors (PDAs). Due to the multiplex advantage of measuring all wavelengths in an interval simultaneously, these solid-state detectors offer about 60 times higher light throughput than the SDM. Although an improvement of the detection limit has been achieved, the physical detection limit imposed by this higher sensitivity has not been reached due to spectral structures that are most likely induced by the detector itself (Stutz and Platt, 1992; Mount et al., 1992; Stutz and Platt, 1997).

The determination of trace gas concentrations by DOAS requires several auxiliary measurements to ensure optimal performance of the instrument (Stutz, 1996):

- Atmospheric background light intensity caused by aerosol scattering of sunlight into the telescope has to be measured by blocking the lamp during a measurement cycle. This background light has to be subtracted from the absorption spectrum.
- The shapes of the emission peaks of xenon lamps, used in most DOAS instruments, change with time and alignment of the instrument and should be monitored regularly.
- As described above, the instrument function H and the spectral position are the most important parameters to analyze DOAS spectra (see below). Their measurement

is therefore essential. Since atomic emission lines are two orders of magnitude narrower than the typical resolutions of DOAS spectrographs, measurement of these lines offer a sufficiently accurate description of H and the spectral position.

- One way to overcome the need for regular determination of H and the spectral position is to calibrate the instrument with absorption cells containing known concentrations of a trace gas. While this seems to be an easy way to avoid the determination of H, one of the most important advantages of DOAS, the absolute measurement of trace gas concentration based on the absorption cross section (see below) is given up. It is often also difficult to accurately determine the concentration of a trace gas in a cell. For example, the concentration of NO_2 in a cell depends on its temperature due to the equilibrium with its dimer N_2O_4 and the photolysis in the light beam (Hofmann et al., 1995). Special care has to be taken in preparing the cell to avoid water on the cell walls, which will form nitrous acid, HONO. Since HONO absorbs in the same wavelength range as NO_2, its presence will introduce problems in the analysis of atmospheric spectra. Experience has shown that water-free cells filled with a mixture of a small amount of NO_2 and ultrapure O_2 at atmospheric pressure show reasonable performance if the NO_2–N_2O_4 equilibrium is accounted for (Harwood and Jones, 1994; Hofmann et al., 1995). This approach is experimentally very challenging and expensive for unstable gases like HONO and NO_3.

Inexpensive computers with large storage capabilities and storage media control today's DOAS instruments. These fast computers make it possible to perform an on-line analysis, which delivers real-time NO_2 concentrations. Nevertheless, the possibility of instrumental problems like shifts in spectral position and aging of the lamp makes it highly desirable, if not necessary, to store and archive all atmospheric absorption spectra as well as all auxiliary spectra. Storing the spectra also provides an opportunity to later reanalyze spectra to prove unequivocally the presence of a certain trace gas concentration.

B.3.2 Analysis of DOAS Spectra

After the measurements described in the preceding section are made, the actual concentrations have to be determined by analyzing the atmospheric absorption spectra (Platt,1994; Stutz and Platt, 1996). To obtain reproducible DOAS results, it is necessary that the different steps described below are well documented for each instrument.

B.3.2.1 Determination of the Absorption Cross Section for the Instrument

As described above, measurement with an instrument with a limited spectral resolution changes the shape and size of the absorptions and also the corresponding absorption cross section. As long as these changes are identical for the atmospheric measurement and the absorption cross section, Lambert-Beer's law can be used to determine the concentration.

Two basic approaches can be used to determine instrument-specific absorption cross sections. The first approach is the calibration of the instrument by measuring the absorption of the gas in a reference cell with known content. As described above, several experimental problems are connected with this approach for NO_2, and its application to unstable gases such as HONO or NO_3 is even more difficult. The main disadvantage is the loss of DOAS as an absolute technique.

The second approach is to use spectrally high-resolution absorption cross sections (about 20–100 times better resolved than the actual instrument), which have been published in the literature, for example, for NO_2 (Harwood and Jones, 1994; Merienne et al., 1995; Harder et al., 1997; and Vandaele et al., 1998). By using the measured instrumental function H and the spectral position, these cross sections can be adapted to the individual instrument with high accuracy (Stutz, 1996). The adaptation algorithm is based on the convolution of a simulated high-resolution spectrum (calculated with Lambert-Beer's law) with H, and the integration of this spectrum according to the spectral position of individual pixels. Since the accuracy of the published absorption cross sections is approximately 3–10% (see Harder et al. [1997] for a review of published NO_2 absorption cross sections) and the error of the adaptation procedure is approximately 1%, the total error of this method is approximately 3–10%. It should be added that to obtain more accurate measurements of the absorption cross-section concentrations in the future, past measurements could be corrected. Besides its easier experimental realization (only the measurement of atomic emission lines are required), the accuracy is certainly higher than for the first approach, since it is improbable that a calibration in the field is more accurate than intensive laboratory studies. The origin of the absorption cross sections should always be reported with DOAS results. In all research DOAS instruments, this last approach is used because it can be considered an absolute method to determine ambient trace gas concentrations.

B.3.2.2 Filtering Procedure

The separation of the absorptions into differential and broadband parts is an essential part of DOAS. No unique or favored method exists to perform this separation. In general, all high-pass filtering procedures can be used, as long as they do not change the differential absorption too much. Independent of what

filtering method is used, it is essential that the absorption cross section, or a simulated reference absorption spectrum used in the analysis, is treated in the same way and that the differential absorption cross section fits the filtered absorption spectra. The filtering procedure should be well documented since it can strongly influence the size of the absorption and the differential cross section.

It is also possible to omit a filtering of the spectra and include a higher order polynomial in the separation procedure to describe the broadband structures (see below).

B.3.2.3 Separation Algorithm

The analysis of the absorption spectra is one of the main problems in the application of DOAS. Figure B-3 shows the different absorbers and other spectral structures that have to be separated in the analysis of NO_2 and HONO in the wavelength range from 300 to 400 nm.

The evaluation procedure is typically based on a model that describes the physical behavior of the logarithm of DOAS spectra, $\ln(I'_0(\lambda)/I(\lambda))$. The model is most often a function that consists of a linear combination of reference spectra (which are obtained by simulation or measurement for the specific instrument) and a polynomial to describe broad structures (for a mathematical description, see Stutz and Platt, 1996). A linear least squares fitting procedure is then used to optimize the scaling factors for the reference spectra, a_j, and polynomial parameters, with the goal of minimizing the difference between measured and modeled spectra. The scaling factors a_j are the result of the fit and can be used to calculate the concentration C_j of the respective trace gases: $C_j = a_j/(\sigma_j \times L)$. In the case of filtering procedures applied to the spectra before the actual separation process, the degree of the polynomial can be set to 1. If additional filtering is needed, higher degrees of polynomials can be chosen.

One of the problems in DOAS is the shift in spectral position of the atmospheric spectrum. If this shift is large (in the range of tens of pixels), systematic errors are introduced due to the imperfect alignment. More advanced analysis procedures allow the automatic alignment of the references to the measured spectrum. This can lead to considerable improvement of the analysis, but also introduces additional problems that supercede the scope of this report (see Stutz and Platt, 1996, for additional information).

Numerical simulations have shown that no interferences between absorbers larger than the error of the concentration calculated by the fit occur, as long as the reference spectra are accurately aligned and there are no unidentified structures in the spectra (Stutz, 1996). Problems can occur if the quality of the reference spectra is poor or if they contain structures of more than one absorber (as can be the case of HONO and NO_2).

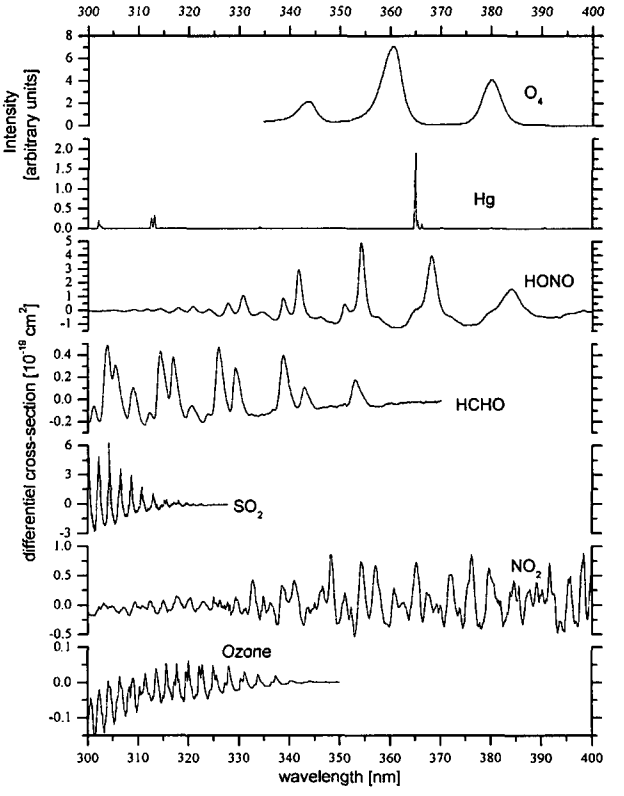

Figure B-3. Known differential absorptions and mercury emission lines in the wavelength range typically used to monitor NO_2 and HONO. The region around 370 nm is often preferred for NO_2 measurements, because around 440 nm, where the strongest differential NO_2 absorptions are found, Xe lamps have strong emission peaks.

B.3.2.4 Errors

Besides deriving the trace gas concentration, the task of the evaluation procedure is also to estimate the random error Δa_j of the scaling parameters a_j and, therefore, of the measured trace gas concentrations (Stutz and Platt, 1996; Hausmann et al., 1999). Both tasks can be solved with linear least squares methods if no instrumental problems are encountered. Δa_j is proportional to a factor determined by the fitted reference spectra and the polynomial, and the noise in the spectrum or, if present, unexplained structures other than noise (Stutz and Platt, 1996). It is important to note that, due to changing conditions in the atmosphere, the noise, and therefore the error, of individual measurements can vary and always has to be reported.

While the above-described determination of the error considers only random errors, several sources of systematic

errors have been found. An uncorrected spectral alignment or change in dispersion of the reference spectra due to a drift of the spectrograph, as discussed above, can lead to systematically wrong concentrations. Also, additional spectral structures caused by the instrument or by unknown absorbers are often found to introduce problems.

B.4 Theoretical Considerations about DOAS

As with all experimental methods, several requirements must be met to make it useful for the intended measurement. The following aspects have to be considered for DOAS:

B.4.1 Linearity

The linearity of DOAS has so far not been discussed in the literature. To determine the linear behavior of DOAS, numerical simulations have been performed as follows: The high-resolution absorption cross section by Harder et al. (1997) has been used to simulate absorption spectra in the column density (column density = C × L) range from 5×10^{15} cm^{-2} to 2×10^{19} cm^{-2} (the lower end was determined by truncation errors in the simulation). These spectra were then analyzed by the DOAS procedure using the spectrum for 5×10^{16} cm^{-2} arbitrarily as the reference spectrum. The concentrations derived by this analysis were compared to those used in the simulation. If the column density was smaller than 2×10^{18} cm^{-2}, no deviation from the linear behavior could be found above 0.1%. At column densities above 2×10^{18} cm^{-2}, saturation of the NO_2 absorption occurred. In summary, as long as the high-resolution absorption is not in saturation, DOAS is linear with respect to the relation of differential optical density to concentration. If the limit of saturation is reached, the analysis of smaller absorption bands of the same trace gas or shortening the light path might be considered as possible solutions.

B.4.2 Random Error of the Measurement

As discussed above, the random error of DOAS measurements, in a case where no instrumental problems or unknown spectral structures are encountered, is proportional to the noise in the spectrum. A short qualitative description of the behavior of the random error for only one absorber in different situations will be given. A more quantitative description can be found in Stutz and Platt (1996).

If we consider the errors of $\sigma(\lambda)$ and L as nonrandom, the error of the concentration C is proportional to the error of the differential absorption cross section:

$$\Delta C = \frac{1}{\sigma(\lambda') \times L} \times \Delta D' \qquad \text{(B-5)}$$

The error of D′ depends only on the noise in the spectra and, therefore, on the error of $I(\lambda')$ and $I'_0(\lambda')$:

$$\Delta D' = \sqrt{\left(\frac{\Delta I'_0(\lambda')}{I'_0(\lambda')}\right)^2 + \left(\frac{\Delta I(\lambda')}{I(\lambda')}\right)^2} \qquad \text{(B-6)}$$

If we assume, for simplicity, that $I'_0(\lambda') = (1 + \alpha) \times I(\lambda')$, where the factor α gives a nonlinear measure of the strength of the absorption, we can gain some qualitative information.

In the case of very small absorption, α will approach zero and we can write the error of C as:

$$\Delta C = \frac{1}{\sigma(\lambda') \times L} \times \sqrt{2} \times \frac{\Delta I'_0(\lambda)}{I'_0(\lambda)} \qquad \text{(B-7)}$$

The error will therefore approach a constant value, which is dependent only on the light intensity and is independent of the concentration. In most detectors the intensity is proportional to the number of photons counted by the detector, and, therefore, Poisson statistics applies for the error of the intensity. In this case the error of the concentration will be proportional to $(I'_0(\lambda'))^{-0.5}$.

The situation is more difficult when we consider large absorptions. In this case the relative error of $I(\lambda')$, and also possibly the error in $I'_0(\lambda')$, increases because the absorption (absolute and differential) will decrease the intensity. The error of the concentration will then depend on the concentration and on the light intensity. An exact description of this phenomenon can only be achieved by considering the shape of the absorption cross section and is beyond the scope of this report.

The material described here only considers the error of the intensity at two wavelengths. Since DOAS typically uses a wavelength range, the error is much smaller. Similar to an averaging procedure, one expects approximately a 10 times smaller error if 200 pixels of a detector are used for an analysis. The exact improvement of the analysis depends on the shape of the spectrum and can be derived by considering a least squares procedure. Stutz and Platt (1996) have mentioned that one can derive precise concentrations even if the noise of the spectrum is larger than the actual absorption structures.

B.4.3 Possible Systematic Errors

The most common systematic errors in DOAS are spectral misalignment and unknown spectral structures. While spectral misalignment can often be corrected in measured spectra, this procedure introduces additional errors and also makes the analysis very difficult. Also, in contrast to the linear least squares fit, the nonlinear methods used to correct misalignment are non-analytical and special care must therefore be taken when applying them (Stutz and Platt, 1996).

So far no method has been found to correct for unknown spectral structures, and the only possible way to attack this problem is to identify the sources of the structures. In the case of unknown absorbers, the reference spectra of these absorbers have to be included in the analysis. If the structures are caused by instrumental problems, they have to be removed by changes in the hardware.

B.4.4 Accuracy of DOAS

The overall accuracy of DOAS for NO_2 and other trace gases is usually dominated by the uncertainties in the absorption cross sections. Only in situations of low or very high concentrations do the random errors of the intensity dominate. It is therefore desirable to increase the accuracy of the absorption cross-section data.

B.5 Current State of the Art

To assess the current state of the art of DOAS instruments one has to distinguish between commercial and research instruments. Not much is known about the available commercial DOAS instruments because their construction and especially their analysis software is proprietary. The current state of the art of research instruments is better documented in the literature (Platt, 1994; Plane and Smith, 1995; Stutz and Platt, 1997; and references therein). These instruments are all similar in their construction, the main differences being in the length of the light path and in the analysis software. Typical detection limits for nitrogen oxides are listed in Table B-1 (Platt, 1994; Plane and Smith, 1995; Stutz and Platt, 1997).

Table B-1. Detection Limits of Research DOAS Instruments for Various Nitrogen Oxides

Trace Gas	Typical Absorption Path Length (km)	Detection Limit (pptv)
NO	0.2	200–300
NO_2	5	50–100
HONO	5	50–100
NO_3	10	1–2

The determination of the accuracy of DOAS instruments is problematic for several reasons. Since DOAS instruments are typically not calibrated, the only possibility to compare instruments is by simultaneous measurements in ambient air. The largest uncertainty of strongly absorbing species like NO_2 is typically the error of the absorption cross section. Experiments in the past have shown that the agreement between DOAS systems is improved if all instruments use the same absorption cross section to derive the concentrations (Camy-Peyret et al., 1996). Another problem with intercomparing DOAS instruments and comparing them to other techniques is the spatial averaging over the absorption path (Camy-Peyret et al., 1996). Comparing measurements of DOAS systems of several kilometers path length with in situ measurements close to sources, i.e., in a city, is particularly problematic. In the following paragraphs several of these comparisons are discussed.

Two intercomparisons of research DOAS instruments were performed in the framework of the Tropospheric Optical Absorption Spectroscopy (TOPAS) project of the EUROTRAC program (Bösenberg et al., 1997). The first campaign in Brussels, Belgium (Camy-Peyret et al., 1996), revealed many of the problems discussed above. Eight DOAS instruments were compared in a polluted urban environment. Despite the differences of optical setups of the instruments, in an environment with nearby NO_X sources the agreement was very good, with correlation coefficients above 0.97 for the measured concentrations of O_3, SO_2, and NO_2. The authors concluded that the general agreement among the instruments was better than 2 ppbv NO_2 in the relatively polluted environment.

To reduce the problems of spatial averaging, a second campaign took place in fall 1994 at the Weybourne Atmospheric Observatory in north Norfolk, U.K. This site typically receives well-mixed air, and differences due to spatial averaging were not expected. Seven DOAS instruments were compared to each other and to in situ analyzers for O_3, SO_2 (both EPA-approved systems), and NO_2 (chemiluminescence + photolytic converter). The intercomparison of the DOAS instruments and the comparison with other techniques showed very good agreement. Unfortunately problems with the chemiluminescence NO_X monitor prevented an accurate comparison of the NO_2 concentrations. All DOAS instruments agreed with the in situ O_3 and SO_2 analyzers within 5–10% (Bösenberg et al., 1997).

A more recent comparison of state-of-the-art DOAS instruments was published by Geyer et al. (1999). During a campaign near Berlin in 1998 measurements of NO_3 by DOAS and by MIESR were compared, showing agreement within the error limits of the instruments. During the same campaign a DOAS system based on an open 15-m base path-length multireflection cell was compared to an in situ NO_2 chemiluminescence analyzer with photolytic converter (Pätz et al., 2000). In this setup the DOAS instrument only observed the small air mass inside the open cell. The cell was mounted within a few meters of the sample inlet of the in situ analyzer; the values should therefore be free of any spatial averaging effects. Figure B-4 shows a correlation plot of the DOAS and chemiluminescence measurements. The two instruments agree within 1% over a 2-week period ($\approx$1000 data points).

The most recent intercomparison was made during the SOS field campaign in Nashville, TN, in summer 1999. Three different techniques were compared with each other: a system based on the photolytic conversion of NO_2 and detection of NO by chemiluminescence, LIF, and the newest generation of DOAS research instruments with a 1.35-km folded light path (total absorption length 2.7 km). Figure B-5a shows the measurements of the DOAS and the chemiluminescence instrument during a 3-day period in June. To compare the DOAS values, which were recorded with a lower time resolution, we averaged the chemiluminescence measurements over the exposure time of the DOAS system. The correlation plot (see Figure B-5b) shows that on average the instruments agree within 2%. The larger scatter in the data compared to Figure B-4 can be explained by the spatial

averaging in this case. The in situ monitors sampled at a 10-m height, while the DOAS light beam was located about 100 m away covering a 2- to 36-m height interval and a horizontal distance of 1.3 km. The DOAS system had an average detection limit of 200–400 pptv.

B.6 Summary

DOAS is a powerful technique to monitor air pollutants like NO_2 or NO. Its main advantage is the ability to measure absolute trace gas concentrations over an extended light path. For air quality monitoring this averaging is an advantage because influences of strong local sources are diminished. The comparison of Figure B-4 with Figure B-5b show how large these uncertainties can become.

Intercomparison experiments have shown that the DOAS instruments agree well with each other and in situ techniques if the spatial averaging of the DOAS is eliminated. Larger scatter is observed in cases where the long-path DOAS data are compared with in situ measurements. The detection limits for NO_2 reported in the literature vary for different light path lengths, but they are in general approximately 50–100 pptv for a 5-km absorption path length (Platt, 1994; Plane and Smith, 1995; Stutz and Platt, 1997). State-of-the-art instruments give a HONO detection limit of approximately 50–100 pptv (5-km light path). DOAS is currently the only technique able to monitor NO_3 radicals over an extended period. The detection limit for NO_3 is approximately 1–2 pptv.

The main challenge today for DOAS is integrating the complexity of the method into an instrument that can be operated by nonspecialists while avoiding all the possible problems outlined in this report. Several commercial instruments attempt this, but it remains to be seen if they will succeed.

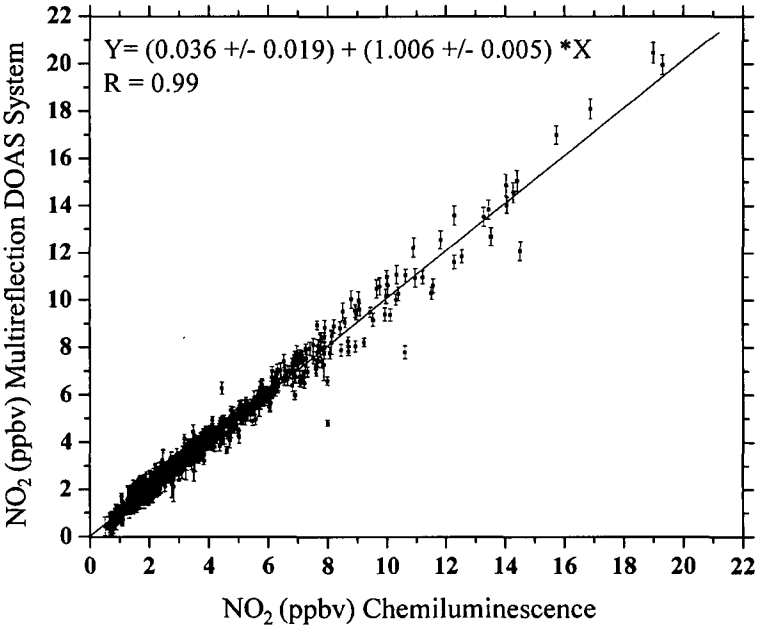

Figure B-4. Intercomparison of a chemiluminescence detector with photolytic converter (B. Alicke, A. Geyer, H.W. Pätz, and A. Volz-Thomas unpublished data) and a DOAS system with a 15-mm-long multireflection cell setup. Both instruments were located within a few meters from each other. Due to the optical setup of the DOAS system, the problem of spatial averaging was avoided. The agreement between the two techniques is excellent. The equation in the graph is the result of a weighted linear least squares fit. Errors are two times standard deviation.

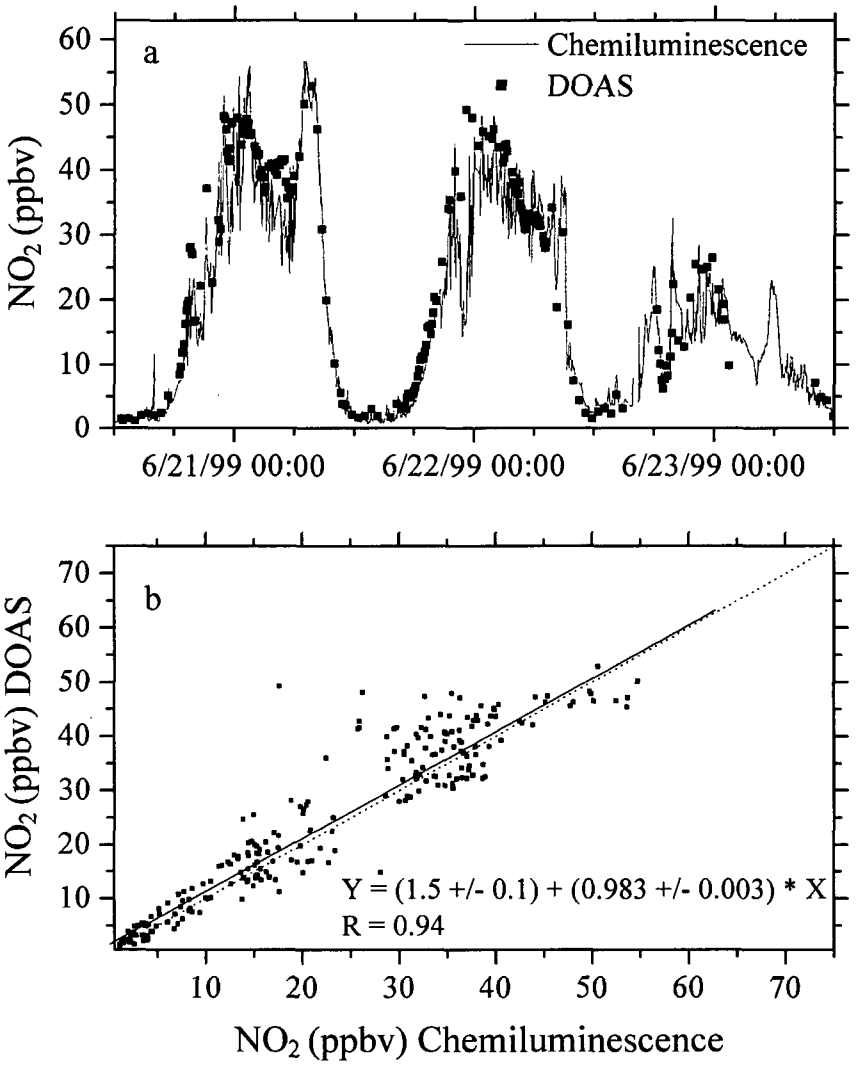

Figure B-5. Intercomparison of a long-path DOAS system (1.3-km light path length) with an in situ chemiluminescence analyzer with photolytic converter (see Appendix C in this report) during the SOS '99 field intensive in Nashville, TN: (a) shows the mixing ratios determined by both instruments. The differences can mostly be explained by the different air masses observed by both instruments. (b) shows a correlation plot, where the data of the chemiluminescence analyzer were integrated over the longer integration time of the DOAS measurements. The slope of 0.983 ± 0.03 shows the excellent agreement between the instruments. The scatter is again caused by the observation of the different air masses. This also explains the non-negligible intercept.

B.7 References

Axelsson, H., Galle, B., Gustavsson, K., Regnarsson, P., and Rudin, M. 1990. A transmitting/receiving telescope for DOAS-measurements using retroreflector technique. *Techn. Dig. Series* 4:641–644.

Bösenberg, D., Brassington, D., and Simon, P.C., eds. 1997. *Instrument Development for Atmospheric Research and Monitoring*. Berlin: Springer-Verlag.

Camy-Peyret, C., Bergqvist, B., Galle, B., Carleer, M., Clerbaux, C., Colin, R., Fayt, C., Goutail, F., Nunes-Pinharanda, M., Pommereau, J.P., Hausmann, M., Platt, U., Pundt, I., Rudolph, T., Hermans, C., Simon P.C., Vandaele, A.C., Plane, J.M.C., and Smith, N. 1996. Intercomparison of instruments for tropospheric measurements using differential optical absorption spectroscopy. *J. Atmos. Chem.* 23:51–80.

Geyer, A., Alicke, B., Mihelcic, D., Stutz, J., and Platt, U. 1999. Comparison of tropospheric NO_3 radical measurements by differential optical absorption spectroscopy and matrix isolation electron spin resonance. *J. Geophys. Res.* 104:26097–26105.

Harder, J.W., Brault, J.W., Johnston, P.V., and Mount, G.H. 1997. Temperature dependent NO_2 cross sections at high spectral resolution. *J. Geophys. Res.* 102:3861–3879.

Harwood, M.H., and Jones, R.L. 1994. Temperature dependent ultraviolet-visible absorption cross sections of NO_2 and N_2O_4—Low-temperature measurements of the equilibrium constant for $2NO_2 \leftrightarrow N_2O_4$. *J. Geophys. Res.* 99:22955–22964.

Hausmann, M., Brandenburger, U., Brauers, T., and Dorn, H.P. 1999. Simple Monte Carlo methods to estimate the spectra evaluation error in differential-optical-absorption spectroscopy. *Appl. Opt.* 38:462–475.

Hofmann, D., Bonasoni, P., Demaziere, M., Evangelisti, F., Giovanelli, G., Goldman, A., Goutail, F., Harder, J., Jakoubek, R., Johnston, P., Kerr, J., Matthews, W.A., McElroy, T., McKenzie, R., Mount, G., Platt, U., Stutz, J., Thomas, A., Vanroozendael, M., and Wu, E. 1995. Intercomparison of UV-visible spectrometers for measurements of stratospheric NO_2 for the network for the detection of stratospheric change. *J. Geophys. Res.* 100:16765–16791.

Merienne, M.F., Jenouvrier, A., and Coquart, B. 1995. The NO_2 absorption spectrum 1. absorption cross-sections at ambient temperature in the 300–500 nm region. *J. Atmos. Chem.* 20: 281–297.

Mount, G.H., Sanders, R.W., and Brault, J.W. 1992. Interference effects in Reticon photodiode array detectors. *Appl. Opt.* 31:851–858.

Noxon J.F. 1975. Nitrogen dioxide in the stratosphere and troposphere measured by ground-based absorption spectroscopy. *Science* 189:547–549.

Pätz, H.-W., Corsmeier, U., Glaser, K., Kalthoff, N., Kolahgar, B., Klemp, D., Lerner, A., Neininger, B., Schmitz, T., Schultz, M., Slemr, J., Vogt, U., and Volz-Thomas, A. 2000. Measurements of trace gases and photolysis frequencies during SLOPE96 and a coarse estimate of the local OH concentration from HNO_3 formation. *J. Geophys. Res.* 105:1563–1583.

Perner, D., and Platt, U. 1979. Detection of nitrous acid in the atmosphere by differential optical absorption. *Geophys. Res. Lett.* 6:917–920.

Pierson, A., and Goldstein, J. 1989. Stray light in spectrometers: causes and cures. *Lasers and Optronics,* Sept:67–74.

Plane, J.M.C., and Nien, C.F. 1992. Differential optical absorption spectrometer for measuring atmospheric trace gases. *Rev. Sci. Instr.* 63:1867–1876.

Plane, J.M.C., and Smith, N. 1995. Atmospheric monitoring by differential optical absorption spectroscopy. In *Spectroscopy in Environmental Sciences*, eds., R.E. Hester and R.J.H. Clark, pp. 223–262, London: Wiley.

Platt, U. 1978. Dry deposition of SO_2. *Atmos. Environ.* 12: 363–367.

Platt, U. 1994. Differential optical absorption spectroscopy (DOAS). In *Monitoring by Spectroscopic Techniques*, ed., M.W. Sigrist, New York: John Wiley.

Platt, U., Perner, D., and Pätz, H. 1979. Simultaneous measurement of atmospheric CH_2O, O_3, and NO_2 by differential optical absorption. *J. Geophys. Res.* 84:6329–6335.

Platt, U., and Perner, D. 1983. Measurements of atmospheric trace gases by long path differential UV/visible absorption spectroscopy. In *Optical and Laser Remote Sensing*, eds., D.K. Killinger and A. Mooradien, pp. 95–105, Berlin: Springer.

Ritz, D., Hausmann, M., and Platt, U. 1992. An improved open-path multireflection cell for the measurement of NO_2 and NO_3. Proc. Europto series. *Optical methods in atmospheric chemistry*, eds., H.I. Schiff and U. Platt, 1715:200–211.

Stutz, J. 1996. Messung der Konzentration troposphärischer Spurenstoffe mittels Differentieller-Opischer-Absorptionsspektroskopie: Eine neue Generation von Geräten und Algorithmen. Ph.D. thesis, Heidelberg: Univ. Heidelberg.

Stutz, J., and Platt, U. 1992. Problems in using diode arrays for open path DOAS measurements of atmospheric species. Proc. Europto series. *Optical methods in atmospheric chemistry*, eds., H.I. Schiff and U. Platt, 1715:329–340.

Stutz, J., and Platt, U. 1996. Numerical analysis and estimation of the statistical error of differential optical absorption spectroscopy measurements with least-squares methods. *Appl. Opt.* 35:6041–6053.

Stutz, J. and Platt, U. 1997. Improving long-path differential optical absorption spectroscopy (DOAS) with a quartz-fiber mode-mixer. *Appl. Opt.* 36:1105–1115.

Vandaele, A.C., Hermans, C., Simon, P.C., Carleer, M., Colin, R., Fally, S., Merienne, M.F., Jenouvrier, A., and Coquart, B. 1998. Measurements of the NO_2 absorption cross-section from 42 000 cm^{-1} to 10 000 cm^{-1} (238–1000 nm) at 220 K and 294 K. *J. Quant. Spect. Rad. Trans.* 59:171–184.

White, J.U. 1942. Long optical paths of large aperture. *J. Opt. Soc. Am.* 32:285–288.

White, J.U. 1976. Very long optical paths in air. *J. Opt. Soc. Am.* 66:411–416.

Appendix C
Photolytic Conversion of Ambient NO_2

by

Eric Williams
NOAA Aeronomy Laboratory, Boulder, CO

Photolytic conversion of NO_2 to NO is an attractive means of measuring NO_2 for a number of reasons. Photolysis, as opposed to thermal or catalytic conversion, is a process that is understandable from a fundamental physical chemistry standpoint. Absorption cross-section and quantum yield data for this molecule have been accurately determined by a number of investigators. Moreover, photolysis is in principle more specific than thermal conversion. As such it is not subject to potential interferences from thermally labile species such as PAN and peroxynitric acid (HO_2NO_2). Since absorption cross sections for all of the principal reactive nitrogen oxides have been measured, the wavelength range of radiation used for NO_2 photolysis can be adjusted to eliminate interferences from photolysis of other compounds such as nitric acid (HNO_3), PAN, and N_2O_5. There are, however, two reactive nitrogen species that will be interferences due to photolysis that occurs in the wavelength region used for NO_2; these are nitrous acid (HONO) and nitrate radical (NO_3). In most cases, though, the levels of these species will be small compared to NO_2, and in the case of NO_3 photolysis the interference can be eliminated by the use of optical filters (see below).

C.1 Physics and Chemistry of the Measurement

Atmospheric levels of NO_2 can be determined readily by photolysis with UV radiation followed by measurement of the increase in NO by chemiluminescence. This is effected by flowing the sample gas through a photolytic converter, essentially a quartz or Pyrex cell, that is irradiated by a source of intense UV such as a high-pressure Xe lamp. The chemical reaction of interest is

$$NO_2 + h\nu \rightarrow NO + O \qquad R1$$

where hν is in the range 350–400 nm. Since not all of the NO_2 entering the cell is converted, a conversion factor is defined that relates the increase in the amount of NO that exits the cell to the entering NO_2 level. The conversion factor must also account for a competing reaction that occurs in the cell:

$$NO + O_3 \rightarrow NO_2 + O_2 \qquad R2$$

where the ozone (O_3) comes from ambient O_3 or is produced by the very fast reaction

$$O + O_2 \rightarrow O_3 \qquad R3$$

that occurs in the cell during photolysis. Reactions R1–R3 are the same reactions that occur in the atmosphere to interchange NO and NO_2 while conserving O_3. These reactions are commonly referred to as the photostationary state. Viewed from the perspective of these reactions, the photolytic converter does nothing more than change the ratio of NO_2 to NO during gas transit through the cell.

The photolytic rate coefficient, J in units of s^{-1}, that describes the rate of reaction R1 is the wavelength-integrated product of the absorption cross section, the quantum yield of NO production, and the UV photon flux in the cell. The second-order rate coefficient that describes the rate of reaction R2 is k, in units of cm^3 $molec^{-1}$ s^{-1}. If conditions in the photolytic converter can be arranged such that reaction R1 proceeds much faster than reaction R2, then the conversion factor (CF) relating the measured NO increase to the NO_2 concentration is

$$CF = \{J*t/(J*t+k*[O_3]*t)\} * \{1-\exp(-J*t-k*[O_3]*t) \qquad (C\text{-}1)$$

where t is the residence time of the gas sample in the cell and the assumption is made that $[O_3]$ is large compared to [NO]. The

residence time is typically determined by the ratio of the cell volume to the gas flow rate (usually where both are determined at STP). The use of this factor relies on knowledge of J, which usually is difficult to determine because the photon flux through the cell cannot be readily estimated. In practice, CF is determined by direct calibration of the instrument with a known concentration of NO_2. Moreover, under carefully controlled conditions such as using zero air as the sample matrix, the CF determined by NO_2 calibration can be used to calculate J using Equation C-1 above.

C.2 Instrumental Application of NO_2 Photolysis

C.2.1 General Considerations

The use of photolysis in the determination of NO_2 in the atmosphere requires an instrument capable of sensitively measuring NO, such as a chemiluminescence detector. However, since NO is generally present in the atmosphere as well, a photolytic/chemiluminescence NO_2 instrument will actually measure some fraction of NO_X (NO_X = NO + NO_2), that is, all of ambient NO plus the fraction of NO_2 photolyzed in the system. Thus, in order to determine ambient NO_2, a means of separately determining ambient NO from NO produced during photolysis of NO_2 is necessary. If only one instrument is available, then NO and NO_2 may be measured sequentially and the NO present during the NO_2 measurement can be interpolated. In practice, rather than turning the lamp on and off, which induces lamp instability, this has been accomplished by means of a shutter that is capable of blocking all UV radiation from the photolysis cell. The interpolated NO is then subtracted from the measured NO_2 (actually NO_X) and the result divided by CF to yield NO_2. A more desirable arrangement is the use of two instruments, where one is dedicated to the continuous measurement of NO and the other dedicated to continuous measurement of NO_2. Here, every measurement of NO_2 has a corresponding NO data point; thus, no interpolation of NO is required, which results in a more complete and more accurate data set. In this case, calculation of NO_2 involves taking a difference between data from two separate instruments, so care must be taken to ensure that no systematic errors are present between the two instruments. This is best accomplished by acquiring sufficient NO data from the NO_2 (NO_X) instrument to compare to data from the NO instrument.

Calibrations for NO and NO_2 must be performed at regular intervals regardless of the instrumental arrangement. Instrument calibration can be conveniently accomplished by addition to the sample airflow of a small known gas flow (<1% of sample flow) containing a known mixing ratio of the species of interest. Compressed gas cylinders of calibrated NO (generally at low ppmv levels in N_2) are readily available with uncertainty to within ±2%. It is prudent, though, to continually evaluate the standard against others to ensure stability. Compressed gas cylinders containing calibrated mixtures of NO_2 are also available, but there is some question as to long-term stability. Permeation devices containing NO_2 are also commonly employed; these devices must be closely temperature regulated and must be regularly calibrated against other NO_2 standards to ensure accuracy. A third technique is the use of a small O_3 generator (typically a Hg penray lamp) coupled to the primary NO standard in a flow system that can produce precisely known levels of NO_2 by monitoring the loss of NO from O_3 titration. The assumption here is that mass balance applies with respect to NO and NO_2 (i.e., no additional titration of NO_2 to NO_3 and N_2O_5 with subsequent loss to surfaces). Regardless of the method, the concentration of added calibration gas should be similar to the expected atmospheric concentrations.

An artifact signal is usually present when a photolytic converter is used. This signal is observed when it is known that no NO_2 is present in the sample gas (e.g., zero air) and is believed to arise from evaporation of NO or NO_2 from material deposited on the cell walls when irradiated. The artifact appears to be diminished by use of a dichroic beamsplitter (see below) and can be substantially reduced by the use of optical filters to restrict the photolytic wavelength region to 350–400 nm. This artifact is monitored by periodic evaluation of the system with zero air, converted to an equivalent NO_2 concentration, and subtracted from the measured NO_2 levels. This NO_2 artifact level can vary from very low to negligible (0–0.02 ppbv) to high values (>0.10 ppbv) depending on the sampling environment. It can be eliminated by washing the cell with cleaning solution (dilute KF or KOH) followed by rinsing with deionized water. However, it is always prudent to perform regular checks of the system with zero air.

C.2.2 Practical Considerations

Implementation of the photolysis technique is technically straightforward. A glass cell, which in practice is always a cylinder, is installed in the sample gas flow stream. The cell is coated on the outside with a UV reflecting material (common Al foil works well) and irradiated with an intense UV light source. These light sources consist of the lamp, a housing, a stable power supply, and power cables. Because commonly available UV sources also output light in other wavelengths, some means of isolating the 350- to 400-nm region is required. The use of a Pyrex cell will provide short-wavelength cutoff at about 320 nm, and the use of a dichroic beamsplitter can separate UV from longer wavelength light. This latter mirror prevents visible and IR radiation from reaching the photolytic cell, which reduces the temperature increase of the gas in the cell. This, in turn, reduces interferences from thermally labile species such as PAN. Additional optical filters must be used to limit the light entering the cell to 350–400 nm. The benefits of these filters are (1) increased measurement specificity to NO_2 and (2) reduction (or elimination) of the NO_2 artifact. The disadvantage is a loss of conversion efficiency from attenuation of the lamp output beam.

The amount of the attenuation depends on a number of factors such as the number of filters used, filter placement, and alignment. A shutter device is also installed between the light source and the cell since there is always the need to measure NO levels in the system, regardless of whether one instrument or two is used for the measurement of NO_2.

Equation C-1 indicates that only J and t influence the conversion of NO_2 to NO in the cell. With modern flow control devices it is usually an easy matter to control gas flows (and residence time) very precisely. It is therefore imperative that light sources be used that not only have the required intense output in the UV but that also are highly stable in output. Other requirements also exist depending on the sampling platform for the instrument (e.g., aircraft) or the measurement program (e.g., research vs. monitoring). A commonly used light source is a 300-W high-pressure short-arc Xe lamp with an integral reflector. This type of lamp can be obtained with a built-in 320-nm short-wavelength cutoff filter, which is required since otherwise O_3 would be produced in the sample gas stream (and in the ambient environment around the lamp). Power supplies to drive these lamps can provide stable output regulated to better than ±5%. This type of lamp is very convenient to employ because the light beam is collimated and thus easily introduced into photolytic converter cells. Using these lamps and cells with gas residence times of 3–5 s, CF values of 0.4–0.5 are readily obtainable. Under these conditions J is approximately 0.1–0.2 s^{-1}. This provides more than sufficient sensitivity to NO_2 for most chemiluminescence NO detectors. However, gas residence times of 3–5 s also provide sufficient time for reaction R2 above to become significant, and this situation requires that the measured concentrations be corrected during the data reduction process. Further, longer gas residence times also may allow thermolytic conversion of compounds like PAN, which can be a significant interference with respect to NO_2. A better arrangement is to reduce t to less than 1 s in Equation C-1 above, but this requires that J be increased to 0.6 s^{-1} or greater. This has been accomplished.

C.2.3 Current State of the Art

To date three approaches have been employed to obtain adequate conversion efficiency at short gas residence times (see Figure C-1). One technique has been to employ two separate Xe UV sources to irradiate one cell; a second method uses a newly developed quasi-focused Xe UV lamp; and a third method uses a long-arc Hg-Xe lamp system.

A. One approach has been to use a cylindrical (3 cm i.d. × 20 cm) photolytic converter with a conventional 300-W Xe lamp shining into one end and a mirror at the other end. This arrangement, with the use of optics for focusing the beams, substantially increases the photon flux in the cell. Dichroic beamsplitters are used to remove visible and IR radiation, but because the energy input to the cell is substantial, the cell is cooled with a water bath and the gas pressure inside the cell is maintained at subambient (≈250 torr) to eliminate condensation of water from ambient air onto the inner walls of the cell. Conversion efficiency for NO_2 in this system has been measured at 0.5 at a gas residence time of 0.5–1 s. Artifact levels of equivalent NO_2 with this system have been negligible, even when ambient NO_2 levels have been close to the detection limit.

B. Another approach has been to use a newly developed Xe lamp that provides a quasi-focused output. By focusing, the lamp output can be introduced into a smaller cell, increasing the photon flux density. This system uses a 500-W Xe lamp (with a coating to eliminate O_3 production) and an aluminum-foil-coated cylindrical quartz cell (1 cm i.d. × 30 cm) with a UV reflecting mirror on the end opposite the lamp. The beamsplitter is not used in this system in order to improve the conversion efficiency. The cell is water jacketed and cooled by a recirculating water bath with a water reservoir that is maintained at ambient temperature. Gas pressure in the cell is slightly subambient due to the gas flow (2000 sccm) through it. Under these operating conditions no condensation has been observed in the cell even with sample gas dew point temperatures to 28 °C. Depending on the specific lamp used, the NO_2 conversion efficiency for this system has been 0.4–0.8 at a cell residence time of 0.6–0.7 s. Artifact levels for this system have been observed at less than ≈0.04 ppbv in a rural environment to slightly greater than 0.10 ppbv in an urban environment.

C. A third approach uses a short-arc high-pressure 100-W Hg lamp housed in an ellipsoidal reflector that focuses the lamp output into a cylindrical cell. The Hg lamp provides a greater fraction of radiation in the 350- to 400-nm region than do Xe lamps; thus, a lower overall power is required. Long-wavelength and short-wavelength cutoff filters are used to minimize artifact levels to <10 pptv equivalent NO_2. A small fan provides forced-air cooling to the photolysis cell. Further, because the power supply for the Hg lamp is quite compact and lightweight, this entire system (cell, lamp, power supply, cooling components, etc.) is comparable in size and weight to the power supplies of the systems described in 1 and 2 above. During operation a constant cell pressure (≈250 torr) is maintained by a pressure-flow feedback system, and under these conditions the conversion efficiency (again, depending on the specific lamp used) was ≈0.5 at 0.8 s residence time.

C.2.4 Data Reduction Requirements

There are a number of data reduction issues that must be kept in mind when the photolytic NO_2 converter is used. The most obvious requirement is the need for simultaneous measurements of NO. If a single instrument is used to collect NO and NO_2 data, interpolation of NO between NO_2 determinations becomes necessary. If the NO concentrations are not varying widely in the atmosphere, linear interpolation can provide a reasonable approximation of the actual NO levels while NO_2 (actually NO_X) is being measured. On the other hand, if NO is

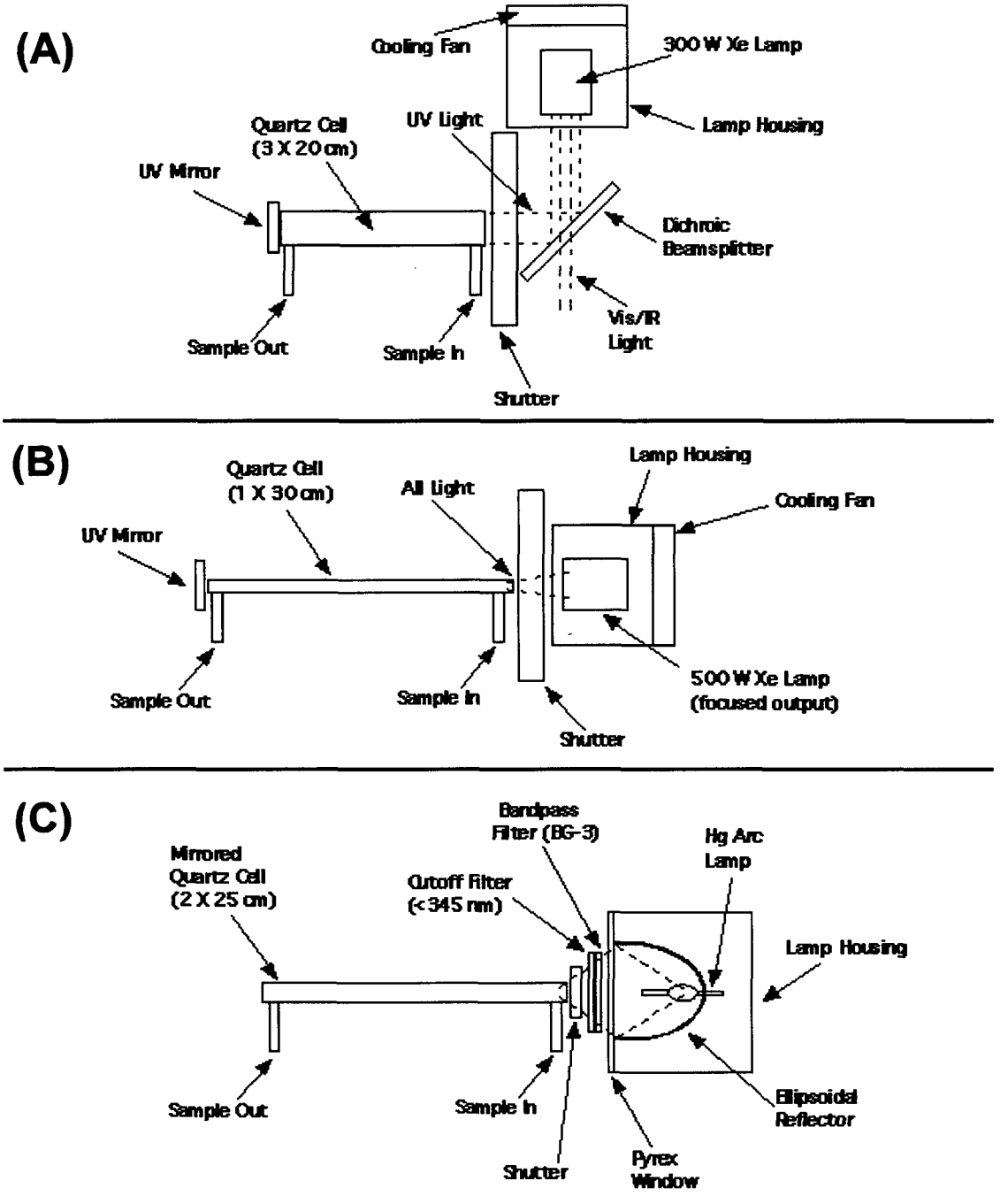

Figure C-1. Configurations for photolytic converters.

changing significantly, then the calculation of NO_2 becomes highly uncertain. This uncertainty can be reduced somewhat by only calculating NO_2 levels at the time when the instrument switches between NO and NO_X measuring modes. However, this technique reduces the total amount of data available. If another instrument can provide simultaneous NO data, then the only issues are that the data be truly simultaneous, that is, any time lags between the measurements be compensated for or eliminated, and that the NO concentrations from each of the instruments be identical (and correct). Under these conditions NO_2 levels can be calculated at high time resolution (1 Hz or faster). A potential problem under these circumstances is the attenuation of concentration fluctuations in the NO_X system due to the presence of the photolytic cell, which acts as a mixing chamber. This problem is manifested in the data reduction by the presence of sharp negative calculated peak NO_2 levels in the middle of a broader positive peak. This problem is due to lower time resolution in the NO_X channel than in the NO channel, which may not have an in-line photolysis cell. The solution to this problem is to match exactly the plumbing configuration and flow rates in the two instruments. This can be accomplished by including a nonilluminated photolysis cell in the NO instrument plumbing and matching the lengths of tubing between the two instruments. This also eliminates any time lags between the measured NO and NO_X and greatly simplifies data reduction.

Unfortunately, this solution can also generate another problem. Since the photolytic converter can be viewed as a mixing volume with a gas residence time determined by the flow rate, there is the possibility that some of the NO in the ambient gas sample can be converted by O_3, according to reaction R2 above. For example, considering only the homogeneous NO/O_3 reaction with ambient O_3 at 100 ppbv, a gas residence time of 4 s in the cell will convert almost 20% of ambient NO to NO_2. Moreover, peroxy radicals (HO_2, RO_2) in the atmosphere can have an effect comparable to O_3 and there also appears to be a heterogeneous process (though smaller in magnitude) involving conversion of NO to NO_2 on the walls of the cell. Clearly, these processes affect the accuracy of both the NO and NO_2 data, since these same reactions may reconvert some of the NO derived by NO_2 photolysis back to NO_2. On the other hand, for a residence time of 1 s in the cell only 5% of ambient NO is converted with ambient O_3 at 100 ppbv; similar effects are expected for conversion by peroxy radicals and heterogeneous processes. It is therefore apparent that short cell residence times are highly desirable, but must be balanced by the need for adequate NO_2 conversion efficiency (i.e., sensitivity). In any case, ambient O_3 levels should be measured along with NO and NO_2 in order to correct the data for these effects. The methods for performing these corrections have been published, but they are beyond the scope of this document.

Assuming that instrument parameters are selected so that adequate sensitivity is available with low levels of interferences and artifacts, the calculation of NO_2 from the measured NO_X can itself be a significant issue. Under many sampling conditions in the atmosphere, the ratio of NO_2 to NO is greater than 3–4, and at night in many cases NO virtually vanishes due to titration with ambient O_3. However, near strong sources of NO, the ratio of NO to NO_2 can be close to, or even exceed, unity. Since the calculation of NO_2 involves taking a difference between measured NO_X and NO, under the latter conditions the calculation involves a small difference between relatively large numbers. This situation, of course, may generate large uncertainties in the derived NO_2 concentrations and points out a fundamental limitation of this technique for NO_2: The background levels against which NO_2 (again, actually NO_X) is measured are usually varying, sometimes rapidly, and are sometimes large enough to make the NO_2 determination highly suspect. Finally, the optimal implementation of this technique actually requires two independent measurements to be conducted simultaneously, though it may be argued that NO_2 data without corresponding NO data are not very useful.

C.2.5 Summary on Photolytic Converters

Photolysis has been used in the determination of NO_2 since the late 1970s and has been shown to provide high-quality data, based on results from field-based instrument intercomparisons. The technique is suited for ground as well as aircraft operation, where fast time response is required. The method is reasonably specific for NO_2, with direct interferences known to occur only with HONO and NO_3. When implemented correctly, interferences from NO_3 and thermally labile species, most notably PAN, are insignificant. For these reasons this method has been the one of choice for researchers in atmospheric chemistry. While generally reliable and straightforward to implement, even via retrofit to existing instruments, the technique nevertheless requires more expensive equipment, both initially and over the long term, and more care and attention to detail during operation than other methods of conversion such as with thermal converters. Also, with the use of high-voltage power supplies and very hot, high-pressure lamps that produce intense UV radiation, safety concerns become paramount.

Appendix D
Laser-Induced Fluorescence Detection of NO_2

by

J.A. Thornton[1], P.J. Wooldridge[1] and R.C. Cohen[1,2]

[1]Department of Chemistry, University of California at Berkeley
[2]Department of Geology and Geophysics and Environmental Energy Technologies Division, Lawrence Berkeley National Laboratory

Laser-induced fluorescence (LIF) detection of NO_2 offers the promise of a combination of simplicity, sensitivity, specificity, accuracy, and long-term reliability that is unparalleled in existing commercial or research-grade techniques for NO_2 detection. Most existing techniques rely on liquid-phase luminescent reactions of NO_2 or on chemical or photolytic conversion of NO_2 to NO followed by detection of the NO. These approaches are subject to an array of interferences from other trace atmospheric species (see Chapter 5). LIF detection, by contrast, can be configured so that it has remarkable specificity for NO_2. As we show below, the signal can be generated using a high-resolution laser tuned to a specific rotational feature in the electronic spectrum of NO_2. The high spectral resolution eliminates the possibility of a substantial false signal from another molecule since the probability of another molecule having identical rotational structure in its absorption spectrum and comparable fluorescent behavior is near zero.

A typical LIF apparatus for NO_2 detection uses a laser oriented at right angles to both the sample flow and to a photomultiplier tube (PMT). Figure D-1 is a schematic of the laser and detection assemblies developed at the University of California, Berkeley. Fluorescent photons are imaged onto the PMT and the average count rate is proportional to the NO_2 mixing ratio. The detection limit is set by noise in the stray light that reaches the PMT, and the sensitivity is determined by a product of the laser power and the absorption and fluorescence efficiencies of NO_2. Early attempts at LIF detection of NO_2 were not competitive with other approaches because laser and detector technology were not sufficiently advanced to allow high sensitivity or high specificity in a compact, portable instrument. Also, the demand for more specific techniques was low because the limitations of other techniques were not as well understood as they are today.

Recently, we have incorporated new laser and detector technologies into an LIF sensor that is accurate (±5%, 1σ), sensitive (15 pptv/10 s, S/N = 2; 1-pptv detection limit), precisely calibrated (drifts of less than 1%/month), free from interferences, and relatively low maintenance (Thornton et al., 1999). This research-grade system was designed for aircraft use and in the remote troposphere where NO_2 concentrations below 100 pptv are typical. We have also made substantial progress toward an LIF system based on a commercially available tunable diode laser that demonstrates a sensitivity of 10 ppbv/10 s. These results suggest that within a year or two LIF instrumentation with all the capabilities necessary for atmospheric monitoring in urban and rural areas will be available at a price competitive with existing commercial instrumentation.

a) Early designs for LIF NO_2 sensors. Before 1997, designs for LIF detection of NO_2 did not emphasize specificity. The lasers used in these instruments were not tunable, precluding discrimination against interferences by tuning on and off of a rotational resonance unique to NO_2. For example, Tucker et al. (1975) used a He-Cd laser with nonresonant detection and achieved a detection limit of 2040 pptv/10 s. George and O'Brien (1991) used a frequency-doubled Nd^{3+}:YAG laser (532 nm) with detection of fluorescence from 580–900 nm to achieve a sensitivity to NO_2 of 2500 pptv with 10-s averaging in a more portable configuration. They took advantage of the long fluorescence lifetime of NO_2 to discriminate against some of the resonant background scatter and used an NO_2 scrubbing step

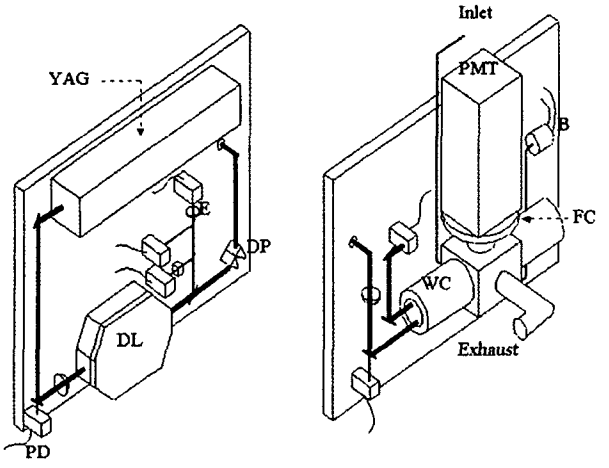

Figure D-1. Schematic of the UC Berkeley LIF NO_2 instrument. The core of the instrument is mounted on a breadboard, one side holding the laser subsystem and the other side the detection axis. A frequency-doubled Nd^{3+}:YAG laser (YAG) at 532 nm pumps a custom-built dye laser (DL). The output (585 nm) is sampled by fused-silica beam splitters to monitor power, frequency (by measuring transmittance through an NO_2 reference cell shown as a cube), and linewidth (measured with an external etalon [E]). Six photodiode detectors (PD) are used to measure laser power at various points along the beam path. A set of dispersion prisms (DP) is used to separate the 585-nm light from the 532-nm light, which is then dumped. The 585-nm light is then sent through a hole in the breadboard to the detection side to the multipass white cell (WC). The pressure in the WC is measured with a manometer (100-torr Baratron [B]). NO_2 fluorescence is collected and sent through a series of optical filters housed in the filter changer (FC) to a photomultiplier tube in its TE-cooled housing (PMT).

(reducing NO_2 to NO using $FeSO_4$) to demonstrate specificity of the technique to NO_2. In the first attempt to use spectroscopic features of NO_2 to ensure specificity in an atmospheric sensor, Fong and Brune (1997) developed an LIF instrument employing a tunable dye laser as the excitation source. They excited NO_2 at 564 nm with detection using a red-sensitive PMT (8% quantum efficiency) filtered to a bandwidth of approximately 200 nm. By tuning the laser on and off of a rotational resonance in the excitation spectrum, this instrument demonstrated its specificity for NO_2. However, the sensitivity of the Fong and Brune prototype was limited by the combination of a modest signal rate—0.012 count/s/pptv—and a high background count rate—approximately 1000 counts/s. The reported instrument sensitivity, 1085 pptv/10 s, was only about a factor of 2.5 better than that of George and O'Brien.

b) LIF systems with parts-per-trillion sensitivity. A UC Berkeley–Harvard University collaboration produced a tremendous advance in LIF sensitivity to NO_2 through attention to eliminating sources of laser scatter and at the same time designing a detection cell with efficient collection of fluorescent photons. The instrument was designed to detect NO_2 aboard the ER-2 aircraft in the lower stratosphere (Perkins et al., in preparation, 1999). This aircraft-borne instrument uses a Nd^{3+}:YAG pumped dye laser that is tuned on and off an NO_2 resonance near 585 nm. Detection of the total fluorescence integrated from 750 nm to the long-wavelength cutoff of a GaAs PMT (850 nm) occurs simultaneously with the pulsed laser. The ER-2 instrument participated in NASA's 1997 Photochemistry of Ozone Loss in the Arctic in Summer (POLARIS) experiment (Newman et al., 1999). During this deployment, Perkins et al. (in preparation, 1999) demonstrated a detection limit of 10–50 pptv, limited by systematic noise in the background, and a sensitivity of 40–80 pptv/10 s at the ambient pressure (< 200 torr). An informal intercomparison with a photolysis-chemiluminescence (PC) instrument developed by Del Negro et al. (1999) showed strong correspondence between the two approaches. A linear regression of 13075 simultaneous measurements by the two instruments obtained on 27 separate flights over a 6-month span gives $[NO_2]^{LIF}=1.07*[NO_2]^{PC}$ and an $R^2=0.95$. At pressures above 200 torr, the ER-2 instrument's sensitivity degrades due to pressure broadening and an increase in background noise associated with 2nd Stokes Nitrogen Raman scattering. Nonetheless, the sensitivity of this instrument is more than a factor of 10 improvement over the LIF instrument designed by Fong and Brune and within a factor of 2 of the best PC instruments.

At UC Berkeley, we improved on this approach, reducing the detection limit to 1 pptv, enabling operation at any pressure within the atmosphere without loss of sensitivity, and improving the sensitivity by more than a factor of 3, to 15 pptv/10 s. The instrument is described in detail in Thornton et al. (in press, November 1999). To achieve these results, the instrument is operated at low pressure in combination with a time-gated photon counting technique. We also redesigned the detection chamber moving the multipass optics further away from the fluorescence collection region to reduce the probability of scattered light reaching the detector. The combination of reduced pressure and the time-gated photon counting technique substantially reduces background noise (by more than 95%) associated with the laser light scattering off of the mirrors, walls, and gas sample and reaching the photocathode. Photon counting begins only after the laser pulse has left the detection chamber (a delay of about 50 ns), at which point the laser-induced background noise has decayed to zero while ≈85% of the NO_2 fluorescence signal remains due to the long lifetime ($t \approx 115$ ns) at 4 torr. Although the signal rate of this experiment is low, approximately 0.1 count/s/pptv, the noise is also extremely low, about 4 counts/s. Thus, a signal-to-noise ratio of 2 for 15 pptv NO_2 in 10 s is achieved using the Berkeley LIF instrument. Another important improvement over the ER-2 instrument was the redesign of the dye pump system, which extended the mean time between failures from tens of hours to several weeks.

D.1 Sampling and Calibration

The Berkeley LIF instrument samples the atmosphere by continuously pumping air through the instrument at a rate of 1.5 standard liters per minute (slpm). This results in a residence time in the tubing and the detection chamber of approximately 1 s. A stainless steel pinhole held in a stainless steel fitting is used as the inlet, and the tubing used to move air from the sampling region to the detection chamber is PFA Teflon. On the downstream side of the pinhole, the pressure is maintained below 100 torr by a 10-cfm rotary vane pump. The low pressure essentially eliminates concerns that the $NO+O_3$ reaction can cause an increase in the NO_2 concentration during the transit time from the inlet to the detection point since the rate of this reaction drops by almost a factor of 10 from its value at atmospheric pressure. The calibration procedure includes a series of tests of instrument performance, stability, and response to a known source of NO_2.

1. Calibrations are performed in dry air every 3–5 h using a cylinder of zero air and a cylinder of 5.08 ± 0.10 ppmv NO_2 in N_2 (Scott Specialty Gases with ACULIFEÒ coating) for dynamic dilution over the range 2.5–150 ppbv. Two mass-flow controllers are used to obtain the desired concentration range. An additional solenoid valve directly following the NO_2 flow controller provides a hard zero for the calibrations and prevents contamination of the sample flow.

2. Standard additions are performed to an atmospheric sample every 15 h. During a standard addition, NO_2 is added to the atmospheric sample stream just prior to the detection cell. This provides a diagnostic for the effect environmental factors such as water vapor have on the fluorescence signal. We observe a 3.5% effect in the fluorescence signal due to variation of 0.01 in the mole fraction of atmospheric water vapor.

3. The background signal in zero-grade dry air is measured by adding dry air every 3–5 h to maintain an accurate and precise measure of the instrumental zero.

4. The sensitivity to N_2-Raman scatter is measured every 20 min. In the N_2-Raman detection mode, zero air is flowed into the detection chamber at various rates to observe the number density dependence of the Raman signal. We then use the measured Raman sensitivity to normalize for changes in laser alignment and optical throughput from the signal. Extensive observations in the lab and in the field show that the ratio of the instrument response to N_2 Raman and to NO_2 is constant to better than ±2%.

D.2 Field Trials and Intercomparisons

Performance of the UC Berkeley LIF instrument has been tested during three field deployments, two in the foothills of the Sierra Nevada (25 July–31 October 1998 and 1 September–15 November 1999) and one in Nashville, TN, as part of SOS '99 (15 June–15 July 1999). The Sierra experiments were at a rural research site located on a ponderosa pine plantation (owned and operated by Sierra Pacific Industries) 50 miles east of Sacramento, CA, at an elevation of 4000 ft. The plantation is adjacent to the University of California Blodgett Research Forest in Georgetown, CA. The site is characterized by a strong diurnal cycle in atmospheric composition with abundances of NO_x, VOCs, and O_3 typical of the clean continental boundary layer observed regularly in the morning and increases in the concentration of all of these species as air is transported from the Central Valley into the foothills every afternoon. In the evening the flow reverses and downslope flow brings in clean air again. Figure D-2 shows observations of NO_2 (30-s averages) from a 14-day period, 16–29 August 1998, that indicate the regularity of the meteorology and of the sensitivity of the LIF technique.

Substantial improvements were made to our approach prior to deployment from 15 June–15 July 1999 as part of SOS '99 in Nashville, TN. These improvements are the basis for our current estimates of sensitivity (15 pptv/10 s, S/N = 2; 1-pptv detection limit). The Berkeley LIF NO_2 measurements were part of an extensive suite of chemical measurements made at the Cornelia Fort Airpark 8 km northeast of downtown Nashville http://www.al.noaa.gov/WWWHD/pubdocs/SOS/SOS99.html. Part of our objective was an informal intercomparison of the relatively new LIF approach with existing techniques for observation of NO_2. The suite of NO_2 measurements at Cornelia Fort included NOAA Aeronomy Laboratory PC (Williams), EPA PC (Kronmiller), EPA luminol (Wheeler), EPA DOAS (Kronmiller), and the University of Heidelberg/UCLA DOAS (Stutz).

As of this writing (November 1999), only the PC observations by Williams are considered final and available for comparison to our LIF measurements. The Cornelia Fort experiment was designed with this intercomparison in mind. Air was brought down from the sampling tower through a 5-cm-i.d. PFA tube using a 200-L/min blower common to both instruments, which were located in adjacent trailers. The Berkeley instrument drew off the main flow approximately 5 cm below the NOAA instrument at a flow rate of 1.5 l/min using the pinhole sampling system described above. After the pinhole, the air was pumped through approximately 5 m of 6-mm-i.d. PFA tubing to the detection cell of the LIF instrument by a 10-cfm rotary vane pump. Both instruments had similar residence times in the plumbing from the sample point to the instrument. Although the pressure drop in the LIF instrument reduces the impact of gas-phase processes, effects of surfaces in the sampling lines, if any, should be common to both instruments.

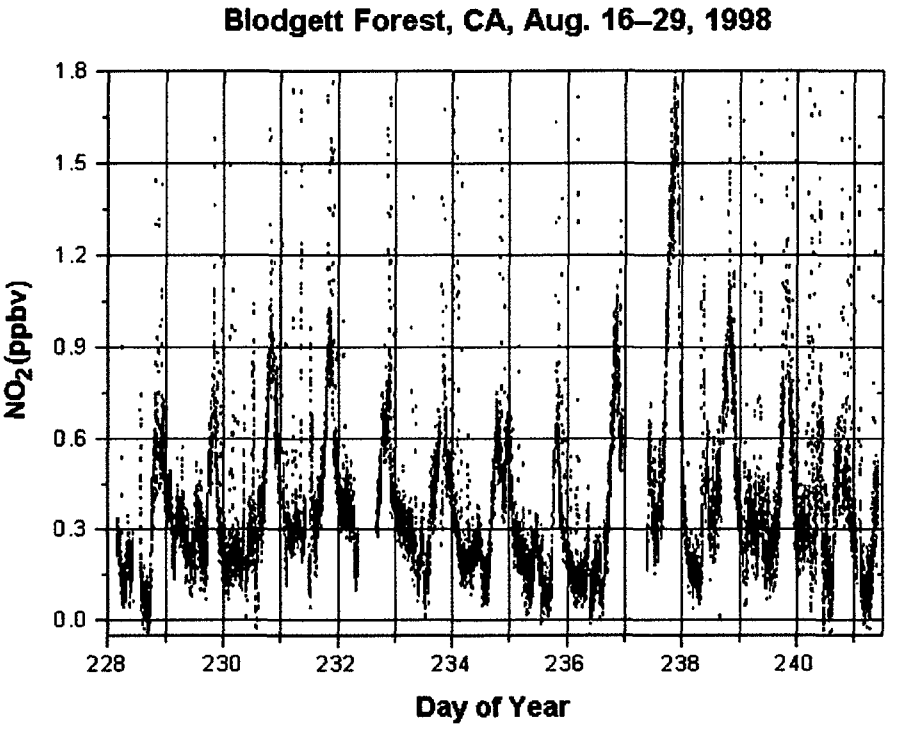

Figure D-2. NO_2 concentration plotted as 30-s averages vs. time for the 2-week period 16–29 August 1998 at UC Blodgett Forest Research Station. Points that are far from the mean are due to air from the site's diesel generator.

NO_2 concentrations measured at Cornelia Fort Airpark by the Berkeley LIF instrument and by the NOAA PC instrument were compared on a point-by-point basis for the period from 17 June 1999 to 14 July 1999. The time recorded by the Berkeley instrument was synchronized to the NOAA time base by comparing structures in the 10-s average Berkeley and 1-min NOAA measurements. The Berkeley measurement time base was then shifted to match the NOAA time base and the Berkeley measurements were averaged to 1 min. Figure D-3 shows observations for the two instruments from 12 p.m. on 20 June to 12 p.m. on 21 June. Figure D-4 shows an intercomparison of observations using data collected by the Berkeley LIF instrument and by the PC instrument operated by Williams of NOAA. The results show remarkable agreement. For the first two-thirds of the campaign, the PC measurements were on average 4% higher than the LIF measurements. The zero offset between the instruments, if any, is below 20 pptv. An $R^2 = 0.984$ for the linear fit is an indication of the near perfect agreement between the two observations. Nonetheless, the effect of variations in instrument calibration on individual days is evident as stripes in the data with different slopes at high concentration. We have not yet identified which instrument has a varying calibration, although efforts to show the calibration of the LIF experiment are precise to a few percent give us confidence that all of the variations are not due to the LIF instrument (Thornton et al., in press, November 1999). After 6 July 1999, a substantial change in the calibration of one of the two instruments occurred. From this point forward to 15 July, when the experiment ended, the PC instrument reported measurements 9% lower than the LIF observations with a measurable offset of 97 pptv. The $R^2 = 0.988$ again indicates the strong correspondence between observations from the two instruments. We do yet not understand the source of the shift observed. In this context, it is important to note that it is only the extreme precision of the two instruments that allows these relatively subtle variations to be observed and evaluated. Few NO_2 measurements are of the quality necessary to investigate differences of less than 10%.

D.3 Future LIF Systems

Rapid progress in laser and detector technology make it likely that LIF approaches to NO_2 detection will soon be routine. In our group at UC Berkeley we have developed a prototype LIF instrument based on a commercial tunable external cavity diode laser. The diode laser operates in the 638-nm range at 4 mW average power, and red-shifted fluorescence is collected and

imaged onto a cooled GaAs PMT. Currently, the prototype has a signal-to-noise ratio of approximately 3 at 1 ppbv NO_2 after 10-s averaging. Improvements in laser technology, the use of large area single photon counting avalanche photodiode detectors, higher quality optics, and incremental improvements to the design of the optical system for collecting fluorescence are expected to increase the sensitivity of this prototype by a factor of 1000 over the next year. The instrument will weigh less than 80 lb, will be smaller than 0.5 m^3 including all components, and will be robust enough to be operated continuously for months in routine monitoring situations with only minor maintenance. We estimate the cost of parts for such an LIF instrument will be on the order of $25,000.

D.4 Acknowledgments

This work was supported by the Office of Science, U.S. Department of Energy, under Contract No. DE-AC03-76SF00098, through the UC Energy Institute, and by NASA, through its Instrument Incubator Program under Contract No. NAS1-99053. Observations in Nashville, TN, were supported by NOAA's Office of Global Programs under Grant No. NA96-GP0482.

D.5 References

Del Negro, L.A., Fahey, D.W., Gao, R.S., Donnelly, S.G., Keim, E.R., Neuman, J.A., Cohen, R.C., Perkins, K.K., Koch, L.C., Salawitch, R.J., Lloyd, S.A., Proffitt, M.H., Margitan, J., Stimpfle, R.M., Bonne, G.P., Voss, P.B., Wennberg, P.O., McElroy, C.T., Swartz, W.H., Kusterer, T.L., Anderson, D.E., Lait, L.R., and Bui, T.P. 1999. Comparison of modeled and observed values of NO_2 and JNO_2 during the POLARIS mission. *J. Geophys. Res.* 104(D21):26687–26703.

Fong, C., and Brune, W.H. 1997. A laser induced fluorescence instrument for measuring tropospheric NO_2. *Rev. Sci. Instrum.* 68(11):4253–4262.

George, L.A., and O'Brien, R.J. 1991. Prototype FAGE Determination of NO_2. *J. Atmos. Chem.* 12:195–209.

Newman, P.A., Fahey, David W., Brune, William H., Kurylo, Michael J., Kawa, S. Randolph. 1999. Preface: Photochemistry of ozone loss in the arctic region in summer (POLARIS). Special section, *J. Geophys. Res.* 104(D21):26,481–26,495.

Perkins, K.K., 2000. An airborne laser-induced fluorescence instrument for in situ detection of stratospheric NO_2, Ph.D. thesis, Harvard University.

Thornton, J.A., Wooldridge, P.J., and Cohen, R.C. 2000. Atmospheric NO_2: In situ laser-induced fluorescence detection at parts per trillion mixing ratios. *Anal. Chem.* 72(3):528–539.

Tucker, A.W., Birnbaum, M., and Fincher, C.L. 1975. Atmospheric NO_2 determination by 442 nm laser induced fluorescence. *Appl. Opt.* 14(6):1418–1421.

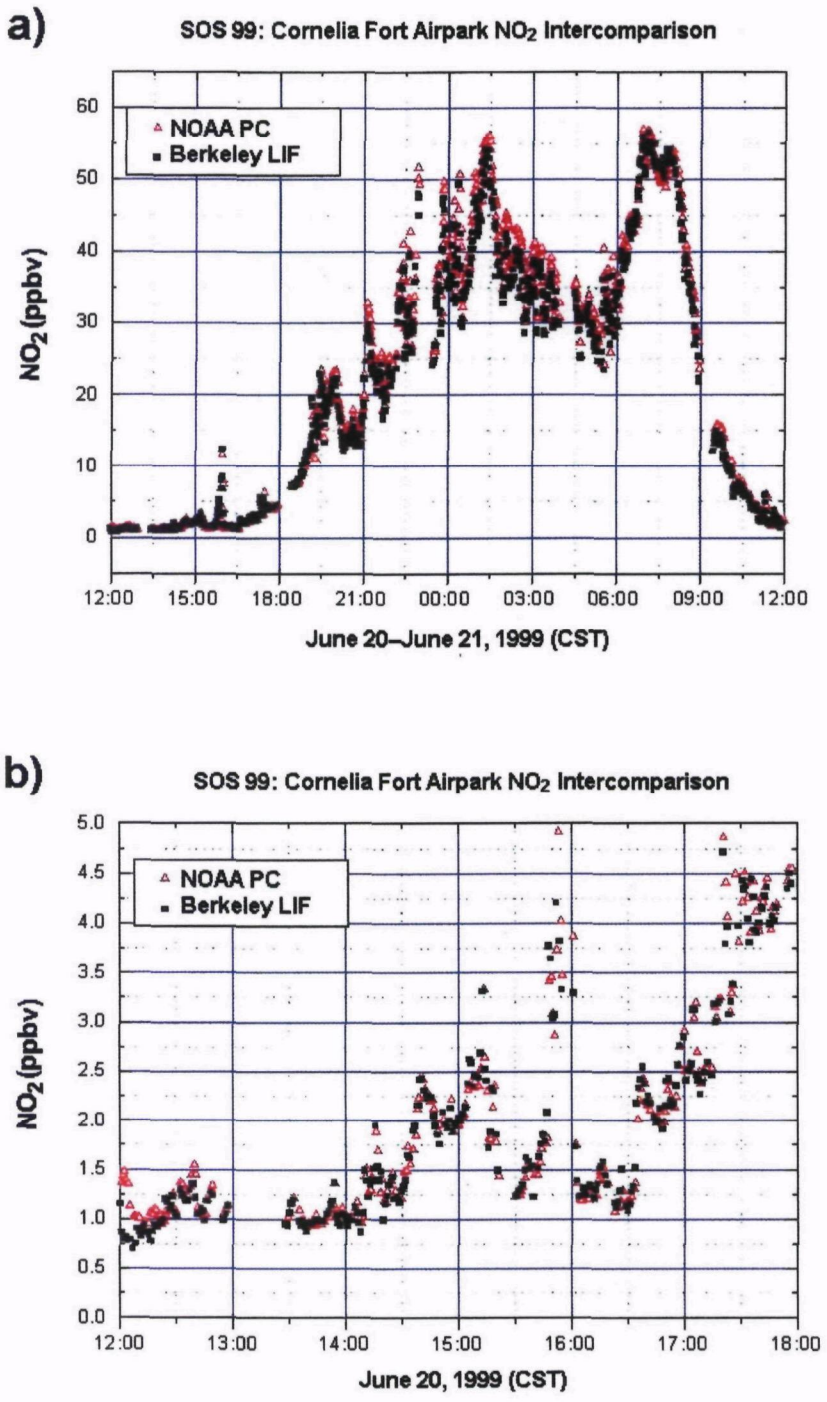

Figure D-3. NO_2 concentration plotted as 1-min averages vs. time at Cornelia Fort Airpark, Nashville, TN. Data measured by the Berkeley LIF instrument are shown as open circles, and those measured by the NOAA PC instrument are shown as crosses. a) Data for the entire 1-day period from 12 p.m. (CST) on 20 June to 12 p.m. on 21 June 1999. b) Data for the period from 12 p.m. to 6 p.m. (CST) on 20 June when the concentration of NO_2 was less than 5 ppbv.

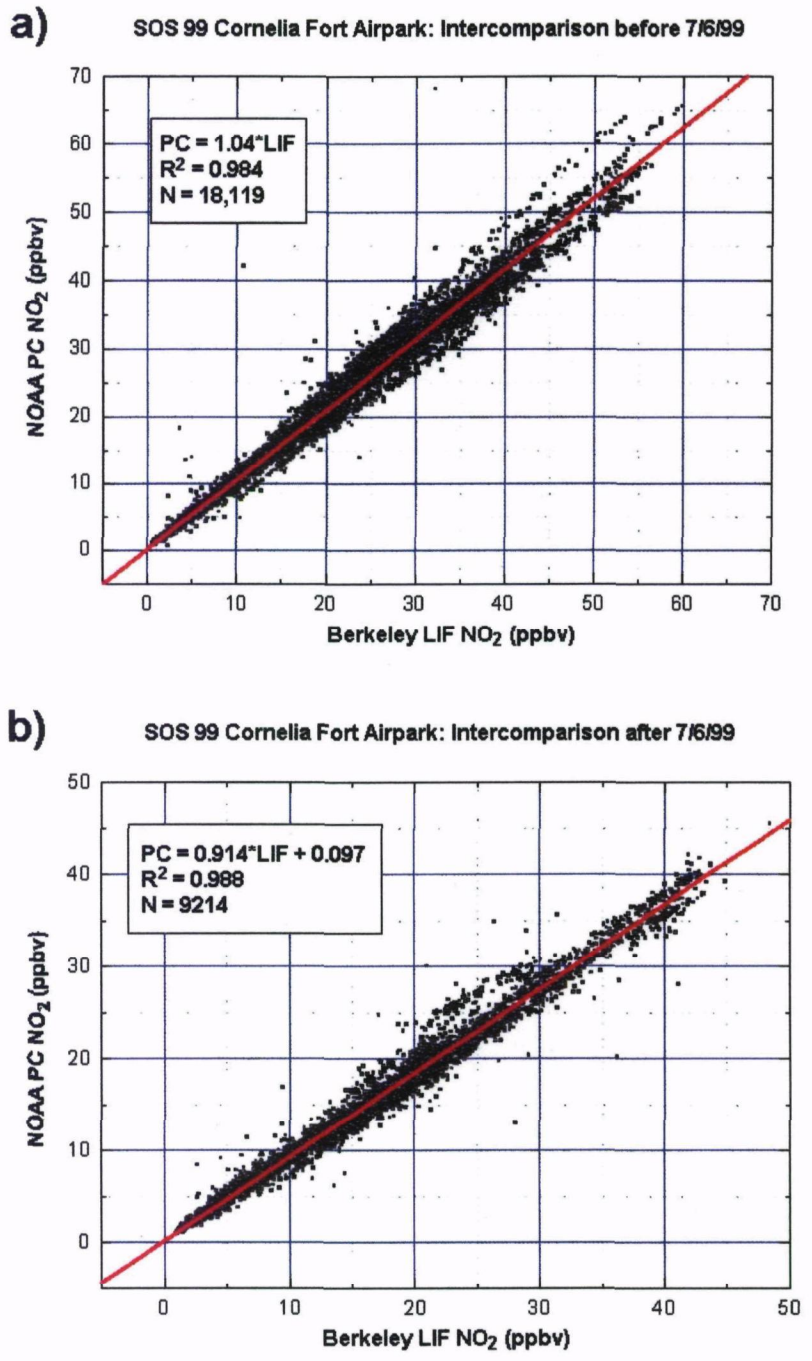

Figure D-4. Southern Oxidants Study, Nashville 1999, Cornelia Fort Airpark NO_2 intercomparison plots. NO_2 data measured with NOAA's PC instrument is plotted vs. that measured with UC Berkeley's LIF instrument. A least squares best fit line is drawn through the data. a) Data from the period 17 June to 7 July 1999 are plotted and a best fit line forced through (0,0) has a slope of 1.04 and an $R^2 = 0.988$. b) Data from the period 7 July to 14 July 1999 are plotted and a best fit line has a slope of 0.914 with an $R^2 = 0.988$. The figures show that while over the entire campaign the two instruments agreed very well on average, there were at least two distinct populations in which the two instruments were calibrated differently to more than 10%.

Appendix E
Application of a Luminol-Based Approach to Monitoring NO_2, NO_X, and NO_Y

by

William A. McClenny, U.S. EPA, and
K. Kronmiller and M. Wheeler, ManTech Environmental Technology, Inc.

The U.S. EPA has funded the evaluation of two approaches for improved nitrogen oxides monitoring in urban atmospheres at the Battelle laboratories in Columbus, OH. The detector used in these two approaches is a luminol-based detector obtained commercially as the Model LMA-3 available from Scintrex (Toronto, Canada). Based on the results as documented in EPA Report 600/R-95/031 (Work Assignment 43 of EPA Contract 68-DO-0007—see Spicer et.al., 1995), a similar system was assembled for monitoring at the Cornelia Fort monitoring site near downtown Nashville, TN, in the 1999 SOS summer field study in that city. The system was operated successfully at this site and led to some of the monitoring results that are presented in Chapter 6 of this report.

The system is shown schematically in Figures E-1 and E-2. Figure E-1 shows the principal components of the system. The thermal converter for NO_Y to NO conversion was placed at the top of the monitoring tower at the Cornelia Fort monitoring site so that compounds such as HNO_3 would be immediately converted to NO and thereby minimize losses to tubing walls. Residence times in the sampling lines were minimized by the use of auxiliary air pumps to pull ambient air through the relatively long sampling lines that stretched from the top of the monitoring tower to the trailer that housed the monitoring equipment. As shown in Figure E-1, a second pump pulled air through the sample conditioner and exhausted it into a sampling manifold for the luminol-based monitor and for a supplemental measurement by a Model 42 chemiluminescence monitor (TEI, Franklin, MA). Routing of the sample streams inside the multipath converter is shown in Figure E-2. By means of valves V1–V3, the sample air was routed in three ways, each path being available for 5 min and repeating every 15 min. With a path through V1 and V3, NO_2 in the air sample was directly monitored. With a path through V1, V2, and V3, NO in the sample stream was converted to NO_2 by the chromium trioxide oxidizer so that NO_X was monitored by the LMA-3. With V2 and V3 open, the sample passed through the Mo thermal converter and then through the chromium trioxide converter to provide a number of NO_2 molecules equal to the NO_Y.

The approach illustrated in Figures E-1 and E-2 provides NO_2, NO_X, and NO_Y, and NO_Z can be obtained by difference. Thus, four priority components (see Chapter 4) requested by the scientists working with AQMs are obtained with the luminol-based detector.

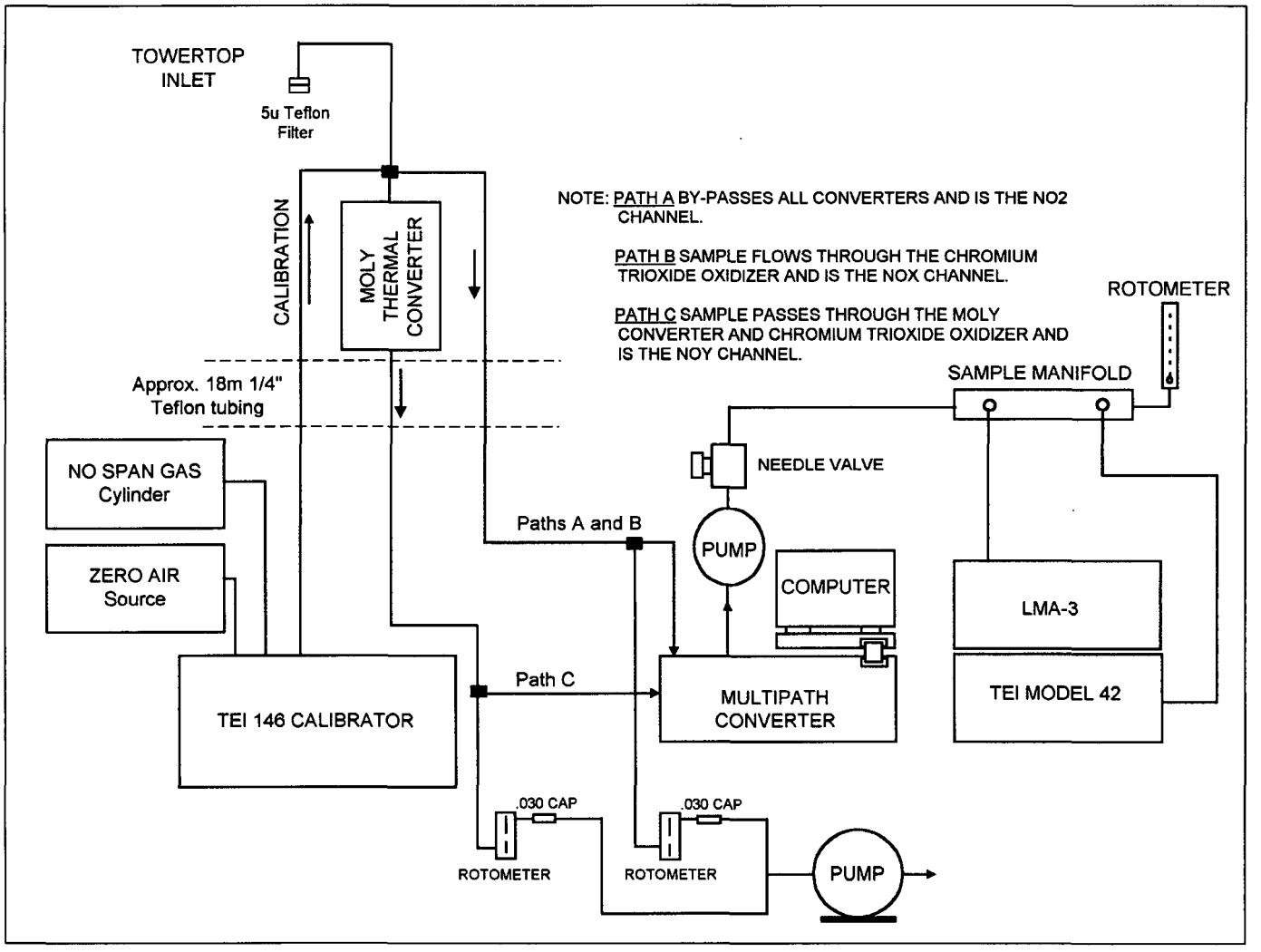

Figure E-1. LMA-3 field setup for SOS '99, Nashville, TN.

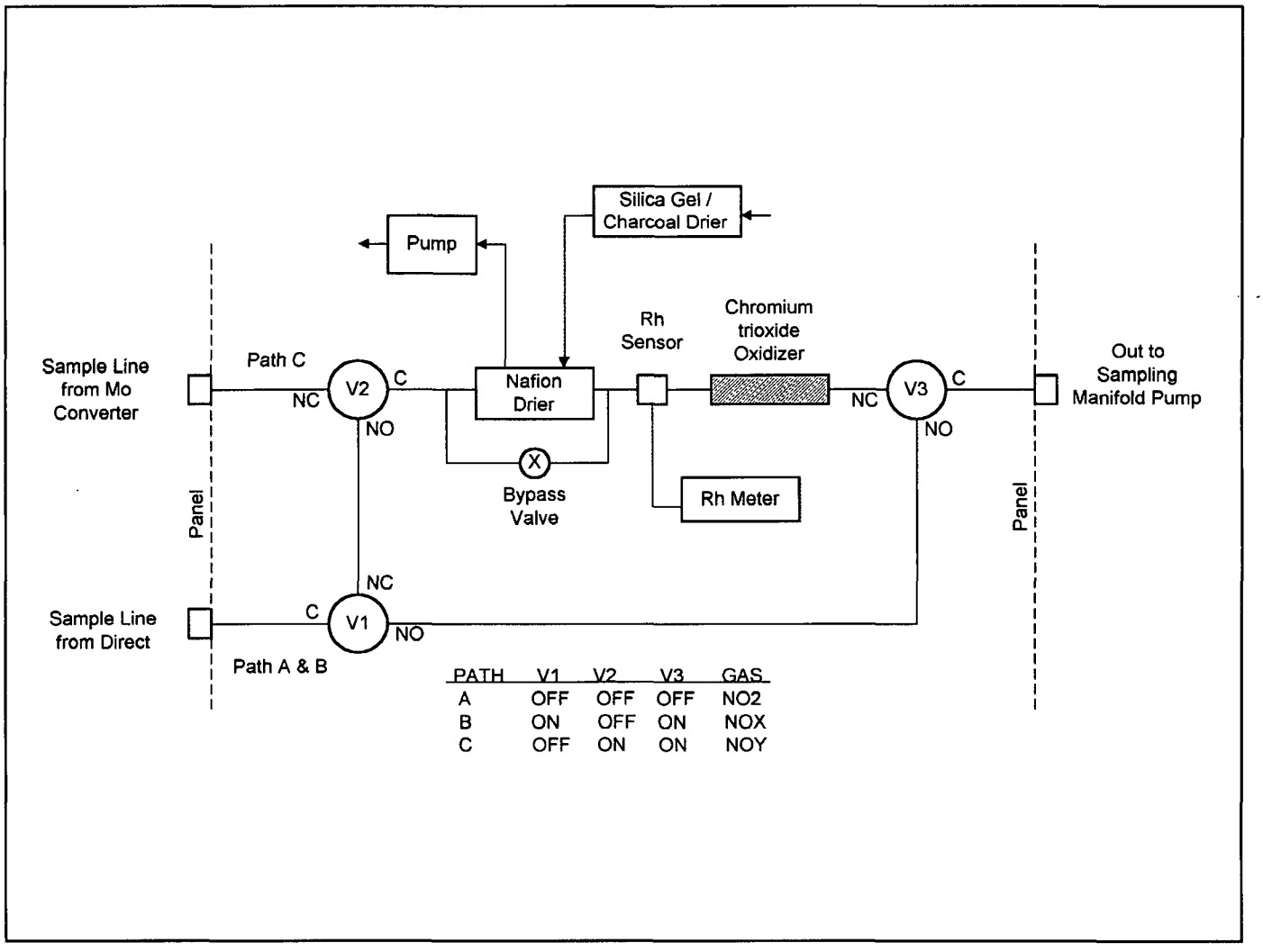

Figure E-2. LMA-3 NO_y multipath converter.